AL ZOUBI, RUFAIDA M., Ph.D. Molecular Level Studies on the Cannabinoid Receptor Type 1 (CB1): Biased Signaling and MD Simulations. (2018)
Directed by Dr. Patricia H. Reggio. 116 pp.

The endocannabinoid system has been historically targeted for medicinal purposes through the use of cannabis. Two cannabinoid receptors, CB1 and CB2, have been identified as the mediators of the biological effects of the main psychoactive component in *Cannabis sativa*; delta-9-tetrahydrocannabinol. The CB1 receptor is a class A G-protein coupled receptor (GPCR), and is the most abundant neuro-modulatory receptor in the CNS. With its location at presynaptic termini, it regulates the function of other receptors, including the dopamine, serotonin, GABA, opioid and glutamate receptors.

Many potential therapeutic applications targeting the CB1 receptor are under investigation. However, the unformed knowledge in drug-receptor interactions at the molecular level, and in the CB1 receptor signaling properties, has hampered the transition of many synthesized CB1 receptor agonists and antagonists to clinical use. In the studies to be presented, computational and mutational methods are employed to improve our understanding of the CB1 receptor structure, its conformational changes during activation, and the dynamics of drug-receptor interaction.

In the first chapter, background information on the CB1 receptor is provided; including its structure, drugs that act at the CB1 receptor, G-protein and β-arrestin mediated signaling pathways, as well as, CB1 receptor regulation by other proteins.

The second chapter includes a discussion of the biased signaling through class A GPCRs in general and through the CB1 receptor specifically. A set of hypothesis-driven

mutations on the CB1 receptor yielded a CB1 receptor that exhibits biased signaling through the β-arrestin pathway. Results from this study provide better understanding of the molecular mechanisms of biased signaling at the CB1 receptor specifically, and in Class A GPCRs in general. In addition, biased mutants developed here should assist structure-based drug design of CB1 receptor ligands with β-arrestin functional selectivity.

In the third chapter, molecular dynamics simulations are presented that were used to investigate the docking of 5-(4-chlorophenyl)-N-[(1R,2R)-2-hydroxycyclohexyl]-6-(2-methoxyethoxy)-3-pyridinecarboxamide (14h) inside the CB1 receptor. 14h has been described previously as a peripherally selective, high affinity CB1 receptor antagonist. However, the compound exhibits higher affinity for the human CB1 receptor compared to rodent CB1. Recent inactive state crystal structures (PDB ID: 5TGZ, 5U09) of the CB1 receptor have been published showing the membrane proximal region of the N-terminus invading the receptor binding pocket, steering an important interaction site (K3.28) away from binding pocket. Thus, results from the docking study will help in the remodeling of the CB1 receptor's N-terminus based on a mutational study that identified an N-terminal residue (M106 in rodent CB1 compared to I105 in human CB1) as the determinant of the species differential affinity of 14h at the CB1 receptor.

The fourth chapter is focused on the biarylpyrazole derivative; 5-(4-Chlorophenyl)-1-(2,4-dichloro-phenyl)-4-methyl-N-(piperidin-1-yl)-1H-pyrazole-3-carboxamide (SR-141716A (SR)). SR is a potent and a selective CB1 receptor antagonist and inverse agonist. The lack of force field parameters for SR has hampered the study of its interaction dynamics with the receptor in a lipid bilayer. This work describes the

development of missing CHARMM force field parameters for SR based on a previously published parameterization method for drug-like molecules, as well as an all atom MD simulation study of SR in a fully hydrated bilayer. Generated parameters were successful in reproducing target data from SR crystal structures equilibrated at the MP2/6-31G* level of theory. MD simulations show that SR can adopt multiple orientations in the lipid bilayer, it can rotate in all directions and move freely between leaflets.

Advances in crystallization and expression techniques made the crystallization of the CB1 receptor possible. However, those techniques, as well as, the static nature of the crystal structures, compromise the structural information for the receptor and undermine the dynamics of drug-receptor interactions. Computational, as well as, mutational studies would provide ancillary information that enhance our understanding of the CB1 receptor. Current studies increase our molecular level understanding of the conformational changes that accompany CB1 receptor activation. They also highlight the dynamics of drug-receptor interactions in a bilayer. Results from these studies will aid the development of new ligands that target the CB1 receptor.

MOLECULAR LEVEL STUDIES ON THE CANNABINOID RECEPTOR TYPE 1 (CB1): BIASED SIGNALING AND MD SIMULATIONS

by

Rufaida M. Al Zoubi

A Dissertation Submitted to
the Faculty of The Graduate School at
The University of North Carolina at Greensboro
in Partial Fulfillment
of the Requirements for the Degree
Doctor of Philosophy

Greensboro
2018

Approved by

Patricia Reggio
Committee Chair

To

my parents and family in law, for their endless love.

my husband Loai, for who he is and his endless support.

my daughters Rand and Sham, for their unconditional love.

APPROVAL PAGE

This dissertation, written by Rufaida M. Al Zoubi, has been approved by the following committee of the Faculty of The Graduate School at The University of North Carolina at Greensboro.

Committee Chair Patricia Reggio

Committee Members E. Will Taylor

Kimberly Peterson

Sherri McFarland

March 14, 2018
Date of Acceptance by Committee

March 14, 2018
Date of Final Oral Examination

ACKNOWLEDGMENTS

Special thanks and appreciation to my Ph.D. advisor, Dr. Patricia Reggio for all her support and mentoring, for inspiring critical thinking, and for believing in the abilities of her students. Dow P. Hurst and Diane L. Lynch for their patience in answering all my questions, and to all members of the Reggio`s lab for making a family-like environment in the lab.

I am also grateful for Dr. Norman Chiu for guidance, and for committee members; Dr. E. Will Taylor, Dr. Sherri McFarland, Dr. Kimberly Peterson for reviewing my dissertation. Dr. Mary Abood, Luciana Magalhaes Leo, and Pingwei Zhao at Temple University for constructing CB1 receptor mutants and running cellular assays. The Department of Chemistry and Biochemistry at UNCG, and Jordan University of Science and Technology for funding my study.

This research was supported in part by the National Institute on Drug Abuse (NIDA DA03934).

TABLE OF CONTENTS

Page

LIST OF TABLES

Page

LIST OF FIGURES

Page

LIST OF ABBREVIATIONS

Å	Angstrom
BW	Ballesteros–Weinstein residue numbering system in GPCRs that uses the X.YY format; X denotes the transmembrane helix number and (YY) denotes residue position relative to the most conserved residue in the helix (X.50).[1]
EC	Extracellular
GPCR	G-Protein Coupled Receptors
HF	Hartree-Fock
IC	Intracellular
MD	Molecular Dynamics
MM	Molecular Mechanics
MPR	Membrane Proximal Region
PES	Potential Energy Surface
POPC	1-Palmitoyl-2-Oleoyl-Phosphatidyl-Choline
QM	Quantum Mechanical
TMH	Trans-Membrane Helix
WT	Wild Type

CHAPTER I

INTRODUCTION

Overview

The CB1 receptor is a class A (Rhodopsin-like) GPCR that was first determined and characterized as the receptor protein for Δ^9-THC -the major psychoactive constituent in *Cannabis Sativa* (Marijuana)- from rat brain preparations in 1988.[2] Cloning of the CB1 receptor from rat cerebral cortex[3] followed by cloning of human CB1 receptor from brain stem[4] prompted an ongoing research in the cannabinoid field. Another cannabinoid receptor subtype (CB2) was identified in 1993 that shows 44% overall identity to human CB1 receptor and 68% identity in the transmembrane region.[5] The CB1 receptor is highly expressed in the central and the peripheral nervous system, with high concentrations in the basal ganglia, cerebellum, cerebral cortex, hippocampus, and the emetic centers in the brain stem. An expression pattern that correlates with the analgesic, cognitive, psychomotor, and anti-emetic effects of cannabinoids. In addition. It is also expressed in the nucleus accumbens and ventral tegmental areas which are involved in reward, and food intake. On the other hand, the CB2 receptor is located primarily throughout the immune system.[6-9]

Many potential therapeutic applications for CB1 agonists are under investigation including anti-emesis and appetite stimulation for AIDs patients, symptomatic relief of neuropathic pain in patients with multiple sclerosis and spinal cord injury, and, inhibition

of angiogenesis and growth of malignant tumors. However, psychoactive side effects limit the use of these agonists.

CB1 receptor ligands have been shown to induce a complex pattern of intracellular effects that are ligand as well as cell-specific. Binding of a ligand induces distinct conformational changes in the receptor that will eventually translate into distinct intracellular signaling pathways through coupling to different intracellular effector proteins that can mediate receptor desensitization, trafficking, and signaling. The complex cellular components as well as concomitant expression of other proteins that either regulate the CB1 receptor or are regulated by the CB1 receptor will affect therapeutic outcome of targeting the CB1 receptor.

This chapter will be focused on CB1 receptor structure, ligands, signaling, and regulation by other intracellular proteins to provide the basis for the three subsequent chapters in this dissertation.

Cannabinoid Receptors Phylogeny and Structure

Cannabinoid receptors share the general class A GPCRs' topology that includes an extracellular N terminus, seven transmembrane helices (TMHs) joined by extracellular (EC) and intracellular (IC) loops of varied lengths, and an intracellular C terminus that begins with short alpha helical segment (Helix 8) oriented parallel to the cell membrane. The binding site for the endogenous ligand is generally formed by the EC core within the TMH bundle, and may extend to EC loops, referred to as the orthosteric binding site. Ligands may also bind to distinct (allosteric) binding sites in the receptor.

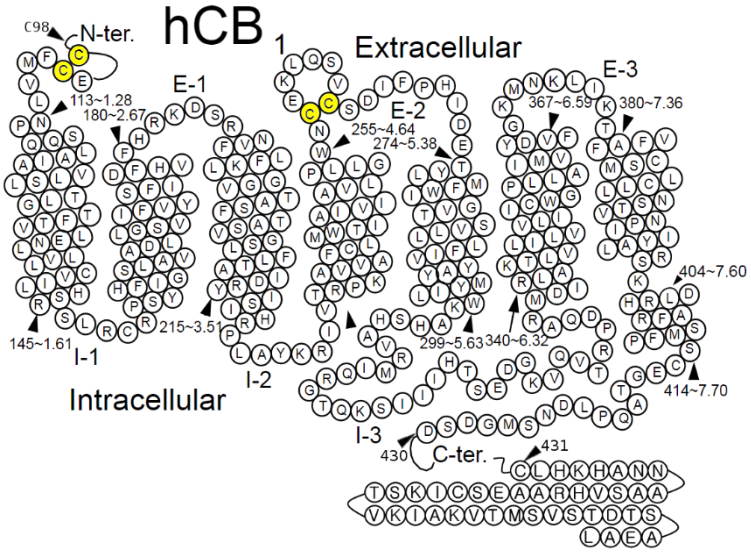

Figure 1. Helix Net Representation for the hCB1 Receptor. Disulfide bonds within the second extracellular loop and the N-terminus are yellow labeled.

Different phylogenetic studies and multidimensional scaling analysis of Class A GPCRs classify cannabinoid receptors (CB1/CB2) into one cluster of class A GPCRs along with the endothelial differentiation G-protein coupled receptors (EDGRs) (including Sphingosine 1-phosphate receptor (S1P) and Lysophosphatidic acid receptor(LPA)).[10-13] Receptors from those families recognize lipid-derived ligands and share common sequence divergence from other Class A GPCRs. Specifically, the absence of helix kinking proline residues in TMH2 and TMH5, and the absence of disulfide bridge between EC-2 loop and C3.25 at the EC end of TMH3. Instead, they share an internal disulfide bridge in the EC-2 loop, a conserved PxxGWN motif at the EC end of TMH4 in addition to a Y5.39 that pi-pi stack with W4.64 in that motif resulting in a similar conformation of the EC2 loop in those receptors as can be seen in their crystal structures.[14-17] At the binding site, they share a common basic residue (K/R 3.28) on

TMH3 and an aromatic residue (F/Y 2.57) on TMH2. In addition, the S1P1 receptor is like CB1/CB2 in the presence of E1.49 at TMH1. E1.49 has been reported as the site of interaction of pregnenolone (an endogenous negative allosteric modulator that protects the brain from *cannabis* intoxication) with CB1,[18] while the LPA1 receptor shares a W5.43 that has been shown to affect antagonist binding to the cannabinoid receptors.[19]

Endocannabinoids

The CB1 receptor is located primarily on presynaptic termini, it acts in response to endogenous arachidonic acid derivatives (endocannabinoids) synthesized on demand following postsynaptic depolarization, these are N-arachidonoylethanolamine (Anandamide, AEA) and sn-2-arachidonoylglycerol (2-AG), (see Fig. 2).[20-22] Activation of CB1 receptor by 2-AG modulates two short-term forms of synaptic plasticity; depolarization induced suppression of inhibition (DSI) and depolarization induced suppression of excitation (DSE). Thus, 2-AG acts as retrograde messenger that inhibits the ongoing release of GABA and Glutamate from presynaptic neurons.[23] 2-AG and AEA are rapidly degraded enzymatically by monoacylglycerol lipase (MAGL) and the fatty acid amide hydrolase (FAAH).[24]

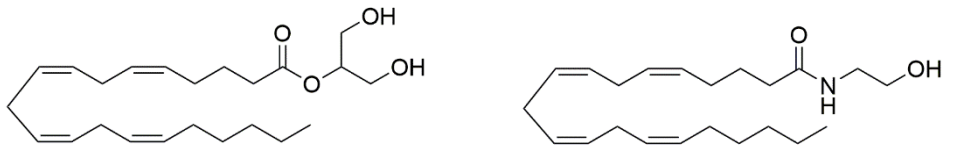

2-arachidonoylglycerol (2-AG) **N-arachidonoylethanolamine (AEA)**

Figure 2. Endogenous CB1 Receptor Ligands.

CB1 Receptor Ligands

Non-endogenous CB1 receptor agonists that target the orthosteric binding site of the receptor are grouped into the classical cannabinoids (e.g., **Δ^9-THC** and (-)-11-hydroxy-Δ^8-THC-dimethylheptyl (**HU210**)), non-classical cannabinoids (e.g., ([2-[(1R,2R,5R)-5-hydroxy-2-(3-hydroxy propyl)cyclohexyl]-5-(2-methyloctan-2-yl)phenol] (**CP-55940**)), and the aminoalkylindoles (e.g., ((R)-(1)-[2,3-dihydro-5-methyl-3-(4-morpholinylmethyl)pyrrolo[1,2,3-de]-1,4-benzoxazin-6-yl]-1-napthalenylmethanone (**WIN55212-2**)). The first CB1 antagonist ([5-(4-chlorophenyl)-1-(2,4-dichloro-phenyl)-4-methyl-N-(piperidin-1-yl)-1H-pyrazole-3-carboxamide] (**SR141716A**)), was described by Sanofi Recherche in 1994, it displays nano-molar CB1 affinity and acts as a selective CB1 inverse agonist (see Fig. 3).[25, 26]

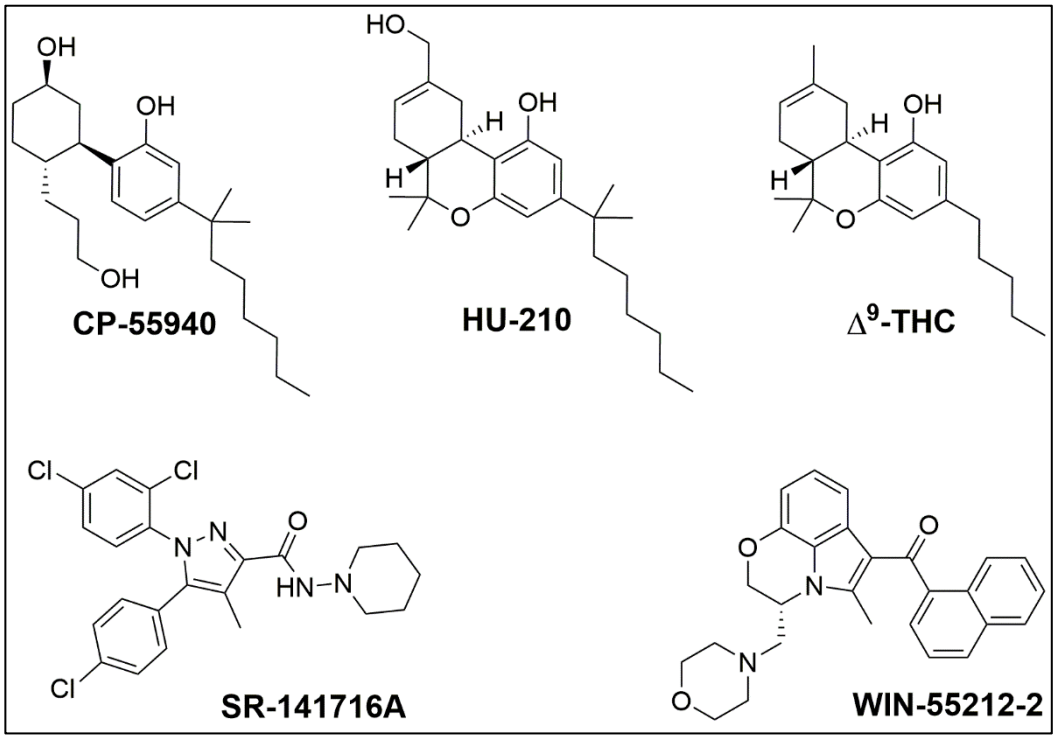

Figure 3. Non-Endogenous Ligands for the CB1 Receptor. Agonists (CP-55941, HU210, Δ9-THC, WIN-55212) and the antagonist/inverse agonist SR-141716A.

Signaling via the CB1 Receptor

Activation of the CB1 receptor inhibits forskolin-stimulated adenylyl cyclase via coupling to PTX-sensitive G-protein (Gαi/o), and increases phosphorylation of extracellular signal-regulated kinase 1/2 (pERK1/2) via G-protein dependent and β-arrestin-1 dependent pathways.[27] Gαi/o mediated decrease in cAMP upon CB1 activation activates G-protein-coupled inwardly rectifying potassium channels (GIRKs) and inhibits N-type and P/Q type voltage-gated calcium channels, inhibiting presynaptic neurotransmitter release. Stimulation of CB1 also leads to phosphorylation and activation of mitogen-activated protein kinases (MAPK), such as p38 MAPK and c-Jun

N-terminal kinase, which can regulate nuclear transcription factors.[28-30] While CB1 couples mainly through Gαi/o type G-protein, coupling to other G-protein types under special circumstances has been also reported. As an example; coupling to Gαs has been suggested in striatal neurons and in transfected CHO cells treated with PTX as well as in L341A/A342L mutant CB1 receptor accounting for the increase in intracellular cAMP upon treatment with CB1 agonist.[31, 32] The increase in cAMP has been attributed in a later study at Howlett's Lab to reduced Gi/o function.[33] In addition, WIN55212-2 has been shown to increase intracellular calcium in transfected HEK293 cells and in cultured hippocampal neurons via coupling to Gαq/11.[34]

Phosphorylation and Subsequent β-Arrestin Recruitment

Mammalian cells express seven isoforms of G protein-coupled receptor kinases (GRKs), those are GRK1-7. While GRK1/7 are primarily found in the retina and regulate opsins, other GRKs (GRK2,3,5,6) are widely expressed in the body and in neuronal cells, with limited expression of GRK4 to the cerebellum, testis and kidneys.[35, 36] GRK2 and GRK3 have a pleckstrin homology domain that allows their translocation to the plasma membrane by binding to phosphatidylinositol lipids such as phosphatidylinositol (4,5)-bisphosphate (PIP2) or to the βγ-subunits of activated G-proteins. GRKs 4, 5, and 6 lack the pleckstrin homology domain but are primarily attached via a lipidation to the plasma membrane. In canonical GPCRs signaling pathway, GRKs phosphorylate serine and/or threonine residues at the IC domain of agonist-activated receptors, specifically at the C-terminus and/or the third IC loop.[36] Different GRKs have been reported to result

in distinct phosphorylation patterns at the IC domain of GPCRs that were correlated with the functional selectivity of the activated receptor upon agonist binding.[37]

β-arrestin recruitment to phosphorylated receptor redirects the G-protein dependent signaling state of the receptor to other possible states depending on the receptor itself, the phosphorylation pattern which determines the type of the β-arrestin being recruited to the receptor, the agonist specificity, as well as intracellular components. The two non-visual arrestins; β-arrestin-1 and β-arrestin-2, are expressed ubiquitously in mammalian tissues and mediate GPCRs desensitization, endocytosis, ubiquitination, or the G-protein independent signaling.[38, 39] β-arrestin recruitment to phosphorylated receptor may sterically inhibit G-protein coupling to the activated receptor, thus quenching G-protein signal and reducing receptor's response to repeated stimulation, known as receptor desensitization. On the other hand, β-arrestins may act as scaffolding proteins in which they can mediate clathrin-mediated receptor endocytosis by binding to β(2)-adaptin and clathrin, or they can mediate G-protein independent intracellular signaling pathways by scaffolding the different mitogen-activated-protein-kinase (MAPK) signaling modules, including the ERK1/2, p38MAPK, and c-Jun N-terminal kinases, as well as scaffolding the Src family tyrosine kinases and protein phosphatases.[35, 36, 39, 40]

In addition, the non-canonical, G-protein independent β-arrestin recruitment to GPCRs has been also reported. The reported ability of GRK5 and GRK6 to phosphorylate inactive receptors may explain the ability of β-arrestins to recruit to GPCRs in a G-protein independent way.[41]

Recent studies on the β2AR and the vasopressin receptor using mutational and electron microscopic techniques, reported two possible interaction scenarios of the arrestins with the IC domain of the receptors; the tail-conformation where the arrestin is bound to the C-terminus of the receptor only, and the core-conformation where the arrestin is bound to both the C-terminus and the cytoplasmic core of the receptor. Interacting in the tail conformation, arrestins preserve their ability to mediate G-protein independent signaling, receptor internalization, but not desensitization.[42] Interestingly, GPCR-G-protein-β-arrestin megaplexes have been reported, in which the arrestin is engaged to the GPCR in the tail conformation allowing a concomitant binding of the G-protein with the receptor, these megaplexes explain the ability of some GPCRs to activate G-proteins from internalized compartments.[43] In addition to GRKs, second messenger-dependent protein kinases (PKA, and PKC) have been reported to phosphorylate GPCRs at the IC domain, attenuating G-protein dependent signaling through GPCRs.[44-47]

In the recently published crystal structure of Rhodopsin in complex with the visual arrestin, authors identified a phosphorylation pattern in the C-terminus that is required for effective recruitment of arrestins to the receptor. A short code (PxPxxP/E/D), or a long code (PxxPxxP/E/D) were identified in which the P represents phosphorylated serine or threonine residues, while the x is any amino acid residue. Identified pattern of negatively charged amino acid residues ensures high affinity interaction with the three positive pockets at the N-temrinal domain of activated arrestin.[48] The crystal structure of β-arrestin-1 bound to phosphorylated peptide segment of the vasopressin receptor's C-terminus was also in agreement with proposed motif.[49]

The C-terminus in the CB1 receptor contains multiple serine, threonine, aspartate and glutamate residues. According to the previously proposed phosphorylation code, the membrane proximal segment of the C-terminus which contains D423-NSMGDS-D430 (hCB1 numbering) and the membrane distal segment which contains T460-MSVSTDTSA-E470 are two possible interaction sites at the C-terminus of the CB1 receptor with the β-arrestins. The central segment, on the other hand, contains A439-A-S441 in human / T440-A-S442 in rodents, which implies low if no interaction of the arrestins with the CB1 receptor at this region.

Different studies that investigate the role of GRKs and β-arrestin-1/2 in the desensitization, internalization, or signaling via the CB1 receptor have been reported. Mackies lab demonstrated the role of GRK3 and β-arrestin-2 in CB1 receptor desensitization using *Xenopus* oocytes transfected with rat CB1. Attenuation of G-protein dependent Kir current during an 8 minutes exposure to WIN-55212 required co-expression of both GRK3 and β-arrestin-2. In the same study, truncation mutants of the whole C-terminus (Δ418), or (Δ418-439) did not desensitize while truncation at 439 and at 460 could still desensitize. In addition, S426A, or S430A mutations significantly attenuated desensitization, while they had no effect on the internalization of the receptor evaluated in AtT20 cells treated with WIN-55212.[50] Subsequent study in HEK293 cells shown that the S426A/S430A mutant recruits β-arrestin-2 in a similar extent to the WT receptor, suggesting that the β-arrestin-2 recruitment to the proximal C-terminus confers receptor desensitization, while it can still recruit to the distal region of the C-terminus in the absence of phosphorylation at S426/S430. Thus, β-arrestin-2 recruitment does not

guarantee CB1 receptor desensitization.[51] In a different study, treatment with WIN-55212 resulted in desensitization of CB1 receptor lacking distal residues 419-460 transfected into CB1 knockout autaptic hippocampal neurons, distal segment of the C-terminus thus was directly attached to the transmembrane bundle.[52] It could be concluded from those studies, that the desensitization is linked to β-arrestins being recruited close to the CB1 receptor transmembrane domain, which may imply β-arrestin core conformation binding to the CB1 receptor at the proximal C-terminus that would sterically uncouple G-protein from the CB1.

In further studies on the proximal C-terminus region of the CB1, a recent study using the S426A/S430A CB1 receptor mutant expressed in HEK293 cells, demonstrated an interesting shift in the functional selectivity of WIN-55212 from inducing biased G-protein-dependent pERK1/2 signal at the WT receptor to inducing biased β-arrestin-1-dependent pERK1/2 signal in the mutant receptor. On the other hand, 2-AG induced G-protein dependent followed by β-arrestin-1 dependent pERK1/2 signal in the WT receptor, while its induced pERK1/2 signal was totally β-arrestin-1 dependent in the S426A/S430A CB1. The same study has also demonstrated significantly higher recruitment of β-arrestin-1 to the S426A/S430A CB1 compared to the WT receptor, and a weaker recruitment of β-arrestin-2 to the S426A/S430A CB1 compared to the WT receptor 5 minutes after treatment with WIN-55212.[53] However, an immunoprecipitation study from Howlett's lab, demonstrated that only the proximal phosphorylated C-terminal peptide segment (T419-H436 phosphorylated at S426/S430) competed for the CB1 receptor association with β-arrestin-1, while both phosphorylated

proximal peptide segment and the distal peptide segment (V460-L473 phosphorylated at T468) competed for the association with β-arrestin-2, the study was done using cultured N18TG2 neuroblastoma cells.[54] Those results contradict with the ability of β-arrestin-1 to recruit to the S426A/S430A CB1 receptor. However, the ability of β-arrestin-2 to bind both the proximal and the distal regions of the CB1 receptor's C-terminus could still be valid.

In vivo, S426A/S430A mutant mice were more sensitive to the anti-nociception and hypothermic effects induced by Δ^9-THC and endocannabinoids, with delayed tolerance and increased Δ^9-THC-dependence, while cultured autaptic hippocampal neurons from mutated mice showed enhanced WIN-55212-mediated DSE and reduced agonist-mediated desensitization of DSE.[55]

Reported studies on the distal segment of the C-terminus evaluated its role in receptor internalization as well as desensitization. Mackeis' lab used AtT20 cells stably transfected with truncated rat CB1 receptor mutants and demonstrated that receptors lacking the last 10 amino acid residues (V464Z) could internalize in a similar extent to the WT receptor following WIN-55212 treatment. However, receptor lacking the last 14 amino acid residues (V460Z) did not internalize. Internalization in this study was determined using immunofluorescence confocal microscopy and was determined to be G-protein independent since pretreatment of the cells with cholera toxin or PTX did not prevent internalization.[56] In a later study, the V640Z CB1 receptor did not internalize and failed to recruit β-arrestin-2 to the membrane in AtT20 cells treated with WIN-55212 or CP-55940. However, V640Z CB1 receptor expressed in HEK293 cells internalized to

the same extent as the WT receptor and could recruit the β-arrestin-2 to the membrane.[57] From previous discussion, we could conclude that β-arrestin-2 could bind to both the proximal and the distal regions of the CB1 receptor's C-terminus, truncation of distal C-terminus did not affect β-arrestin-2 recruitment in HEK293 cells, suggesting that it has been recruited to the proximal C-terminus. A possible explanation that β-arrestin-2 could not recruit to the proximal C-terminus of V640Z receptors expressed in AtT20 cells could be the presence of other CB1 receptor coupling proteins that compete with the β-arrestins for the C-terminus, such as the CRIP1A and the SGIP1 proteins which are known to compete with the β-arrestins on binding to the CB1 receptor's C-terminus.[54, 58] Thus, the only available interaction site at the proximal C-terminus in V640Z receptors would be occupied by those proteins that are absent in HEK293 cells.

To determine critical phosphorylation site residues required for internalization, different mutations were introduced to the distal C-terminus region (T460-MSVSTDTSAEA-L473). T461A/S463A, S465A/T466A, and T468A/S469A double mutants showed similar extent of internalization and efficient β-arrestin-2 recruitment to the plasma membrane compared to the WT upon treatment with CP-55940. However, mutating four or all six putative phosphorylation sites (T461A-T466A and T461A-S469A) significantly attenuated CP-55940 induced receptor internalization, and did not show translocation of β-arrestin-2 to the membrane.[57] Results described here are perplexing, since β-arrestin-2 could recruit to the V640Z mutant in HEK293 cells while it could not recruit to T461A-T466A and T461A-S469A mutants in the same cell line. On

the other hand, V640Z CB1 or T461A-S469A transfected into CB1 knock out autaptic hippocampal neurons did not desensitize following WIN-55212 or 2-AG treatment.[52]

Finally, away from the C-terminus, the CB1 receptor's IC3 loop has been reported to be phosphorylated at S317 by PKC in AtT20 cells transfected with rat CB1 receptor. Phosphorylation at S317 has been shown to attenuate CB1 mediated activation of K_{ir} currents.[47]

Reported GRKs that Phosphorylate the CB1 Receptor

As discussed earlier, co-expression of GRK3 and β-arrestin-2 in oocytes have been reported to be essential for CB1 receptor desensitization of WT receptor but not receptors with truncations of the proximal C-terminus.[50] inhibition of GRK2 in N18TG2 cells reduced the internalization of CB1 receptor upon treatment with CP-55940.[54] In another study, knocking down GRK3 or GRK2,3 in HEK293 cells expressing rat CB1 receptors significantly increased the pERK1/2 signal 15 minutes following WIN-55212 treatment, while they had no effect on the S426A/S430A mutant receptor. The same mutant induced significantly lower pERK1/2 signal following WIN-55212 treatment in HEK293 cells with GRK4, GRK5, or GRK6 knock down. In the same study, WIN-55212 has been shown to induce G-protein dependent pERK1/2 signal in the WT receptor, and β-arrestin-1 dependent pERK1/2 signal in S426A/S430A mutant.[53] Results suggest that GRK3 phosphorylates the proximal phosphorylation sites in the CB1 receptor C-terminus, specifically at S426 and S430. This phosphorylation results in desensitization of the receptor. Thus, knocking down of GRK3 would enhance G-protein

dependent pERK1/2 signal in WT receptor. On the other hand, β-arrestin-1 mediated signaling through the CB1 receptor has been reported to be from endocytic pits.[27] GRK4, GRK5, and GRK6 might be involved in the phosphorylation of the distal C-terminus and could be necessary for receptor internalization into those endocytic pits, thus knocking down of those GRKs lowers the β-arrestin-1 mediated pERK1/2 signal in the S426A/S430A mutant.[53]

Altering Cannabinoids Activities in β-Arrestin-1 and β-Arrestin-2 Knockout Mice

In vivo studies evaluating the antinociceptive (tail flick assays) and temperature depressive effects of CB1 receptor agonists in β-arrestin-1 and β-arrestin-2 knockout mice, demonstrated that β-arrestins regulate cannabinoids sensitivity in agonist-selective manner, while they do not affect the density of CB1 receptors in brain membranes which was determined using radioligand binding assays.[59, 60] Deletion of β-arrestin-2 increased Δ^9-THC antinociceptive and temperature depressive efficacy, while it did not affect the efficacy of other ligands such as CP-55940, methanandamide, JWH-073 and O-1812.[59] On the other hand deletion of β-arrestin-1 diminished the effects of CP-55940 in both antinociception, and temperature-depression assays in mice, while it did not affect Δ^9-THC efficacy. Interestingly, CP-55940 produced greater stimulation of [^{35}S]GTPγS binding to membranes from whole brain of β-arrestin1 knockout mice compared to the WT. this may indicate that the antinociceptive and the temperature depressive effects of CP-55940 are not G-protein dependent. In the same study, it has been demonstrated that

the tolerance development to chronic treatment with Δ9-THC or CP-55940 is not β-arrestin-1 dependent.[60]

Other Proteins Regulating the CB1 Receptor

In addition to GRKs and β-arrestins, other intracellular proteins are known to regulate the CB1 receptor. The Src homology 3-domain growth factor receptor-bound 2-like (endophilin) interacting protein 1 (SGIP1), is an 828 amino acid residues protein with N-terminal lipid-binding domain. SGIP1 has been shown to interact with the CB1 receptor C-terminus. Association with the CB1 receptor was verified *in-vivo* using coimmunoprecipitation technique from rat brain homogenates, and *in-vitro* using BRET assay in HEK293 cells transfected with both the CB1 and SGIP1 protein, where similar extend of association has been observed in the presence or absence of CB1 receptor agonist. SGIP1 is expressed in different regions in the brain where it can overlap with the expression of the CB1 receptor. SGIP1 has been shown to inhibit clathrin-mediated endocytosis of the CB1 receptor. It has been also demonstrated that it enhances the CB1 receptor association with β-arrestin-2 but not with b-arrestin-1, and it lowers WIN-55212 induced PTX-sensitive ERK1/2 phosphorylation while not affecting CB1 receptor mediated Gαi/o/q activation.[58] In addition, it has been demonstrated to colocalize at presynaptic termini with the CB1 receptor in cultured cortical neurons, which may explain neuronal compartment-selective endocytosis in which rapid CB1 receptor internalization is observed in neuronal soma, while resistance to endocytosis is observed in presynaptic termini.[58, 61]

The cannabinoid receptor interacting protein 1a (CRIP1a) has been also demonstrated to interact with the C-terminus of the CB1 receptor. CRIP1a is a 164 amino acid residues protein with predicted palmitoylation site but not transmembrane domain, it has high expression in different brain regions including the cerebral cortex, cerebellum, hippocampus, hypothalamus, and caudate nucleus. *In-vivo* co-expression has been determined using coimmunoprecipitation technique from rat brain homogenates,[62] and colocalization with the CB1 receptor at presynaptic termini was also confirmed using immune-histochemical studies in transgenic mice cerebellum.[63] CRIP1a has been reported to attenuate agonist-induced CB1 receptor internalization,[63] and modulate CB1 mediated activation of G proteins in a subtype selective manner.[64] It has been also shown to compete with β-arrestins to the CB1 receptor C-terminus that could affect β-arrestins mediated effects via the CB1 receptor.[54]

CHAPTER II

MUTATIONS AT THE INTRACELLULAR DOMAIN OF THE CB1 RECEPTOR BIAS ITS SIGNALING TOWARDS THE β-ARRESTIN PATHWAY

Introduction

Biased signaling through GPCRs has recently received a special attention in the field of drug research; this is due to the possibility of attaining different therapeutic effects and/or avoiding untoward effects while targeting the same receptor protein.[65] In GPCRs, biased signaling describes the ability of different ligands to stabilize distinct receptor states that vary the ability of the receptor to activate specific transducers, such as activation of different G-proteins and/or signaling through β-arrestins.

Binding of an agonist to the receptor induces several conformational changes in the binding site which lead to distinct conformational changes in the IC domain of the receptor. These changes uncover the IC domains that are important for coupling to different IC effector proteins, thus determining the signaling pathway(s) of the receptor.

Despite the tremendous variation in chemical structures of agonists that bind and activate class A GPCRs, those receptor proteins share common molecular activation mechanisms. A set of amino acid residues that are highly conserved at the majority of non-olfactory members (ligand-modulated receptors) of this class[66] are thought to act as molecular switches that dictate the conformational changes in the receptor upon ligand

binding and thus; dictating the functional selectivity and biased signaling of the receptor. Conserved amino acid residues include the following motifs; NxLV in TMH1, LAxAD in TMH2, D/ERY motif in TMH3, FxxCWxP in TMH6 and NSxxNPxxY motif in TMH7 (see Fig. 4, and Table 1).

Different mutations on class A GPCRs have been used to study multiple downstream signaling cascades from biased mutants. As mentioned in the first chapter, mutating two phosphorylation sites at the C terminus of the CB1 receptor (S426A, S430A in rat CB1) shifted WIN-55212-induced pERK signal via the CB1 receptor from being G-protein biased to being β-arrestin-1 biased.[53] Mutations that included conserved amino acid residues were also employed; mutating the conserved DRY motif at the IC end of TMH3 into AAY biased the signaling of the CB1 receptor and the angiotensin-1A receptor towards the β-arrestin pathway[67, 68]. At the β-2-adrenergic receptor, a triple mutant that included two conserved tyrosine residues (T2.39F, Y3.51G, Y5.58A) exhibited β-arrestin biased signaling determined by measuring the pERK signal in HEK293 cells expressing WT or mutant receptor.[69] In addition, a recent mutational study on the δ-opioid receptor revealed interesting efficacy switching of Naltrindol from antagonist at the WT receptor into a potent β-arrestin biased agonist at D2.50A, N7.45A, and N7.49A mutants [70].

Other mutations that involve the conserved amino acid residues in class A GPCRs are abundant in the literature. However, their exact role in biased signaling is still not well understood because most of these mutations were evaluated for their canonical G-

protein signaling efficacy only, while their efficacy in β-arrestin signaling is yet emerging in the literature.

In this study, three hypothesis-driven single point mutations on I2.43 and S7.57 were proposed to elucidate the mechanism of biased signaling through the CB1 receptor. Those are I2.43A, I2.43T, and S7.57E. As being expected, mutants were successful in biasing the signaling of the CB1 receptor towards the β-arrestin signaling pathway.

The elucidation of the specific conformational changes in the CB1 receptor that result in distinct subsets of downstream signaling pathways through G-protein or β-arrestin, should increase our understanding of biased signaling in CB1 receptor in specific and in Class A GPCRs in general. In addition, the presence of biased CB1 receptor mutants aids the search for potential therapeutic applications via the CB1 receptor.

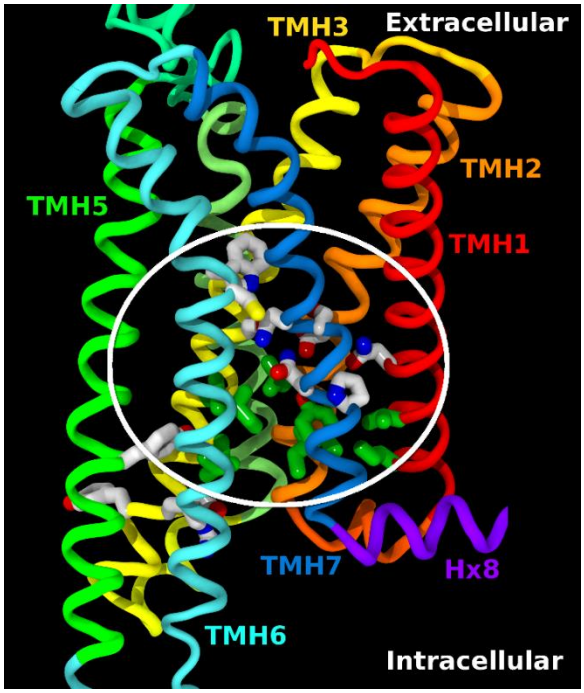

Figure 4. Location of Conserved Amino Acid Residues in Class A GPCRs. Residues displayed in green form an intact hydrophobic layer at the IC domain of the receptor in its inactive state. Residues that contribute to this hydrophobic layer are at locations 1.53, 157, 2.43, 2.46, 3.43, 3.46, 6.37, 6.40, in addition to Y7.53

Table 1. Conserved Residues and Motifs Presented in a Sample of Class A GPCRs. (* BW: Ballesteros–Weinstein residue numbering.[1]), Green highlight represents non-polar amino acid residues, while yellow highlight represents polar amino acid residues.

Helix #	1				2						3				4	5		6							7									
Motif	NxLV				LAxAD						D/ERY							FxxCWxxP							NPxxY									
BW*	1.50	1.51	1.52	1.53	2.43	2.46	2.47	2.48	2.49	2.50	3.39	3.49	3.50	3.51	4.50	5.50	5.58	6.44	6.45	6.46	6.47	6.48	6.49	6.50	7.45	7.46	7.49	7.50	7.51	7.52	7.53	7.60	7.61
Rho	N	F	L	T	L	L	A	V	A	D	A	E	R	Y	W	P	Y	F	L	I	C	W	V	P	A	A	N	P	V	I	Y	F	R
D3	N	G	L	V	V	L	A	V	A	D	S	D	R	Y	W	P	Y	F	I	V	C	W	L	P	N	S	N	P	V	I	Y	F	R
D1	N	T	L	V	I	L	A	V	S	D	S	D	R	Y	W	P	Y	F	V	C	C	W	L	P	N	S	N	P	I	I	Y	F	R
GPR119	N	T	L	V	T	L	A	V	A	D	S	D	R	Y	W	P	F	F	A	L	S	W	T	P	N	S	N	P	L	I	Y	V	R
M2	N	I	L	V	L	L	A	C	A	D	S	D	R	Y	W	P	Y	F	I	I	T	W	A	P	N	S	N	P	A	C	Y	F	K
LPAR1	N	L	L	V	M	L	A	A	A	D	S	E	R	H	W	T	Y	F	I	I	C	W	T	P	N	S	N	P	I	I	Y	M	S
S1P1	N	I	F	V	I	L	A	L	S	D	S	E	R	Y	W	L	Y	F	I	A	C	W	A	P	N	S	N	P	I	I	Y	M	R
CB1	N	L	L	V	I	L	A	V	A	D	S	D	R	Y	W	L	Y	L	I	I	C	W	G	P	N	S	N	P	I	I	Y	L	R
CB2	N	V	A	V	I	L	A	G	A	D	S	D	R	Y	W	L	Y	L	L	I	C	W	F	P	N	S	N	P	V	I	Y	I	R
Orx2	N	V	L	V	I	L	S	L	A	D	S	D	R	W	W	P	Y	F	A	I	C	Y	L	P	N	S	N	P	I	I	Y	F	R
B2AR	N	V	L	V	I	L	A	C	A	D	S	D	R	Y	W	P	Y	F	T	L	C	W	L	P	N	S	N	P	L	I	Y	F	R
A2A	N	V	L	V	V	L	A	A	A	D	S	D	R	Y	W	P	Y	F	A	L	C	W	L	P	N	S	N	P	F	I	Y	F	R
B1AR	N	V	L	V	I	L	A	S	A	D	S	D	R	Y	W	P	Y	F	T	L	C	W	L	P	N	S	N	P	I	I	Y	F	R
MOR	N	F	L	V	I	L	A	L	A	D	S	D	R	Y	W	P	Y	F	I	V	C	W	T	P	N	S	N	P	V	L	Y	F	K
KOR	N	S	L	V	I	L	A	L	A	D	S	D	R	Y	W	P	Y	F	V	V	C	W	T	P	N	S	N	P	I	L	Y	F	K

Methods

Mutagenesis: The I2.43A, I2.43T, and S7.57E mutants of the GFP-tagged human CB1 (GFP-hCB1) in the vector pcDNA3 were constructed using the QuikChange site-directed mutagenesis kit (Agilent, Wilmington, DE) as described by the manufacturer. DNA sequencing subsequently confirmed the presence of only the desired mutation.

Cell culture and transfections: Human embryonic kidney (HEK293) cells (ATCC CRL-1573) were cultivated in growth medium consisting of Dulbecco's Modified Eagle's medium (DMEM) with 4.5 g/L glucose, L-glutamine and sodium pyruvate purchased from Corning (Corning, NY), and 10% fetal bovine serum (FBS) purchased from HyClone (Logan, UT). Cells were grown in 75cm^2 flasks at 37°C and 5% CO_2 until 80-90% confluent and then resuspended by incubation with 2ml of 1mM EDTA in phosphate-buffered saline (PBS). Growth medium was then added, and mechanical dissociation was performed. Cells were passaged weekly at a sub-cultivation ratio of 1:10.

Stably transfected cell lines were obtained by transfecting HEK293 cells with wild-type or mutant GFP-hCB1 plasmids in a 24-well plate using Lipofectamine 2000, as described by the manufacturer (Invitrogen, Carlsbad, CA). Transfected cells were then resuspended and transferred to 100mm tissue culture dishes. On the next day cells were incubated in selection medium, containing growth medium and 800µg/ml G418 (Enzo Life Sciences, Farmingdale, NY). Cells were maintained in selection medium for 2 weeks before single colonies were selected for expansion. GFP-hCB1 expression was confirmed by analysis of GFP fluorescence. Briefly, cells were grown on glass coverslips and fixed

in 4% Paraformaldehyde for 20min at room temperature. Coverslips were mounted on microscope slides with Fluoromount-G mounting medium (Southern Biotech, Birmingham, AL) and imaged in an upright epi-fluorescence microscope (Nikon, Tokyo, Japan) at 20x magnification.

In-cell western: Cells were grown to 90% confluence in 96-well plates and serum-starved with DMEM overnight before the assay. Pertussis toxin (Sigma, St. Louis, MO) 200 ng/ml treatment was administered overnight in DMEM while cells were serum-starved. Cells were then incubated with room temperature HBSS (Corning) for 20min before treatment with CB1 agonist 2-arachidonoylglycerol (2-AG) obtained from NIDA Drug Supply in 0.1% dimethyl sulfoxide (Sigma) in DMEM. Cells were then fixed with 4% Paraformaldehyde for 15min on ice and 45min at room temperature, permeabilized with 100% methanol at -20°C for 20min and incubated with LI-COR blocking buffer (LI-COR; Lincoln, NE) for one hour and 30min with gentle shaking. Primary antibodies rabbit monoclonal anti-phospho-ERK1/2 (1:100; Cell Signaling Technology, Danvers, MA) and mouse monoclonal anti-GFP tag clone GF28R (1:500; ThermoFisher) were applied overnight in a cold room, and then secondary antibodies goat anti-rabbit IgG 800CW (1:500; LI-COR) and goat anti-mouse IgG 680RD (1:500; LI-COR) were applied for 1h at room temperature. The plate was dried and then scanned using a LI-COR Odyssey IR Imager set at 169 µM resolution, 3.4 focus offset, and 6 to 7 intensities. Data were analyzed using Excel (Microsoft Corp., Redmond, WA) and Prism 4.0 (GraphPad Software, San Diego, CA) software. pERK signal normalized to the CB1 receptor

expression (GFP signal) at each time point and calculated as fold change with respect to the pERK normalized signal from vehicle treated WT expressing cells.

Results

Different reports have shown that the CB1 receptor activates the extracellular signal-regulated kinases (ERK1/2) via both G-protein and β-arrestin dependent pathways. [27, 53, 71-74] Treatment of the CB1 receptor by the endogenous ligand, 2-AG, resulted in an early PTX-sensitive phosphorylated ERK1/2 (pERK1/2) signal, followed by PTX-insensitive pERK1/2 signal that was diminished using small interfering RNA vector against β-arrestin-1.[27, 53, 72, 73]

In the current study, the three mutants were stably transfected into HEK293 cells and expression was evaluated by immunofluorescence technique, (see Fig. 5). CB1 receptor endogenous ligand, 2-AG, has been used to evaluate the signaling paradigm of mutant CB1 receptors due to its ability to activate both signaling pathways. In-cell western immunolabelling of the pERK was used to measure 2-AG-induced pERK signal in HEK293 cells stably transfected with GFP-tagged WT and mutant CB1 receptors, with and without pretreatment with PTX, and at different time points. GFP protein was immunolabelled and its signal was used to normalize the pERK signal for the CB1 receptor expression. At the WT receptor, treatment with 2-AG resulted in pERK signal that peaks at 15 minutes. Pre-treatment with PTX abolishes the 5 minutes pERK signal while significantly reduces the 10, and 15 minutes signal (see Fig. 6,7,8). In agreement with previous reports, results from the WT indicate that the 2-AG activates the G-protein

signaling pathway through the CB1 receptor resulting in an early (5 minutes) pERK signal that peaks at 10 minutes, subsequent phosphorylation of the CB1 receptor by GRKs calls for the β-arrestins and induces β-arrestin dependent pERK signal detected at 10 minutes and extends beyond 30 minutes, while peaking at 15 minutes.[27, 53]

At the molecular level, it could be inferred that the binding of 2-AG to the WT receptor induces a sequence of conformational changes in which the receptor adopts the canonical G-protein-coupling active state conformation in which the ionic lock is broken between TMH6 and TMH3, followed by β-arrestin-coupling active state conformation in which the ionic lock reforms while the IC end of TMH7 hinges out allowing interaction with the β-arrestin (see Discussion). Such conformational changes are protein-ligand dependent and are not affected by the pretreatment with PTX. Thus, the β-arrestin dependent pERK signal commences later than the G-protein dependent pERK signal at the WT type receptor treated with 2-AG.

I2.43A and I2.43T mutants exhibit β-arrestin biased signaling paradigm: In class A GPCRs, the amino acid residue at 2.43 is a highly conserved amino acid residue that is part of the hydrophobic layer at the IC domain of the receptor, and being packed against Y7.53 in the receptor's inactive state. The I2.43A and I2.43T mutations were expected to bias the signaling of the CB1 receptor towards the β-arrestin pathway. This is because those mutations would disturb the hydrophobic layer in the TMH1/2/7 region, and would enhance the trans rotameric state of Y7.53 by either reducing the steric clash at that region (I2.43A mutant), or via forming H-bond interaction with Y7.53 (I2.43T mutant) (see Discussion).

Dose response curves at the WT and I2.43A and I2.43T mutant receptors were determined 15 minutes after treatment with 2-AG. Emax for the mutants were comparable to the WT receptor, this is due to the normalization to the CB1 receptor expression. However, pEC50 value from the I2.43T mutant receptor has shown statistically significant difference from the WT receptor, with pEC50 values for the WT and the I2.43T mutant receptors being 4.73 ± 0.09 and 5.16 ± 0.06 respectively. The pERK signal for the I2.43A and I2.43T mutants pretreated with PTX was not statistically significant from the mutant receptors without PTX treatment at all time points, suggesting that both mutants signal through β-arrestin only.

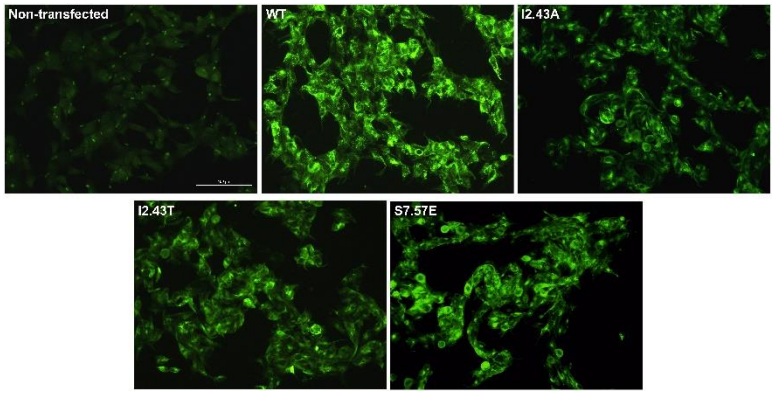

Figure 5. Stable Expression of WT and Mutant CB1 Receptors in HEK293 Cells. Cells non-transfected, or stably transfected with WT and mutant GFP-tagged hCB1 receptor. Cells were imaged under epi-flourescence microscope.

For the I2.43T mutant, it can be noticed that unlike the WT receptor, the β-arrestin dependent pERK signal through this mutant is detected at 5 minutes, this indicates that the receptor adopts the β-arrestin-coupling active state conformation directly after 2-AG binding. However, 5 minutes pERK signal from the I2.43A mutant was not statistically

different form the 0-time point, and the mutant results in a statistically significant 10 minutes signal when compared to the WT receptor for cells pretreated with PTX.

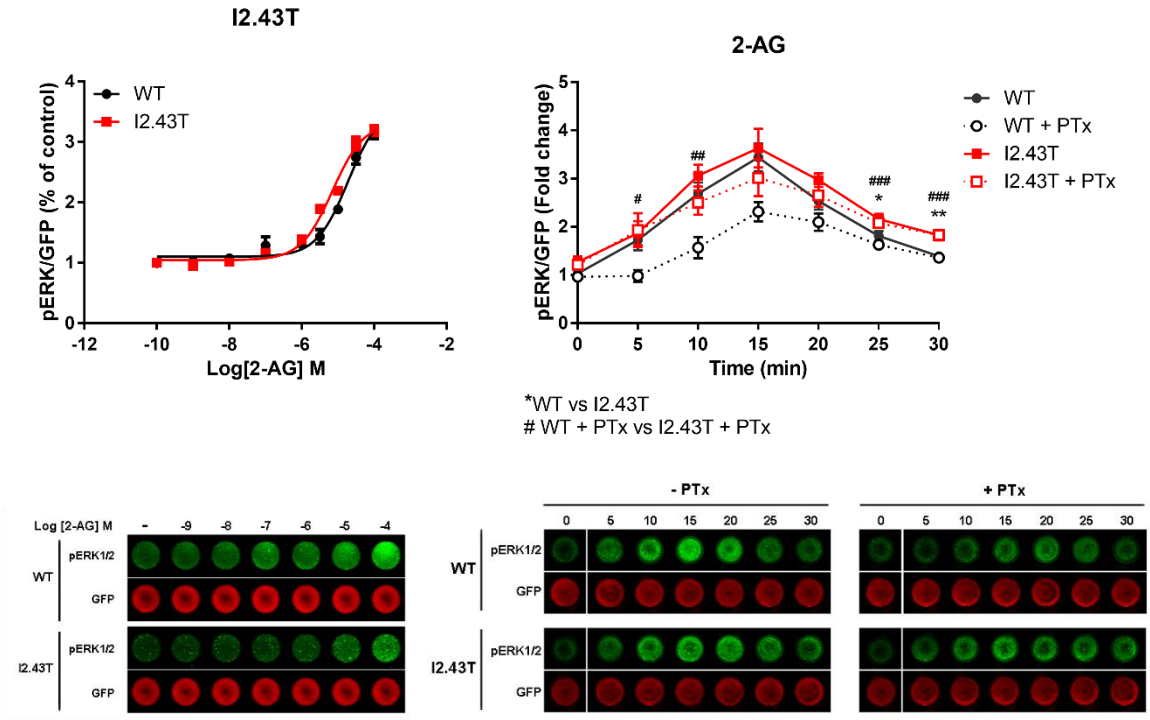

Figure 6. I2.43T Mutant Exhibits β-Arrestin Biased Signaling Paradigm. A) dose response curves 15minutes following treatment by 2-AG for the WT and I2.43T mutant CB1 receptor with pEC50 values of 4.73 ± 0.15 and 5.16 ± 0.09 respectively (pEC50 values determined by non-linear regression using least squares fitting analysis, n=3). B) HEK293 cells expressing GFP-hCB1 treated with 7μM 2-AG. Statistical significance of the differences was assessed using two-way analysis of variance and test., */#, *p* _ 0.03; **/##, *p* _ 0.002; ***/###, *p* _ 0.0002. C) In-cell western blots for HEK293 cells stably transfected with GFP-tagged WT and I2.43T mutant CB1 receptor before and after treatment with 2-AG. D) In-cell western blots for HEK293 cells stably transfected with GFP-tagged WT and I2.43T mutant CB1 receptor and treated with 7μM 2-AG with and without pre-treatment with 200 ng/ml PTX. Each data point represents the mean ± S.E (error bars) of at least three independent experiments.

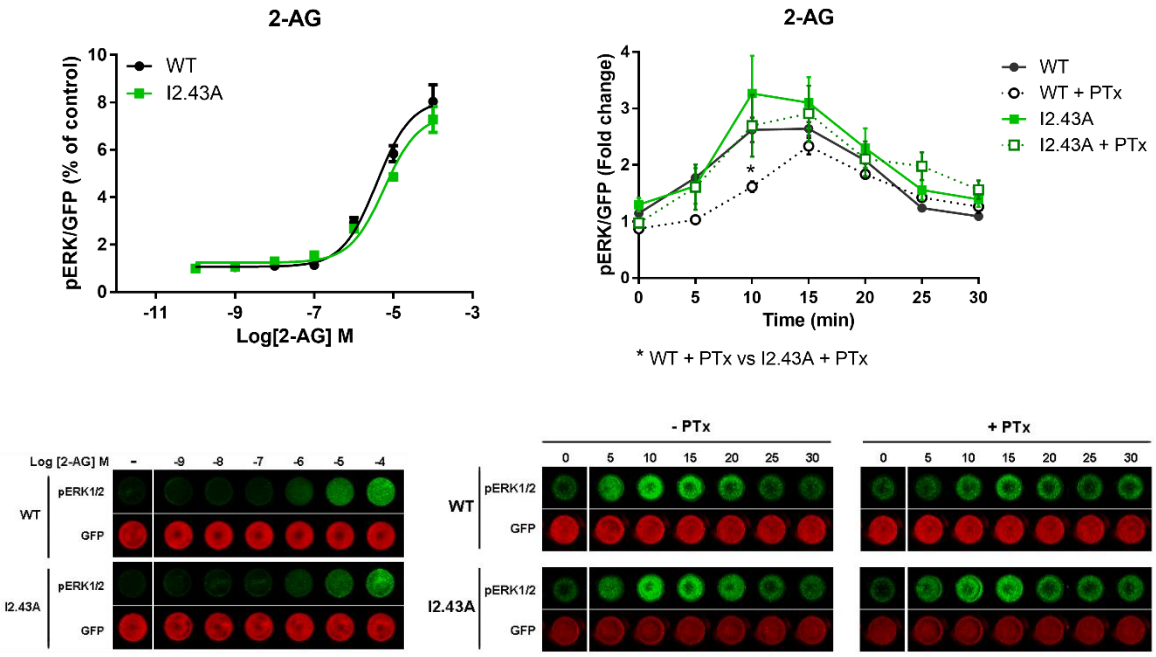

Figure 7. I2.43A Mutant Exhibits β-Arrestin Biased Signaling Paradigm. A) dose response curves 15minutes following treatment by 2-AG for the WT and I2.43A mutant CB1 receptor with pEC50 values of 5.42 ± 0.10 and 5.23 ± 0.09 respectively (pEC50 values determined by non-linear regression using least squares fitting analysis, n=3). B) HEK293 cells expressing GFP-hCB1 treated with 6μM 2-AG. Statistical significance of the differences was assessed using two-way analysis of variance and Bonferroni's test., *, *p* _ 0.03. C) In-cell western blots for HEK293 cells stably transfected with GFP-tagged WT and I2.43A mutant CB1 receptor before and after treatment with 2-AG. D) In-cell western blots for HEK293 cells stably transfected with GFP-tagged WT and I2.43A mutant CB1 receptor and treated with 6μM 2-AG with and without pre-treatment with 200 ng/ml PTX. Each data point represents the mean ± S.E (error bars) of at least three independent experiments.

The S7.57E mutant exhibits β-arrestin biased signaling paradigm: The amino acid residue at 7.57 resides at the elbow between TMH7 and H8. This residue does not show high conservation among class A GPCRs, but the S7.57E mutant was aimed to stabilize the highly conserved Y7.53 in trans conformation (see Discussion).

Dose response curves at the WT and S7.57E mutant receptors were determined 15 minutes after treatment with 2-AG. pEC50 value for 2-AG at the mutant receptor was comparable to the WT receptor, with pEC50 values 5.68 ± 0.25, and 5.30 ± 0.13 respectively. The pERK signal for the S7.57E mutant pretreated with PTX was not statistically significant from the mutant receptors without PTX treatment at all time points, suggesting that the generated pERK signal from the mutant is through β-arrestin only. At 10 minutes, the mutant shows a statistically lower pERK signal compared to the WT receptor, and no statistical difference was observed between the WT and the mutant receptor pretreated with PTX. The results suggest that the mutant receptor is biased towards the β-arrestin signaling pathway, yet it does not show robust 10 minutes or 15 minutes signal as for the I2.43T mutant. A possible explanation of the reduced efficacy of the mutant would be the presence of a lysine residue at the IC1 loop that might be interacting with this glutamate residue and holding TMH7/H8 elbow region in position, or that the glutamate residue increases the bulk at the opening at TMH7 resulting in steric clash with the arrestin upon binding.

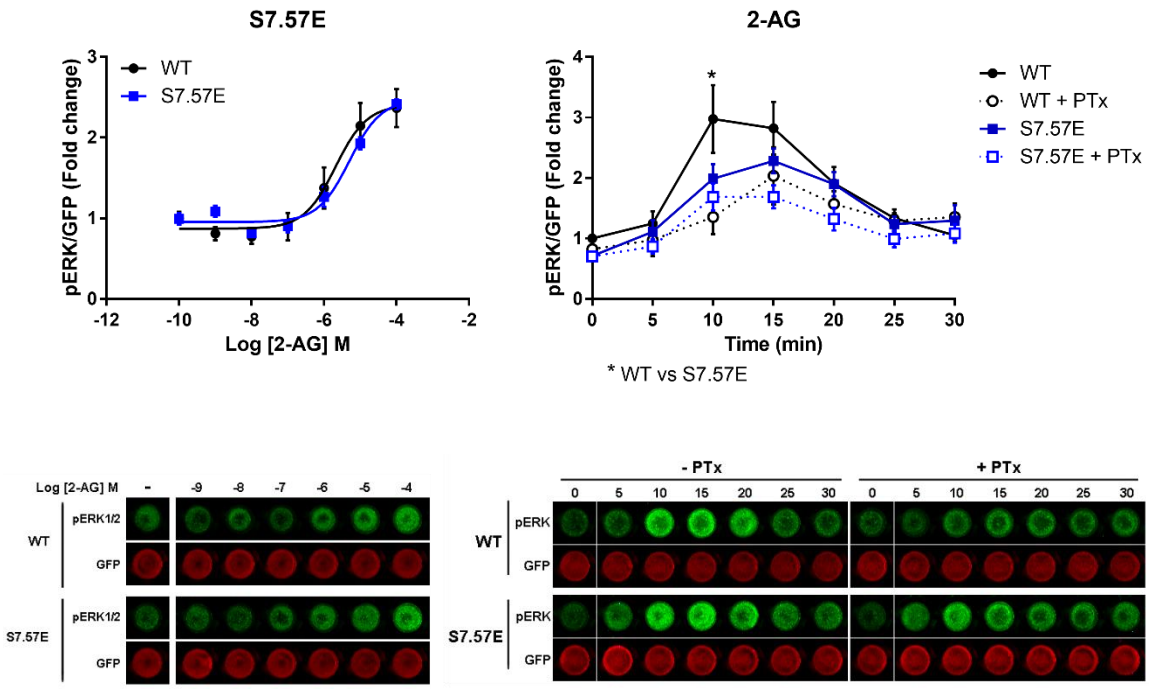

Figure 8. S7.57E Mutant Exhibits β-Arrestin Biased Signaling Paradigm. A) dose response curves 15minutes following treatment by 2-AG for the WT and S7.57E mutant CB1 receptor with pEC50 values of 5.68 ± 0.25 and 5.30 ± 0.13 respectively (pEC50 values determined by non-linear regression using least squares fitting analysis, n=4). B) HEK293 cells expressing GFP-hCB1 treated with 7μM 2-AG. Statistical significance of the differences was assessed using two-way analysis of variance and Bonferroni's test., */#, *p* _ 0.03. C) In-cell western blots for HEK293 cells stably transfected with GFP-tagged WT and S7.57E mutant CB1 receptor before and after treatment with 2-AG. D) In-cell western blots for HEK293 cells stably transfected with GFP-tagged WT and S7.57E mutant CB1 receptor and treated with 7μM 2-AG with and without pre-treatment with 200 ng/ml PTX. Each data point represents the mean ± S.E (error bars) of at least three independent experiments.

Discussion

Initial reports of G-protein independent, β-arrestin dependent pERK signal where reported on the β2-adrenergic receptor (β2AR). Treatment of HEK293 cells expressing a mutant β2-adrenergic receptor ($\beta2AR^{TYY}$) with Isoproterenol (non-biased agonist), resulted in a pERK signal that was insensitive to H-89 (PKA inhibitor), while significantly dropped by knockdown of either β-arestin 1 or 2 using small interfering RNA, this β-arrestin dependent pERK signal was late (peak 5-10 min) compared to the G-protein dependent pERK signal (peak at 2-3 min).[69] Later, carvedilol, which have been known as β2AR antagonist, was reported to activate the ERK1/2 in a β -arrestin dependent pathway, thus acting as a β -arrestin biased ligand.[75]

Experimental evidence of biased signaling through the CB1 receptor has been reported using the allosteric modulator, ORG-27569, which has been shown to act as a biased β-arestin-1 agonist.[18, 76, 77] In knock-out studies, deletion of β-arrestin 1 and 2 in mice resulted in different efficacies of CB1 receptor agonists in anti-nociception and lowering body temperature suggestive of agonist-specific regulation of β-arrestin 1 / 2 [59, 78]. In addition, a recent *in vitro* study in neuronal models of Huntington Disease (HD) shows that enhancing the $G\alpha_{i/o}$ and $G\beta/\gamma$ biased signaling maybe therapeutically beneficial in HD by normalizing CB1 receptor levels and improving cell viability while agonists that displayed β-arrestin-1 bias resulted in reduced CB1 receptor levels and might be detrimental to CB1 signaling, particularly in HD where CB1 levels are already reduced [72].

Rational behind mutations: an overview of reported conformational changes upon class A GPCRs activation: Multiple efforts in the field of GPCRs have been directed to understand structural changes in the protein upon ligand binding. As a result, the two-state model of receptor activation has been challenged, by showing that different ligands can induce distinct patterns of conformational changes in the receptor. At the CB1 receptor; an *in situ* reconstitution technique to directly measure G protein activation,[79] and a Plasmon Wave-guide Resonance (PWR) spectroscopy study,[80] demonstrated that different agonists induce different conformational changes in CB1 resulting in preferential activation of different G-proteins. In addition, a quantitative mass-spectrometry analysis that measures site-specific conformational changes in the β2-adrenergic receptor using nine different ligands, has shown distinct patterns of conformational changes produced during receptor activation.[81]

However, class A GPCRs still share a common activation mechanism. Different studies using mutations and spectroscopic techniques such as NMR, EPR, MS, and X-ray crystallography, have shown a unique pattern of conformational changes that accompany receptor activation via the G-protein signaling pathway that is distinct from those accompanying the β-arrestin signaling pathway (see Fig. 9).

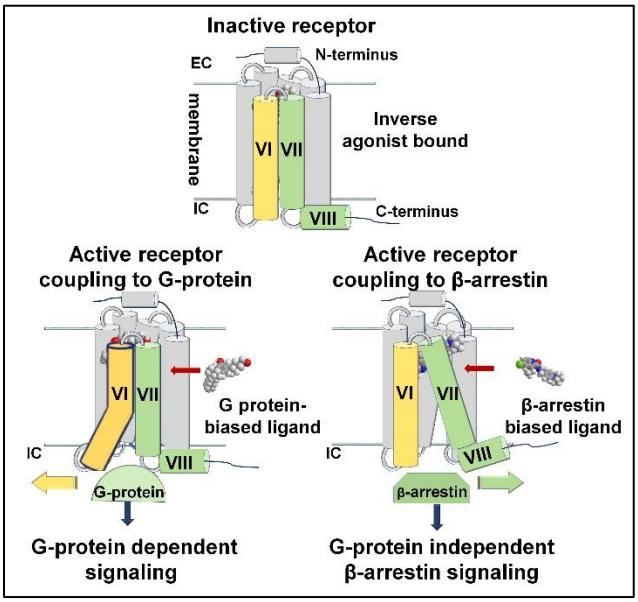

Figure 9. Cartoon Representation of Conformational Changes at the IC Domain of Class A GPCRs. Inactive state (Up): the bundle is closed at the IC domain of the receptor. G-protein-coupling active state conformation (Right): activation includes a movement of the IC domain of TMH6 away from the receptor resulting in an opening in the TMH3/5/6 region. β-arrestin-coupling active state conformation (Left): activation includes an opening between TMH7/1/2 region.

G-protein coupling active state conformational changes: Available active state crystal structures and biophysical studies revealed a set of concerted conformational changes that result in an opening at the intracellular domain of the receptor between TMH 3, 5, and 6 allowing the coupling to the G-protein.[82] Those changes involve: **I)** A counterclockwise rotation (EC view) of the intracellular domain of TMH6, and flexing in TMH6 CWxP hinge region resulting in outward movement of IC end of TMH6 away from TMH3, this will break an ionic interaction between R3.50 and D/E6.30 at the IC ends of TMH3/6.[83-85] Flexing in the CWxP motif, is produced by ligand binding that alters the dihedrals of "toggle switch" residues. For CB1, these are F3.36 and W6.48 (part

of the CWxP motif). The change produced is a shift in W6.48's χ1 dihedral from g+ to trans upon activation.[86, 87] **II)** Packing of TMH7 against TMH3: conserved Y7.53 changes its χ2 dihedral by -60°and interacts with R3.50 in its active rotameric state and with Y5.58 leading to a conserved orientation of R3.50, Y7.53, and Y5.58 in the active state receptors compared to their inactive states.[82] **III)** An amino acid residue at TMH3 (at 3.46) breaks a contact with TMH6 (at 6.37), and forms a contact with Y7.53.[88] **IV)** Rotational movement of TMH3 towards TMH2 that allows direct hydrogen-bond interaction between S3.39 and D2.50 compared to the inactive state in which those residues are bridged by either a water molecule or a sodium ion.[89] **V)** A break in the hydrophobic layer at the intracellular domain of the receptor.[90] (see Fig. 10,11)

Within the previously mentioned conformational changes, it can be noticed that the packing of TMH7 between TMH6 and TMH3 and the triad interaction of Y7.53/R3.50/Y5.58 stabilize TMH6 in its active state's outward conformation. Most importantly, the rotation of TMH3 towards TMH2 seems to be the most crucial in the activation process. During this rotation, a conserved non-polar amino acid residue (L3.43) is translated towards TMH2, which relieves a steric hindrance that would occur between Y7.53 and L3.43 upon activation. In consensus with that, mutating L3.43 to Alanine at the CB1 receptor resulted in highly constitutively active receptor.[91] This can be explained by the absence of a bulky residue, thus allowing the movement of Y7.53 towards TMH3 without steric hindrance (see Table 2, and Fig. 12).

It should be mentioned that the active state crystal structure of the CB1 receptor concur with previously mentioned conformational changes upon G-protein coupling.

Interestingly, Site-directed florescence labeling (SDFL) study using a minimal cysteine receptor with a truncated N terminus (Δ87) and truncated C terminus (Δ417) has shown that CP-55940-induced changes in Bimane fluorescence occurs faster in the Hx8 attached probe (at L7.60) compared to that attached to TMH6 (at A6.34), this may suggest that the inward movement of TMH7/Hx8 precedes the outward movement of TMH6 in G-protein signaling.[92]

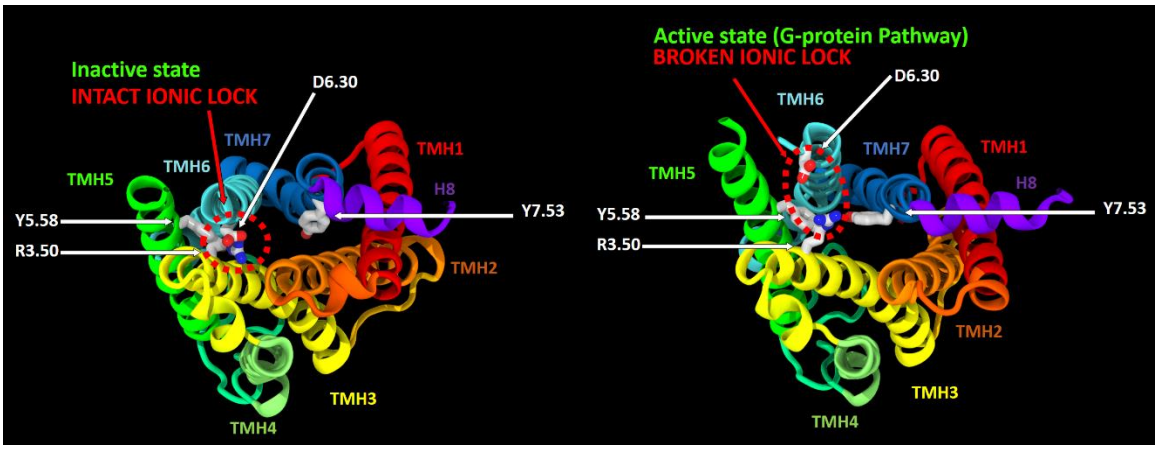

Figure 10. Conserved Conformational Changes at the IC Domain of Class A GPCRs Upon Receptor Activation (G-Protein Coupling State). An IC view showing transmembrane helices rearrangements, and conformational changes in conserved residues; Y7.53, Y 5.58, and R3.50 (shown as sticks) in crystal structures of the CB1 receptor (PDB IDs: 5U09[16], 5XRA[86]): comparing the R*G state (Purple) vs the R state (yellow green); activation includes an inward movement of IC domain of TMH7, allowing Y7.53 to reposition between TMH3 and TMH6 stabilizing the outward movement of TMH6 and interacting with R3.50 and Y5.58. This is accompanied by rotamer change of the χ2 and χ3 dihedrals to trans, while the χ2 dihedral of Y7.53 is shifted by -60 degrees. Black arrows show the direction of TMH6/7 upon activation, while red arrows indicate the conformational changes in R3.50 and Y7.53.

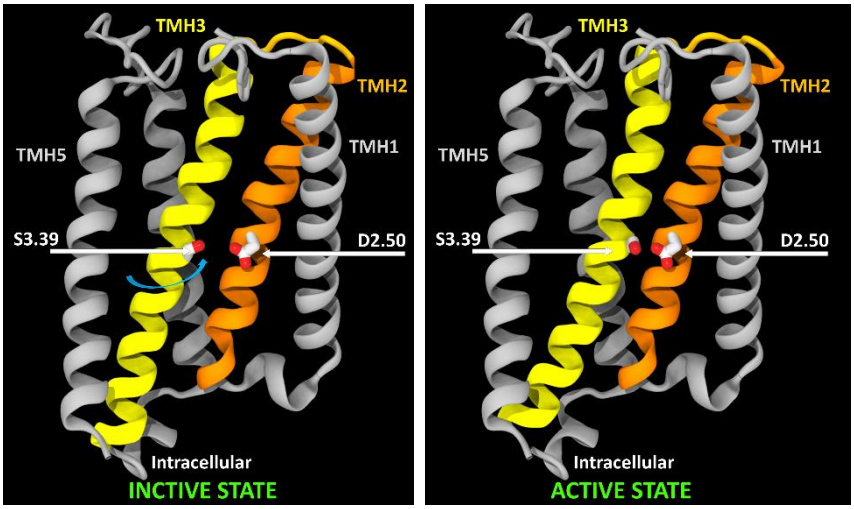

Figure 11. G-protein Coupling Active State of Class A GPCRs Exhibits Rotation of TMH3 Towards TMH2. A side view from the crystal structures of CB1 receptor in its inactive (Left) and active (Right) states. (TMH6 and TMH7 were removed for clarification). TMH2 in orange and TMH3 in yellow. The distance between the Cα atoms of D2.50 and S3.39 is resduced by 1.8 Å and the rotation allows direct H-bond interaction between both residues' side chains.

Table 2. Shorter Distances Between TMH3 and TMH2 Upon Receptor Activation. A conserved axial rotation of TMH3 towards TMH 2 in class A GPCRs results in a decrease in the Cα distance between D2.50/S3.39 and between L2.46/L3.43. Measures were obtained from crystal structures of the CB1 receptor (PDB ID: 5U09[16], 5XRA[86]), Adenosine receptor $A_{2A}R$ (PDB ID: 4EIY[93], 5G53[94]), the β_2AR (PDB ID: 2RH1[95], 3SN6[85]), μ-opioid receptor (PDB ID: 5G53[96], 4DKL[97]), and the muscarinic receptor (PDB ID: 3UON[98], 4MQS[99]).

Receptor	D2.50-S3.39	L2.46-L3.43
CB1	1.8	1.3
$A_{2A}R$	2.3	1.6
β_2AR	0.8	0.5
μOR	1.9	1.1
M2	1.5	1.3

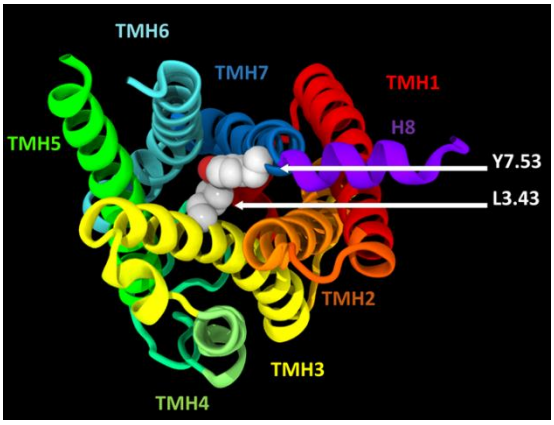

Figure 12. The Role of L3.43 in Stabilizing Inactive State Conformation. Intracellular view of the inactive state crystal structure of the CB1 receptor (PDB ID: 5U09). Conformational change in TMH7 and Y7.53 that lead to G-protein coupling requires the rotation of TMH3 towards TMH2. Without this rotation, L3.43 would sterically hinder TMH7 transition.

β-arrestin coupling active state conformational changes: Few features are yet known that describe the conformational changes associated with the G-protein independent β-arrestin coupling to the receptor. Reported changes involve a movement of the IC domain at TMH7/Hx8 elbow region while preserving the TMH3/6 ionic lock.

At the CB1 receptor, Fay and Farrens demonstrated differences in the CB1 structure stabilized by ORG-27569 (biased β-arrestin-1 ligand) from that stabilized by an orthosteric agonist that activates the G-protein pathway; specifically, TMH6 movement was blocked while TMH7/Hx8 movement was enhanced upon ORG- 27569 binding.[92] Other studies on the arginine-vasopressin receptor and the β2AR have shown a different movement of TMH7 in receptors treated with β-arrestin biased ligands compared to a movement of TMH6 in receptors treated with G-protein activating ligands.[100, 101]

MD simulations at the Reggio's Lab were used to investigate the binding of ORG-27569 to the CB1 receptor (Unpublished). In this simulation, the IC domain of TMH7 and H8 move away from TMH6 resulting in an opening at the IC domain of the receptor, and the Y7.53 was noticed to form stable trans χ1 dihedral conformation throughout the simulation (see Fig. 13). Interestingly, a similar trans χ1 dihedral conformation of Y7.53 is observed in a recently published crystal structure of the 5-HT_{2B} receptor bound to the β-arrestin biased agonist LSD.[102] This change in Y7.53 conformation might suggest a role of Y7.53 in the interaction with the β-arrestin.

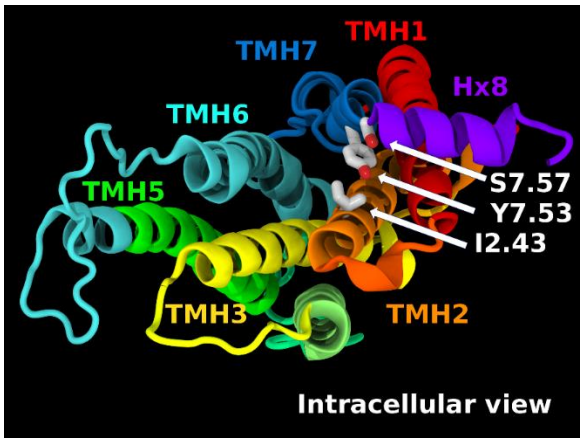

Figure 13. Conformation of Y7.53 in β-Arrestin Active State Conformation at the CB1 Receptor. An intracellular view of the CB1 receptor from a MD simulation with ORG-27569. The figure shows that Y7.53 adopts a trans χ1 dihedral. The I2.43 and the S7.57 are also shown.

Role of water-mediated hydrogen bond network in regulating GPCR function:

The availability of high resolution crystal structures revealed a binding site for sodium ion inside class A GPCRs, in which the sodium ion is coordinated mainly with the highly conserved residue; D2.50. This ion has long been known to act as an allosteric modulator

of many GPCRs. These structures reveal also a water-mediated hydrogen bond network inside the sodium binding pocket, these water molecules coordinate with the sodium ion and interconnect other conserved polar amino acid residues surrounding the pocket; N1.50, S3.39, W6.48, N7.45, N/D7.49, Y7.53, N/S3.35, and S7.46 [70, 93, 103-105]. While the inactive state crystal structure of the CB1 does not show this sodium ion, two different studies on the CB1 receptor suggested a role of the sodium in the stabilization of the inactive state of the receptor.[92, 106]

Different studies have pointed out the role of water in the activation of the GPCRs. [107, 108] However, a set of non-polar conserved amino acids (at positions 1.53, 1.57, 2.43, 2.46, 3.43, 3.46, 6.37, 6.40) form a hydrophobic layer that act as a boundary between the hydrogen bond network and the IC domain of the receptor, preventing the flow of water to the IC domain, and preserving the inactive state of the receptor (see Fig. 4, Table 3). The role of those residues and the conserved Y7.53 in controlling the flow of water from the sodium binding pocket to the IC domain was examined via MD simulations[109-112].

According to previous discussion, it has been hypothesized that mutations that would either break the hydrophobic layer between TMH3/5/6, or that enhance the rotation of TMH3 towards TMH2, or that facilitate the packing of Y7.53 against TMH3, should bias the signal towards G-protein pathway. On the other hand, mutations that break the hydrophobic layer between TMH1/2/7, or those that enhance a trans rotameric state of the Y7.53, would bias the signal towards β-arrestin signaling pathway. Results from I2.43A/T and S7.57E mutations are in accordance with the proposed hypothesis and

were successful in biasing the signaling of the CB1 receptor towards the β-arrestin signaling pathway.

Conclusions

In the current study, the I2.43T mutant could generate an early pERK signal that is similar in the onset time to the G-protein dependent pERK signal in the WT receptor treated with 2AG. A similar result has been reported for ORG-27569 acting on the WT receptor. These findings show that the receptor can adopt a β-arrestin active state conformation directly without prior G-protein active state conformation. The change in the conformation of the receptor is dependent on the ligand-receptor complex and needs to be evaluated for each complex separately to determine the onset of the β-arrestin dependent pERK signal.

Orthosteric CB1 receptor agonists that act as β-arrestin biased ligands are not available yet. The availability of β-arrestin biased mutants would provide a tool to investigate downstream signaling pathways via the β-arrestin and to set structure-based ligand designing rules to design β-arrestin biased ligands. While the resultant functional selectivity of the three mutants agreed with previous observations regarding G-protein vs β-arrestin coupling active state conformations, further studies using MD simulations would reveal detailed mechanism of the effect of these mutations on the receptor's conformation, specifically their impact on the rotameric state of Y7.53.

Table 3. Conservation in Amino Acid Residues Aligning the Sodium Binding Pocket in Class A GPCRs. Table shows consensus residue and other possible amino acids at each position. Table generated from GPCRdb website for class A GPCRs from human species.[113, 114]

TMH	BW	Consensus (%)	Other Amino Acids (%)				Residue in CB1
1	**1.50**	**N (98)**	S (1)	-	-	-	**N**
	1.53	**V (65)**	A (14)	L (7)	T (5)	S/I/F/M (8)	**V**
	1.57	**L (24)**	I (23)	V (20)	F (17)	T/A/Y/S/R/M/N (14)	**I**
2	**2.43**	**L (36)**	I (35)	V (12)	M (8)	F/A/S/T/Y (8)	**I**
	2.46	**L (90)**	M (4)	I (3)	T (1)	V (1)	**L**
	2.50	**D (92)**	N (3)	E/G/H/T (4)	-	-	**D**
3	**3.39**	**S (72)**	G (11)	T (8)	A (3)	C/E/P/Q (1)	**S**
	3.43	**L (73)**	I (10)	V (7)	M (5)	T/G/F/A (4)	**L**
	3.46	**I (56)**	L (16)	M (13)	V (10)	T/A/F (3)	**T**
6	**6.38**	**L (22)**	A (14)	V (13)	F (12)	C/G/I/M/R/S/T/Y (37)	**V**
	6.40	**V (37)**	I (28)	L (15)	M (5)	A/F/H/N/S/T/Y (16)	**L**
	6.48	**W (68)**	F (16)	Y (3)	G (3)	A/M/Q/S/T (7)	**W**
7	**7.45**	**N (67)**	S (11)	H (9)	A (3)	C/I/K/P/Q/R (8)	**N**
	7.46	**S (64)**	C (13)	A (8)	T (6)	F/G/L/N/P/Q/V (8)	**S**
	7.49	**N (72)**	D (20)	H/K/L/S/T (7)	-	-	**N**
	7.53	**Y (89)**	F (4)	L (3)	C (1)	-	**Y**

CHAPTER III

TOWARDS THE REMODELLING OF THE N-TERMINAL REGION OF THE CANNABINOID RECEPTOR (CB1): DOCKING STUDIES AND MOLECULAR DYNAMICS SIMULATIONS

Introduction

Recently published crystal structures of the CB1 receptor show differences between the active (PDB ID: 5XR8, 5XRA[86]) and inactive states (PDB ID: 5TGZ[15], 5U09[16]); specifically, in the N-terminus and at the extracellular domain of the receptor that identifies the ligand binding pocket. In the inactive state structures, the membrane proximal region (MPR) of the N-terminus invades the receptor binding pocket steering an important interaction site (K3.28) away from binding pocket.[115] This residue has been reported as a site of interaction with classical and non-classical cannabinoids and the biarylpyrazole derivatives,[116-118] as well as being an essential interaction site with SR-141716A for its inverse agonist property at the CB1 receptor.[119-122] Resolved structures also lack an internal disulfide bridge at the N-terminus that allosterically modulates the binding affinity of ligands to the receptor.[123]

The CB1 receptor is unique in having a relatively long (114 amino-acid residues) N-terminus compared to other class A GPCRs. Analysis of the amino acid sequence of the MPR of the amino terminus reveals a high conservation in that region (see Fig. 14).

Kendall's lab reported no effect on prolylglycine insertion in the N-terminus (at A73, L86, and E100) of hCB1 receptor expressed in HEK 293T cells on agonist (CP-55940) and antagonist (SR-141716A) binding.[124] In different studies, CP-55940 binding to truncated receptor at the N-terminal region (Δ64, Δ80, Δ89, Δ103 shCB1) was comparable to the WT receptor,[123, 125] while the binding affinity of SR-141716A to the Δ103 shCB1 truncation mutant was higher compared to the WT with retained ability to inhibit basal signaling of the truncated mutant.[123] On the other hand, reduction of the disulfide bridge at the N-terminus C98/C107 reduces CP-55940 efficacy in GTPγS binding assay.[123]

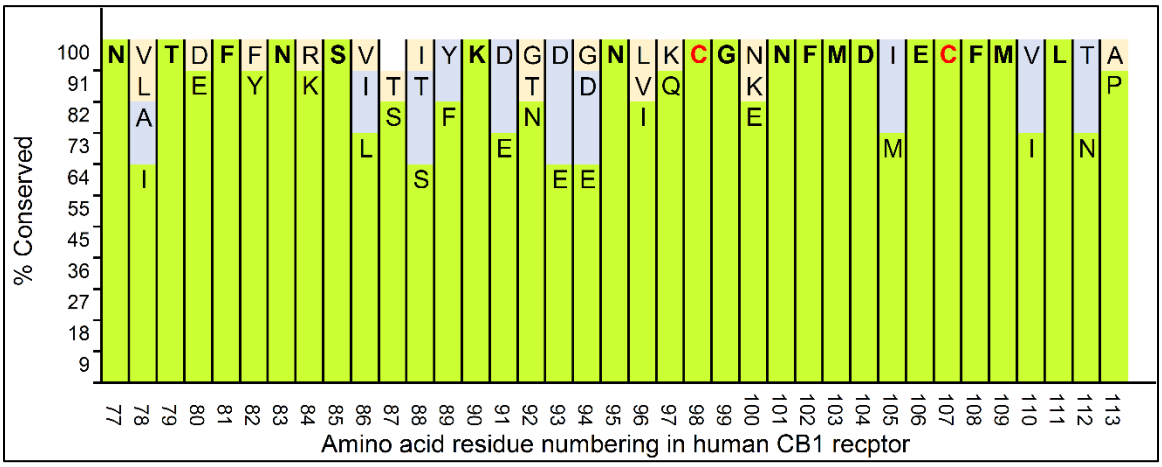

Figure 14. Conserved Amino Acid Residues in the MPR of the N-Terminus in CB1 Receptor. The most conserved residues are colored in light green. Those with 100% conservation among the species analyzed are bolded. The two cysteine residues that form a disulfide bridge are colored in red. Eleven species were used for this graph; Human (Homo sapiens), Chimpanzee (Pan troglodytes), Rhesus macaque (Macaca mulatta), Mouse (Mus musculus), Rat (Rattus norvegicus), Cat (Felis catus), Bovine (Bos Taurus), Zebra finch (Taeniopygia guttate), African clawed frog (Xenopus laevis), Edible frog (Pelophylax esculentus), Roughskin newt (Taricha granulosa). Data obtained from UniProt.org.[126]

The compound [5-(4-chlorophenyl)-N-[(1R,2R)-2-hydroxycyclohexyl]-6-(2-methoxyethoxy)-3-pyridinecarboxamide] **(14h)**, has been described previously as a peripherally selective, high affinity CB1 receptor antagonist[127]. However, this compound has been shown to have higher affinity for the hCB1 receptor compared to rodents CB1 receptor[128]. Mutational, and modelling studies from the Kunos lab identified an N-terminal residue (M106 in rodent CB1 compared to I105 in human CB1) as the determinant of the species differential affinity of this compound at the CB1 receptor, a mutation that did not affect SR-141716A binding to the receptor[128] (see Fig. 14).

We sought to dock **14h** inside the inactive state structure of the CB1 receptor in the effort to model the MPR of the N-terminus. The modeling of the N-terminus will be guided by **14h's** dock, and with the I105M mutation data that affects **14h's** affinity. In this work, we report a molecular dynamics (MD) simulation of **14h** in a fully hydrated 1-palmitoyl-2-oleoyl-phosphatidylcholine (POPC) bilayer, as well as a docking study of **14h** in an inactive state CB1 receptor model based on the CB1 crystal structure (PDB ID: 5U09[16]). Finally, stability of the CB1 receptor with a modeled N-terminus and in complex with **14h** was monitored in a MD simulation.

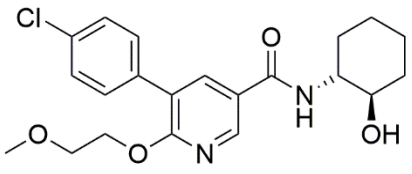

Figure 15. Chemical Structure of 14h.

Methods

Quantum mechanical potential energy scan (QM-PES) for 14h dihedrals:

Crystal structure for **14h** was reported previously,[128] and coordinates were downloaded from Cambridge Crystallographic Data Centre (www.ccdc.cam.ac.uk). Using the crystal structure geometry, energy scans for all dihedrals was performed for **14h** using *ab initio* Hartree-Fock calculations in vacuum at the 6-31G* level as encoded in the Spartan 08 molecular modeling program (Wavefunction, Inc., Irvine, CA). With this, a 360° rotation on each rotatable bond is applied in 10° increments. After rotating each dihedral, single point energy was calculated for each generated conformer. Geometries with local minima were then used as initial geometries for the rotation of subsequent dihedrals. In case of adjacent dihedrals with harmonized effect on the energy of generated conformers, both dihedrals were rotated, and energy surface was plotted to determine the local energy minima of **14h** at those dihedrals.

Preparation of the CB1 receptor bundle for docking and MD simulations:

CB1 crystal structure coordinates were downloaded from the Protein Data Bank (PDB ID: 5U09[16]). The bundle was prepared for MD simulation using Maestro (Schrödinger Release 2016-4: Maestro, Schrödinger, LLC, New York, NY, 2016), missing IC-3 loop and C-termini were added (using Modeller [129, 130]) according to the following: fusion protein at the IC-3 loop was removed and the loop was built according to previous NMR study of this loop region in micelle, which reported three helical regions in the loop; two helical regions extend from TMH5 (L298 –R307), and TMH6 (Q334 – L345), and a third helical domain terminal to TMH5 (I309 – S316).[131] Crystallized ligand and lipids were

deleted, protein preparation wizard implemented in Maestro was used to add hydrogen atoms, connect disulfide bridge, assign bond orders, eliminate crystallographic water molecules, and cap free residues. Prime module in Maestro was used to add missing side chains.[132, 133] The thermostabilizing T210A mutation was mutated back to the WT, and the Glutamate residue at TMH1 (E1.49) which faces lipids was protonated according to pKa calculations and to a previous report.[18] Alpha helical domain of TMH8 was built up to G417 according to previous reports that show that a CB1 receptor with truncation at this point retain cell surface expression and signaling [50, 92, 134-136], and a Palmitoyl group was added to C415.[137] As part of the internal water-mediated hydrogen bond network described in the literature, high-resolution crystal structures revealed consistency in the location of certain water molecules.[70, 93, 103-105] These locations are a) at TMH6/7 interface making H-bond with backbone carbonyls of C6.47 and x7.38, b) at TMH6/7 interface making a H-bond with N7.45/N7.49 and the backbone carbonyl of x6.40, c) at TMH1/7 interface making a H-bond between backbone carbonyls of x7.47 and x1.45, d) in between W6.48 and N7.49. Water molecules at those locations were added to the structure except the one at TMH1/7 interface due to the presence of E1.49. In addition, a sodium ion was placed between D2.50 and S3.39.

Minimization of the bundle: an initial minimization of the hydrogens and water molecules inside the bundle was first done using OPLS3 force field (applying an 8.0 Å extended nonbonded cutoff, a 20.0 Å electrostatic cutoff, and a 4.0 Å hydrogen bond cutoff) in a distant-dependent dielectric constant environment.[15] Then the bundle was minimized in an implicit membrane using Prime which allows the minimization of the

whole bundle by treating the transmembrane region at a low dielectric constant corresponding to the hydrophobic region of the membrane, while the loops being treated at high dielectric constant corresponding to water.[132] With that, the bundle is first oriented in the membrane using OPM data base,[138] and then minimized in 3 iterations of 65 steps per iteration using OPLS3 force field and applying automatic minimization which uses Conjugate Gradient minimization at large RMSD gradients and switches to Truncated Newton method at low gradients.

Prime induced fit docking of 14h in the CB1 receptor: Results from conformational analysis of **14h** were rigidly docked in the CB1 receptor bundle using Prime-induced fit docking[139] and applying the OPLS3 force field for the treatment of the ligand and the receptor. Centroid of residues S1.39 (123), F2.64 (177), V3.32 (196), F268, W5.43 (279), T5.47 (283), W6.48 (356), Y7.53 (397) was used to define the grid box size and center. Receptor and ligand VDW were rescaled to 1.0 with a maximum number of poses being 20. Residues within 5.0 Å of ligand poses were refined allowing optimization of protein side chains. Calculations were carried in an implicit membrane as explained previously.

Modeling of the N-terminus: For the crystal structure, a disulfide bridge was added and the N-terminus was modeled from S88 to E100 using Modeller. Remodeling of the N-terminus was done using Prime Loop refinement module in Maestro which was used to predict a sample of conformations of the N-terminal region (S88 – P113). The location of I105 was restricted within 2Å of its original crystal structure coordinates to fit I105M mutation data.[133]

MD simulations: Isobaric-isothermic (NPT) simulations were performed using the GPU-enabled AMBER16 molecular dynamics package [Case et al., Amber 2016], applying the CHARMM36m[140] and CHARMM36[141] force fields for proteins and lipids respectively, and a stream file that contains **14h** parameters. Initial 5000 steps of restrained minimization were carried using the default CHARMM-GUI protocol for AMBER[142], equilibration and production runs were ran at a temperature of 310K (controlled with Langevin thermostat) and 1atm pressure (controlled with Monte Carlo barostat). Periodic boundary conditions (PBC) were employed. Non-bonded cutoff distance was set to 12 Å, and long-range electrostatic interactions beyond this cutoff were calculated using the Particle Mesh Ewald (PME) method, and bond lengths to hydrogen atoms were constrained using SHAKE algorithm.

MD simulation for **14h** in a POPC bilayer: Two independent all atom MD simulations were performed for **14h** in a POPC bilayer. The simulations were prepared and run like previously described MD simulation for SR-141716A in a POPC bilayer (Chapter IV) with different number of lipids in each leaflet which is 83, in addition, only one molecule of **14h** was added to the water phase in each simulation. Topology and parameter files for **14h** were obtained directly from CGenFF.ParamChem.org server, and were evaluated for the reproduction of crystal structure geometries equilibrated at MP2/6-31G* level of theory, and for the reproduction of dihedrals potential energy scans during the MD simulation. Lipid order parameters and mass density distributions were calculated using LOOS [143], Tcl tools in VMD [144] were used to calculate area per

lipid, H-bond interaction of **14h** with the lipid bilayer, and dihedral angles probability distributions.

MD simulation for the CB1 receptor-**14h** complex in a POPC bilayer: CB1 receptor bundle prepared for the MD simulation as described earlier was fed into the CHARMM-GUI online membrane building tool.[145] Simulation cell (80 Å × 80 Å × 124 Å, with the z-axis being normal to the plane of the bilayer) contained ~75 and 76 POPC molecules on the upper and lower leaflets respectively. The membrane was solvated with TIP3 water (thickness of 18 Å on both sides of the protein) and 0.15 M NaCl. Standard CHARMM-GUI minimization and equilibration steps were performed followed by more than 100ns production runs.[146]

MD simulations were used to investigate interaction dynamics of **14h** with the CB1 receptor at the transmembrane portal, and inside the CB1 receptor binding pocket. To study interaction dynamics at the transmembrane portal, three MD simulations were run where a single molecule of **14h** was placed at the transmembrane portal between TMH1/TMH7 and at different orientations. To study the interaction dynamics of **14h** inside the receptor binding pocket, two different 100ns and 200ns simulations were run, where **14h** was docked inside the CB1 crystal structure, or inside the CB1 receptor crystal structure with modelled N-terminus, respectively.

Tools implemented in VMD [144] were used to measure hydrogen bond interaction of the ligand with the receptor, RMSD of the transmembrane region of the receptor, salt bridge distances of DRY/D6.30 ionic lock, side-chain dihedral changes, and

to calculate the distance between the IC ends between TMH3/TMH6 (Cα distances between R3.50 and D 6.30), and TMH2/TMH7 (Cα distances between Y7.53 and I2.43).

Results

MD simulation of 14h in POPC bilayer: To study the dynamics of **14h** in a lipid bilayer, two independent 300ns all atom MD simulations were run. In both simulations, one **14h** molecule was added to the bulk water, and partitioning into the lipid phase was achieved within the first 100ns of each simulation (see Fig. 16). It could be noticed that **14h** moves from the bulk water into the lipid bilayer by first forming H-bond interaction with the phospholipid headgroups via its cyclohexanol ring. This initial interaction drives the molecule into the lipid in which **14h** would maintain its H-bond interaction with the phospholipid headgroups throughout the simulation.

Area per lipid and lipid order parameters were measured for the whole period of the simulations. Average area per lipid for both simulations was 65 $Å^2$ (RMSD = 1.1 $Å^2$) in agreement with experimental values[147] (see Fig 17). Palmitoyl (sn1), and oleoyl (sn2) acyl chains order parameters (S_{CD}) were also calculated for both simulations and were comparable to experimentally determined order parameters for POPC at 300K[148] (See Fig. 18). (Calculation of lipid order parameters is briefly discussed in Chapter IV).

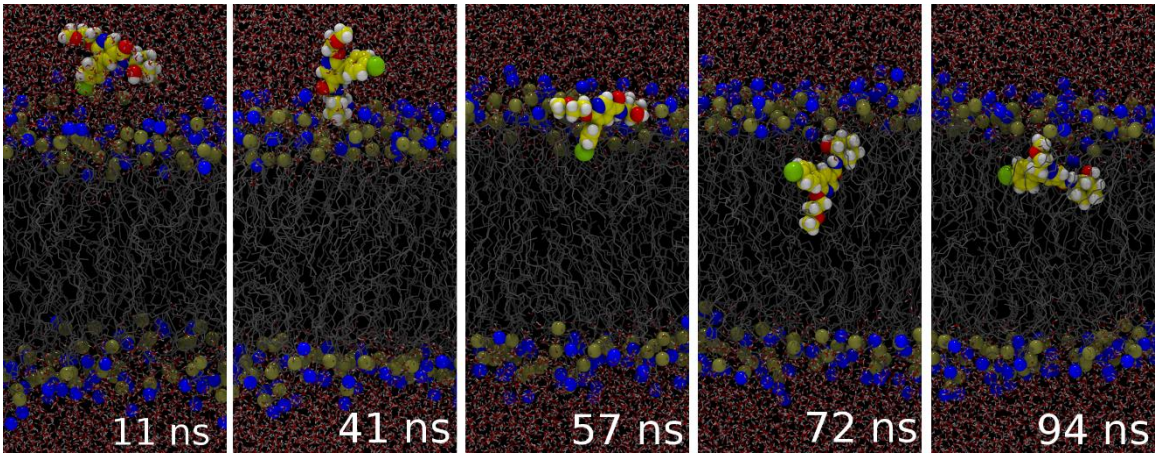

Figure 16. Snapshots from 300ns MD Simulation of 14h in POPC Bilayer. The figure shows the partitioning of **14h** from bulk water into the POPC bilayer. The partitioning of **14h** into the lipid bilayer starts with an interaction of the cyclohexanol ring with the head groups. In the bilayer, **14h** rotates in different directions, while showing two main orientations in the bilayer: vertical (presented at the 72 ns), or horizontal (presented at the 94 ns), with the cyclohexanol ring always near the lipid headgroups. Color Key: Phosphorus (Ochre spheres), Choline Nitrogen (Blue spheres), lipid tails (Silver thin tubes) (hydrogen atoms were not displayed). For **14h**: Carbons (Yellow), Oxygen atoms (Red), Chlorine (yellow green), Hydrogens (White), and Nitrogen (Blue).

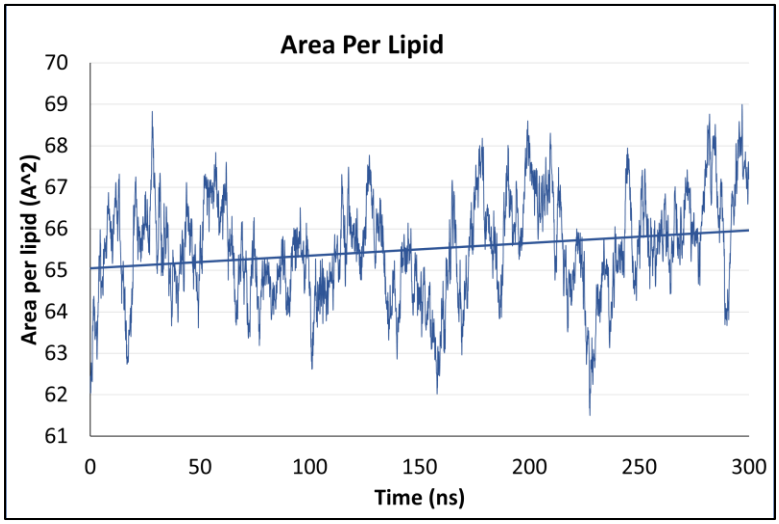

Figure 17. Area per Lipid Calculated for the whole 300ns of both MD Simulations of 14h in POPC Bilayer. The average area per lipid is ~ 65 $Å^2$

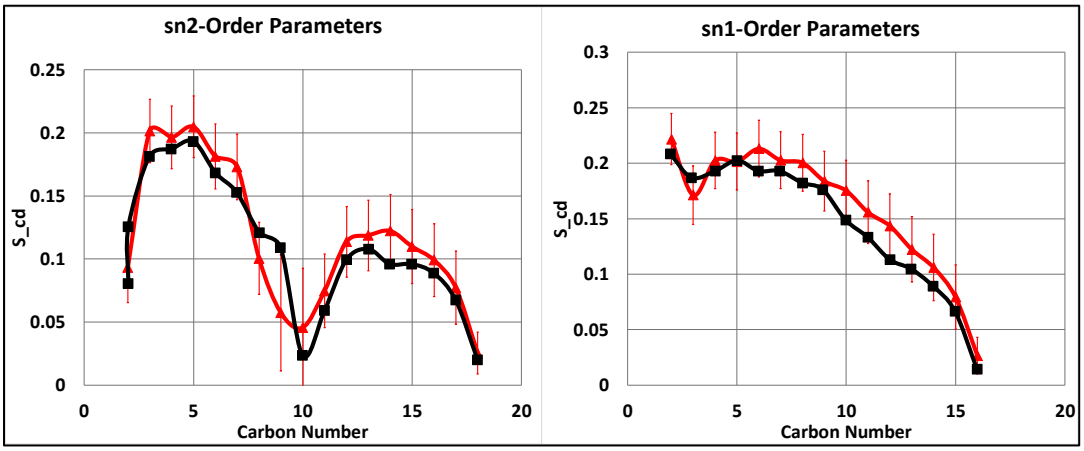

Figure 18. Lipid Order Parameters from MD Simulations of 14h in POPC Bilayer. Calculated lipid order parameters for the sn1 (Palmitoyl) and the sn2 (Oleoyl) chains of POPC. Results from MD simulations of 14h in POPC bilayer (Red), and NMR experimental values[148] (Black). Error bars represent standard error. NMR reference values were extracted by digitizing plotted graph in the reference paper[148].

Density distribution: Density distributions for the bilayer components as well as for **14h** and **14h** subset groups were calculated and determined for the last 200 ns of each simulation. During both simulations, **14h** was retained beneath the phospholipid head groups, this is due to the permanent H-bond interaction of the cyclohexanol group with the lipid head groups and interfacial water molecules (see Fig. 19, and Table 4). The molecule adopts two main orientations in the lipid bilayer; a horizontal orientation parallel to the lipid bilayer with its methoxyethoxy tail forming additional interactions with the phospholipid head groups, or vertically oriented with that tail oriented towards the center of the bilayer.

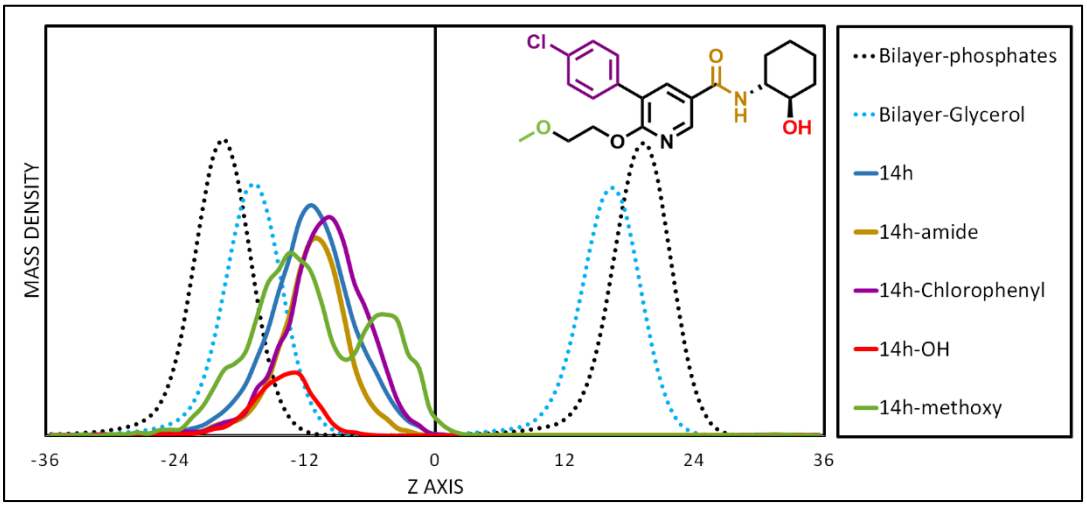

Figure 19. Mass-Density Distributions from MD Simulation of 14h in POPC Bilayer. The density distribution through the Z-axis (normal to the bilayer) is shown. The zero point on the Z-axis represents the center of the bilayer. Phospholipid bilayer components are shown in dotted lines. The whole **14h** compound distribution is in blue line, and **14h** subset groups are colored according to the chemical structure at the top right.

Table 4. Hydrogen Bond Analysis of 14h in the Lipid Bilayer. last 200 ns of the simulation were analyzed and the percentages of the time the ligand sub-groups are interacting with either the phospholipid head groups or interfacial water molecules are listed.

Interacting group	**% interaction time**
Pyridine	26
Amide nitrogen	80
Amide oxygen	23
Hydroxyl group	98
Tail oxygen	36

Dihedrals probability distributions: **14h** dihedrals were measured throughout the simulations of **14h** in the lipid bilayer and compared to QM-PES to validate the quality of ParamChem-generated forcefield parameters for **14h** (see Fig. 20).

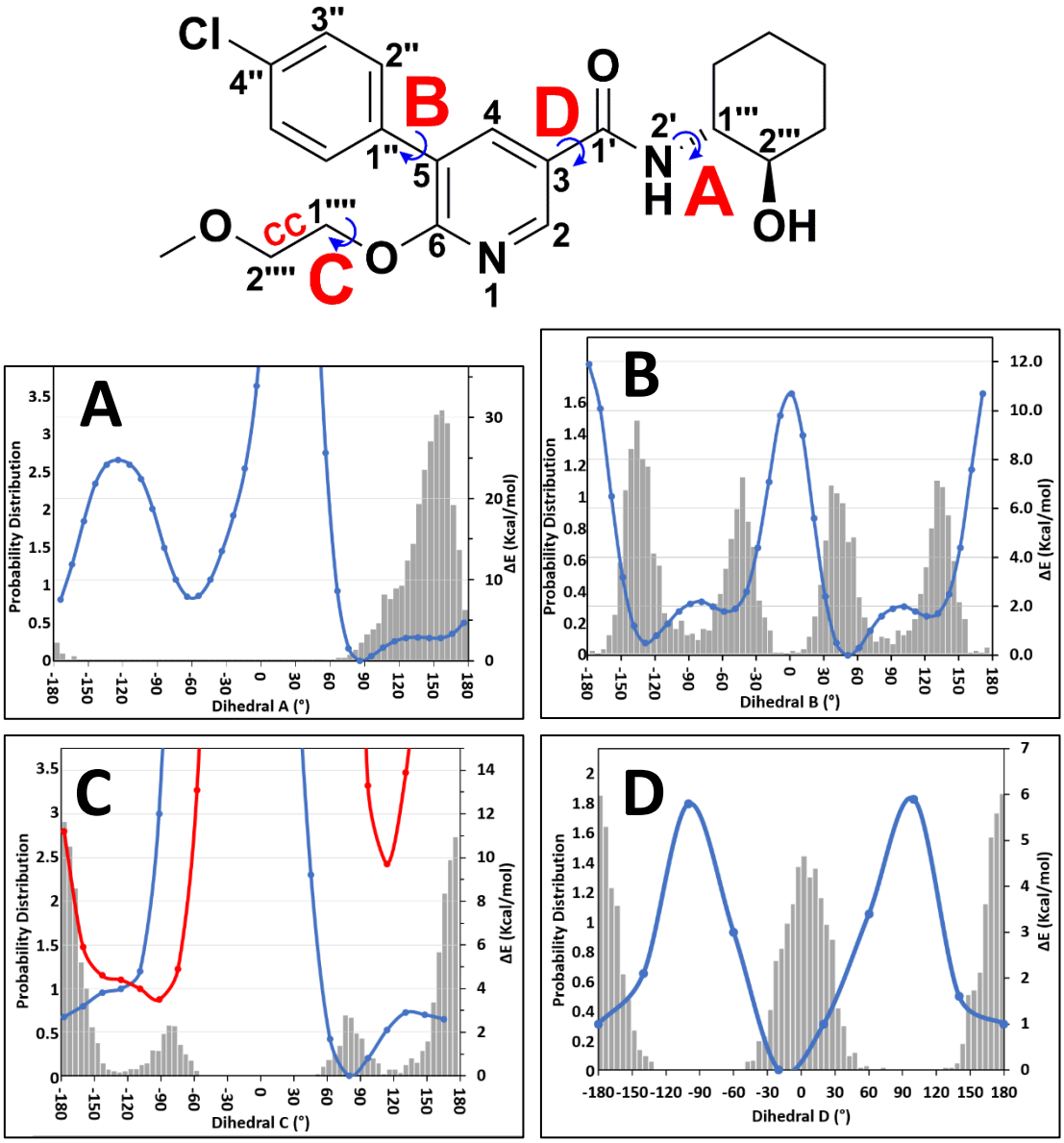

Figure 20. Dihedral Probability Distribution and Energy Profiles for 14h. Probability dihedral distribution from the MD simulation plotted against the dihedral energy profiles determined at the HF/6-31G* level. The chemical structure on top shows the relevant dihedrals; dihedral A (C1'-N1'-C1'''-C2'''), dihedral B (C6-C5-C1''-C2''), dihedral C (C6-O-C1''''-C2''''), and dihedral D (C2-C3-C1'-N2'). For Dihedral C; the blue line represents the energy profile for that dihedral at dihedral CC value of 53°, while the red line represents the dihedral energy profile at dihedral CC value of -67°.

For the dihedral between the amide group and the cyclohexanol ring, gas phase minimal energy determined at the HF/6-31G* level of theory is at ~ 80° corresponding to the formation of intramolecular hydrogen bond between the hydroxyl group and the amide oxygen, this minimum was not prevalent during the MD simulation due to the solvation effect in the bilayer. It can be seen also that a high energy barrier is located at ~ 20° due to the steric clash between the hydroxyl and the amide oxygen at that dihedral value. In addition, the dihedral angle between the amide and the pyridine ring shows local minima at ~ ±40° determined from QM calculations, these local minima were not populated in the MD simulation and were shifted to the 0° due to the nature of the energy force field function which uses a cosine term in the treatment of dihedral energies. However, low energy barrier for that dihedral allows cis-trans isomerization during the simulation. The dihedral probability distribution for the bond between the chlorophenyl ring and the pyridine is consistent with the QM-PES. Finally, the 2-methoxyethoxy tail dihedrals were also determined during the simulation and were consistent with QM-PES.

It is worth mentioning that the crystal structures of **14h** show that the ligand forms intermolecular H-bond that involves the amide group of adjacent compounds. Those structures show also a preferential rotamer of the amide oxygen to be in trans conformation with the lone pair of electrons from the pyridine nitrogen even though the energy barrier between the two conformations is relatively low and energy optimization of both conformers at the HF level of theory results in a low relative energy between the two conformers (~0.1 Kcal/mol), (see Fig. 21).

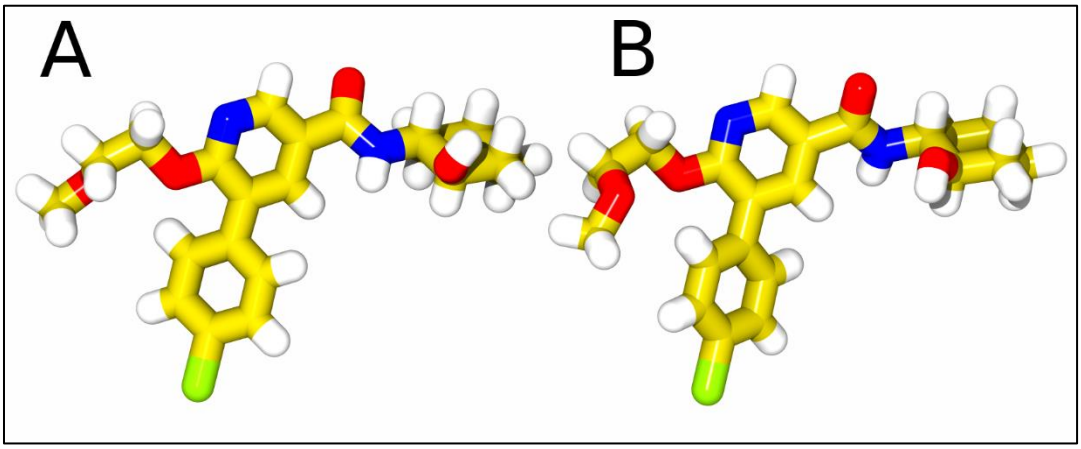

Figure 21. 14h Crystal Structures' Geometry. Structures show trans planar amide which is ~30 degrees rotated from the plane of the pyridine ring, the chlorophenyl ring is rotated ~35° from plane of pyridine, and no-intramolecular H-bond present between the cyclohexanol and the amide oxygen (satisfied in the crystal structure by inert-molecular H-bond between amide nitrogen of one molecule and the carboxamide oxygen from adjacent molecule). Color code: Carbons (Yellow), Oxygen atoms (Red), Chlorine (yellow green), Hydrogens (White).

MD simulations for the CB1 receptor-14h complexes in a POPC bilayer:

Initial interaction of 14h with the CB1 receptor: The CB1 receptor inactive state crystal structures show a transmembrane portal between TMH1 and TMH7 for CB1 receptor antagonists.[15, 16] To study the initial interaction of **14h** with the CB1 receptor, and to investigate the favored orientation of the ligand at the transmembrane portal, three MD simulations were run where one **14h** molecule was placed next to the portal and at different orientations. In all three simulations, **14h** rotated so that the chlorophenyl ring would insert into a groove in the CB1 receptor between TMH1 and TMH7. This groove was aligned by residues I1.35, L1.38, M7.40, and L7.43. On the other hand, the cyclohexanol ring formed intermittent hydrogen bond interaction with the lipid headgroups and E1.31 on top of TMH1 (see Fig. 22). A frame (~46ns from one of the

simulations) where **14h** was placing its chlorophenyl ring deep in the groove was used to run two spawns where the velocities were scrambled. At around 90 ns of the simulations, M7.40 and L7.44 change their χ1 dihedrals allowing the whole structure to fit between TMH1 and TMH7. Specifically, M7.40 changes its χ1 dihedral from g+ to trans, while the L7.44 fixes its χ1 dihedral in trans (see Fig. 23 and Fig. 24). At this stage, the cyclohexanol ring of **14h** would form either a direct or an indirect (via water molecule) intermittent hydrogen bond interactions with the backbone of the N-terminus.

For the sake of docking **14h** inside the CB1 receptor, these simulations elucidated the orientation of **14h** at the transmembrane portal. The simulations demonstrated that **14h** first accesses the receptor binding site with its chlorophenyl ring, while the methoxyethoxy tail is hanging down towards the intracellular of the receptor (see Fig. 23).

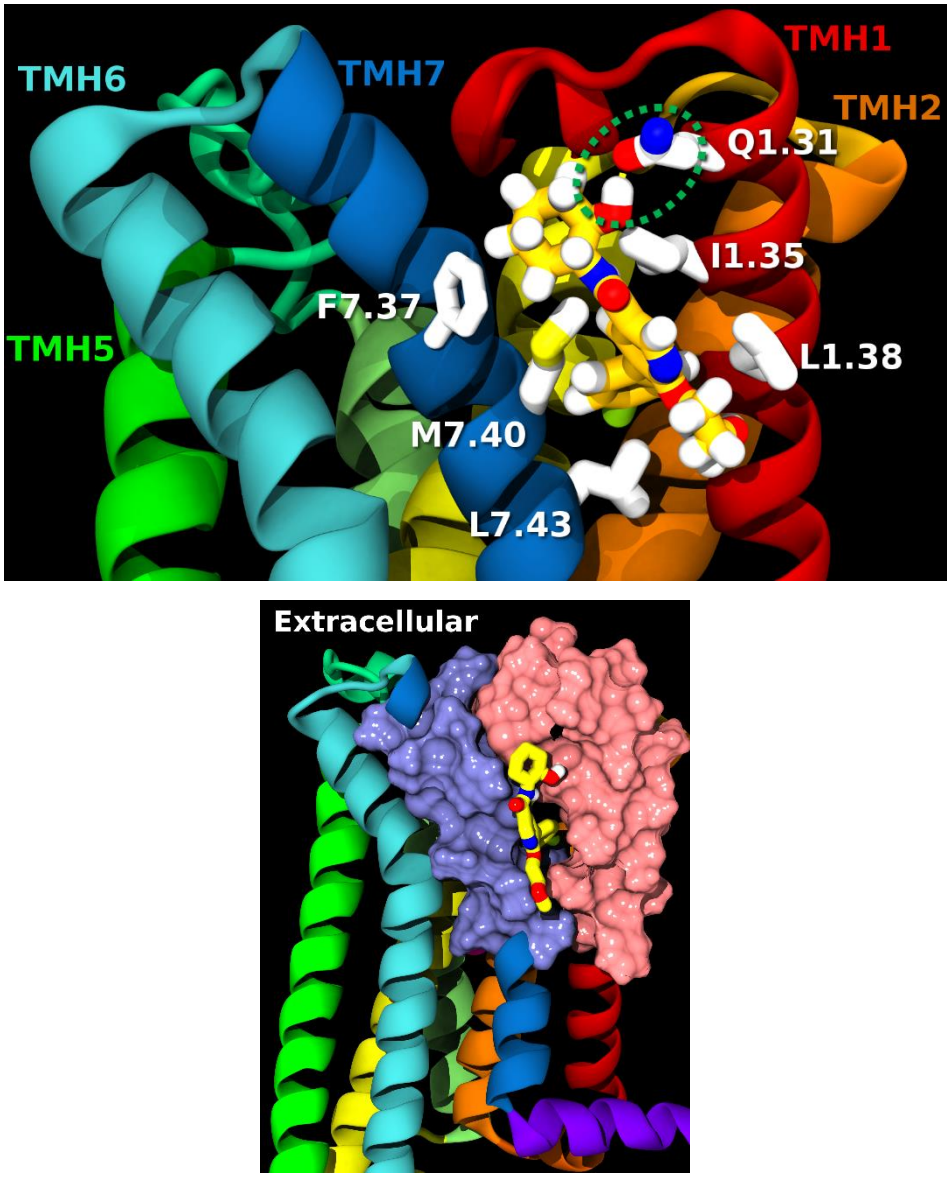

Figure 22. Initial Interaction of 14h with the CB1 Receptor at the TMH1/7 Portal at 46ns. Top) **14h** places its chlorophenyl ring in a groove aligned by hydrophobic residues (M7.40 and L7.44 on TMH7, and I1.35 and L1.38 on TMH1). The cyclohexanol group of **14h** forms stable H-bond interactions with either the Q1.31 on top of TMH1 or with interfacial water molecules around TMH1. Amino acid residues are displayed in white licorice representation. Bottom) Opening between the two helices and the initial insertion of **14h** into the receptor. Surface representation for all amino acid residues aligning the portal between TMH1 and TMH7 including the N-terminus. Color code for **14h**: Carbons (dark Yellow), Oxygen atoms (Red), Chlorine (yellow green), Hydrogens (White).

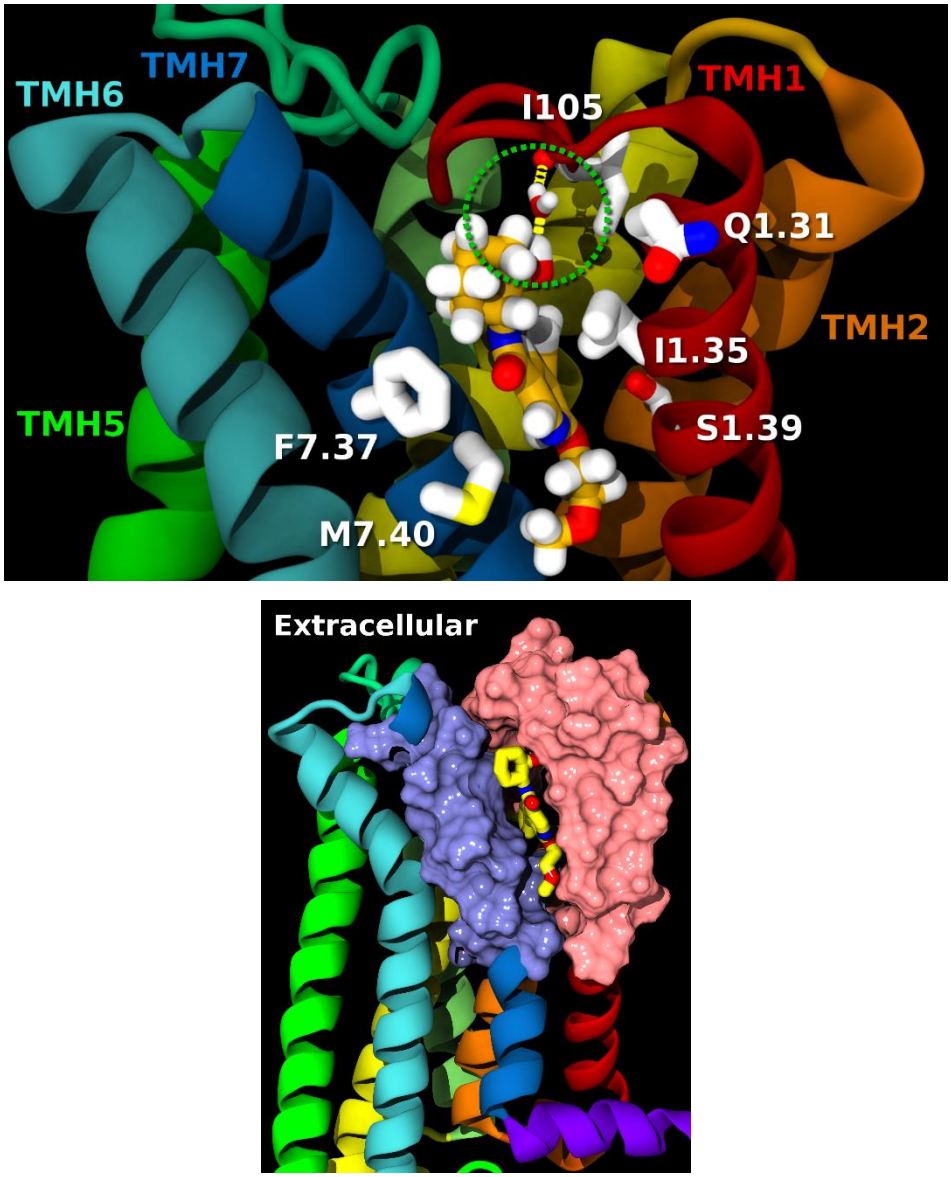

Figure 23. Interaction of 14h with the CB1 Receptor at the TMH1/7 Portal at 90ns. Top) The chlorophenyl ring of **14h** is inside the receptor and the cyclohexanol ring forms indirect H-bond interaction with the backbone of I105 through water molecule. The χ1 dihedral of M7.40 is in trans to allow the chlorophenyl ring to insert between the two helices. Bottom) Surface representation of the residues aligning transmembrane portal including the N-terminus.

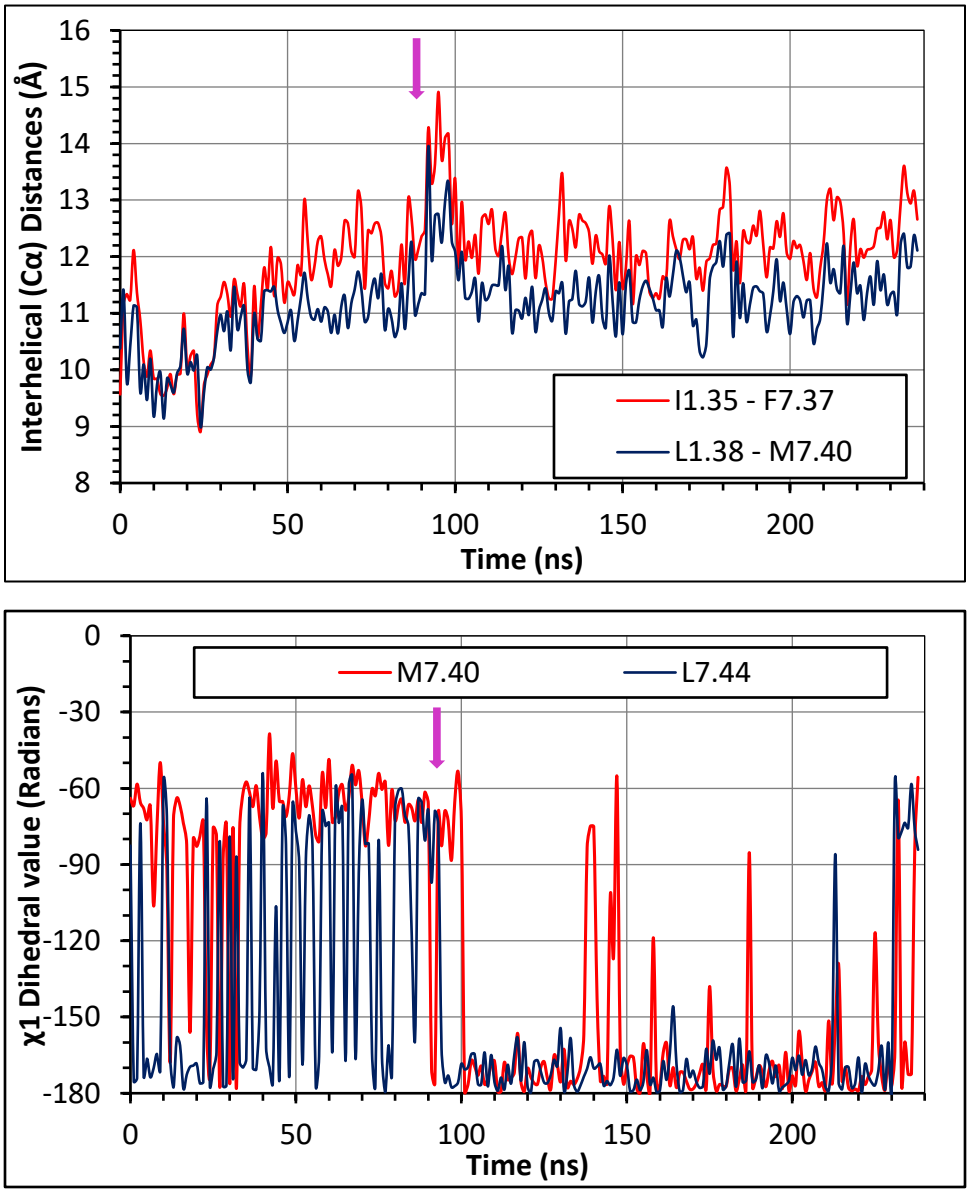

Figure 24. Conformational Changes at the TMH1/7 Portal During Initial Interaction of 14h with the CB1 Receptor. Top) Interhelical (Cα) distances between I1.35 and F7.37, and between L1.38 and M7.40. An increase in the distance between the two helices is observed at ~90ns of the simulation during which the whole **14h** fits in between the two helices. Bottom) Change in the χ1 dihedral of M7.40 and L7.44 is observed at ~90ns of the simulation (dihedral values calculated as the absolute value of the radians).

Docking of 14h inside the CB1 receptor: based on observations from previous simulations, we picked one of the results from prime-induced fit docking where the ligand is oriented so that the cyclohexanol is towards the extracellular side of the receptor and the methoxy-ethoxy tail is pointing towards the sodium binding pocket (see Fig. 25A). This receptor-ligand complex was run eventually in a MD simulation to monitor the stability of the ligand inside the CB1 receptor binding site. In the first 20 ns of the simulation, **14h** shifts from its initial dock to place the chlorophenyl ring near W6.48, while the cyclohexanol ring forms intermittent H-bond interactions with S1.39 (see Fig. 26A, B, C). This simulation was run for a total of 100 ns, and the final dock of **14h** inside the receptor shows that the position of the I105 in the crystal structure fits the I105M mutations data (see Fig. 25B).

Finally, **14h** was docked in the CB1 receptor with a modeled N-terminus. Stability of the CB1–**14h** complex was monitored through a 200ns simulation. Through the simulation, the cyclohexanol ring of **14h** was forming stable VDW interactions with the I105. However, compared to the equilibrated dock of **14h** inside the CB1 receptor with the original crystal structure N-terminus, the amide oxygen rather than the cyclohexanol fits next to S1.39, while the cyclohexanol ring forms additional VDW and intermittent H-bond interactions with E106 or waters inside the binding pocket (see Fig. 26, and Fig. 27).

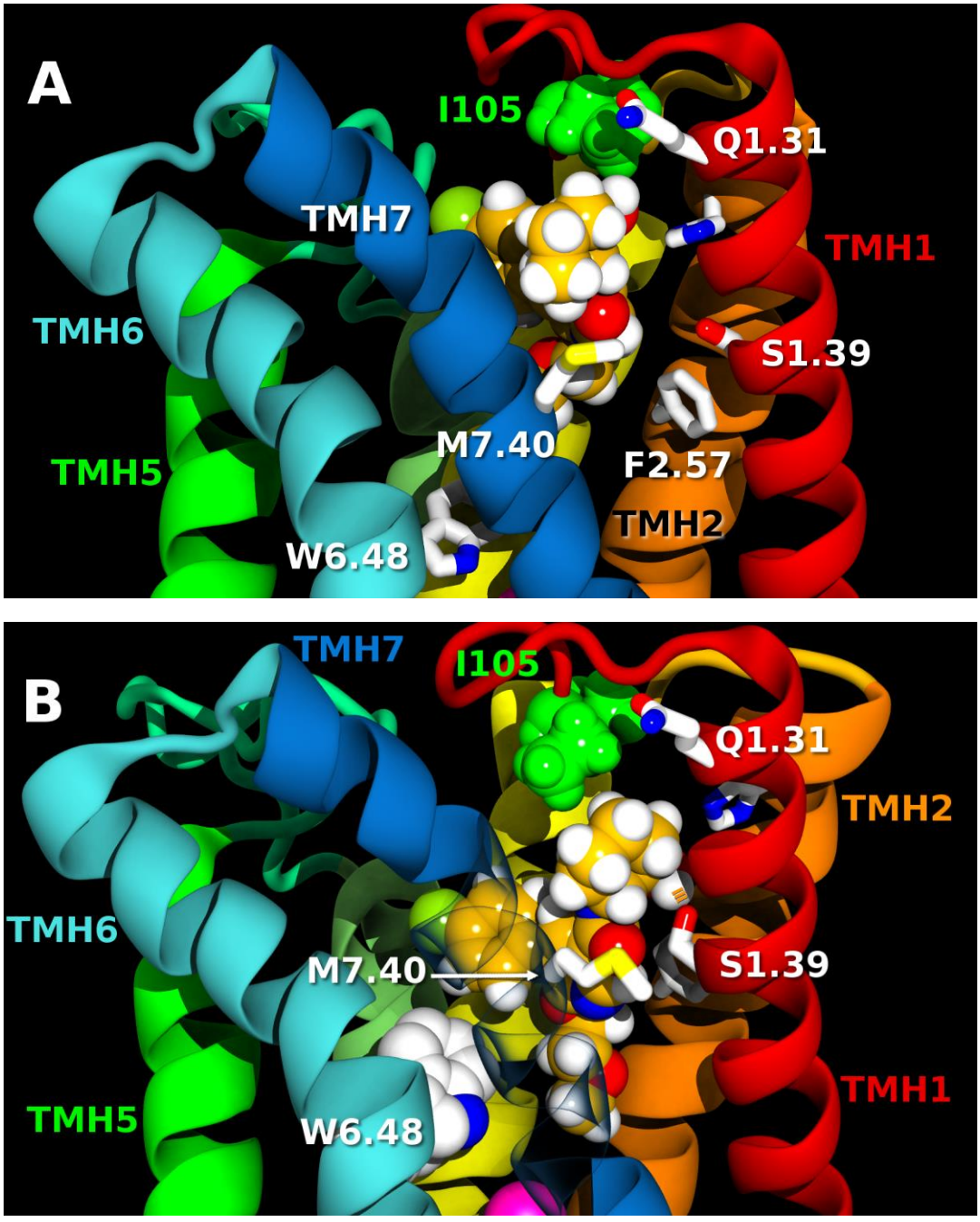

Figure 25. Docking of 14h Inside the CB1 Receptor with the Crystal Structure's N-Terminus. A) initial dock showing **14h** high at the binding site. B) **14h** equilibrated in the CB1 receptor (90ns), the ligand positioned the tail towards the sodium binding pocket (Sodium in magenta sphere), the chlorophenyl ring is on top of W6.48, the cyclohexanol forms H-bond with the S1.39, and I105 (green VDW) forms VDW interaction with **14h**.

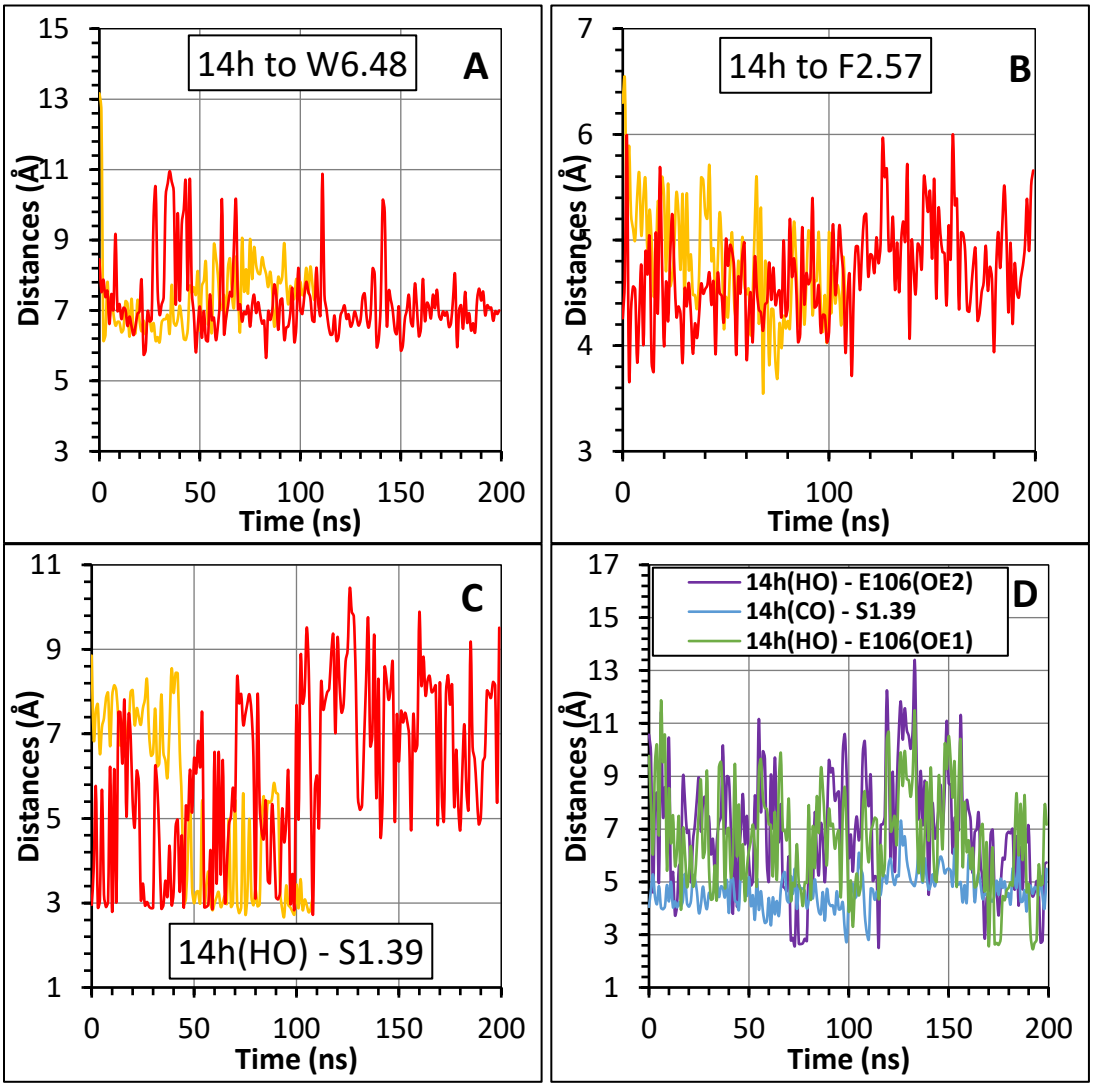

Figure 26. Stability of 14h Docks Inside the CB1 Receptor. For A, B, and C: yellow graphs are for the CB1 receptor with the original N-terminus (100ns simulations), and red graphs are for the CB1 receptor with the modeled N-terminus (200ns simulations). A) distance between the center of mass between the chlorophenyl ring of **14h** and the indole ring of W6.48. B) distance between the center of mass between the pyridine ring in **14h** and the phenyl ring in F2.57. C) Distance between the cyclohexanol hydroxyl oxygen (HO) and the side chain oxygen of S1.39. D) graph shows interatomic distances between (HO) in **14h** and sidechain oxygens of E106, or between the amide oxygen (CO) of **14h** and the sidechain oxygen of S1.39.

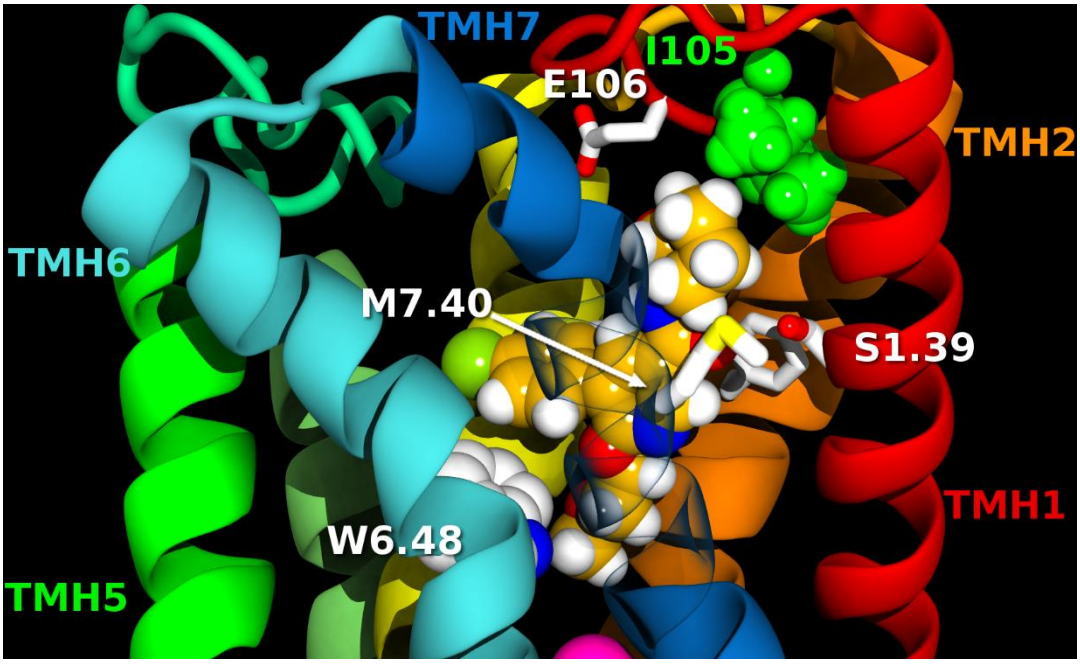

Figure 27. Binding Site of 14h Inside the CB1 Receptor with Modeled N-Terminus (50ns).

For all simulations of **14h** with the CB1 receptor, RMSD of the transmembrane region was monitored. MD simulation with the modelled N-terminus shows stability in the last 100ns of the simulation compared to simulations run on the CB1 crystal structure. The χ1 dihedral for the toggle switch (W6.48) shows better stability at g+ in simulations with **14h** docked inside the receptor. In addition, interhelical distances at the IC domain of the receptor indicate stability of the bundles in the inactive state. It can be noticed that the modelled N-terminus improved the stability of the CB1 receptor in its inactive state compared to the original crystal structure, this can be seen in the comparably shorter intrahelical distances at the IC domain of the receptor especially in the last 100ns of the simulation (see Fig. 28).

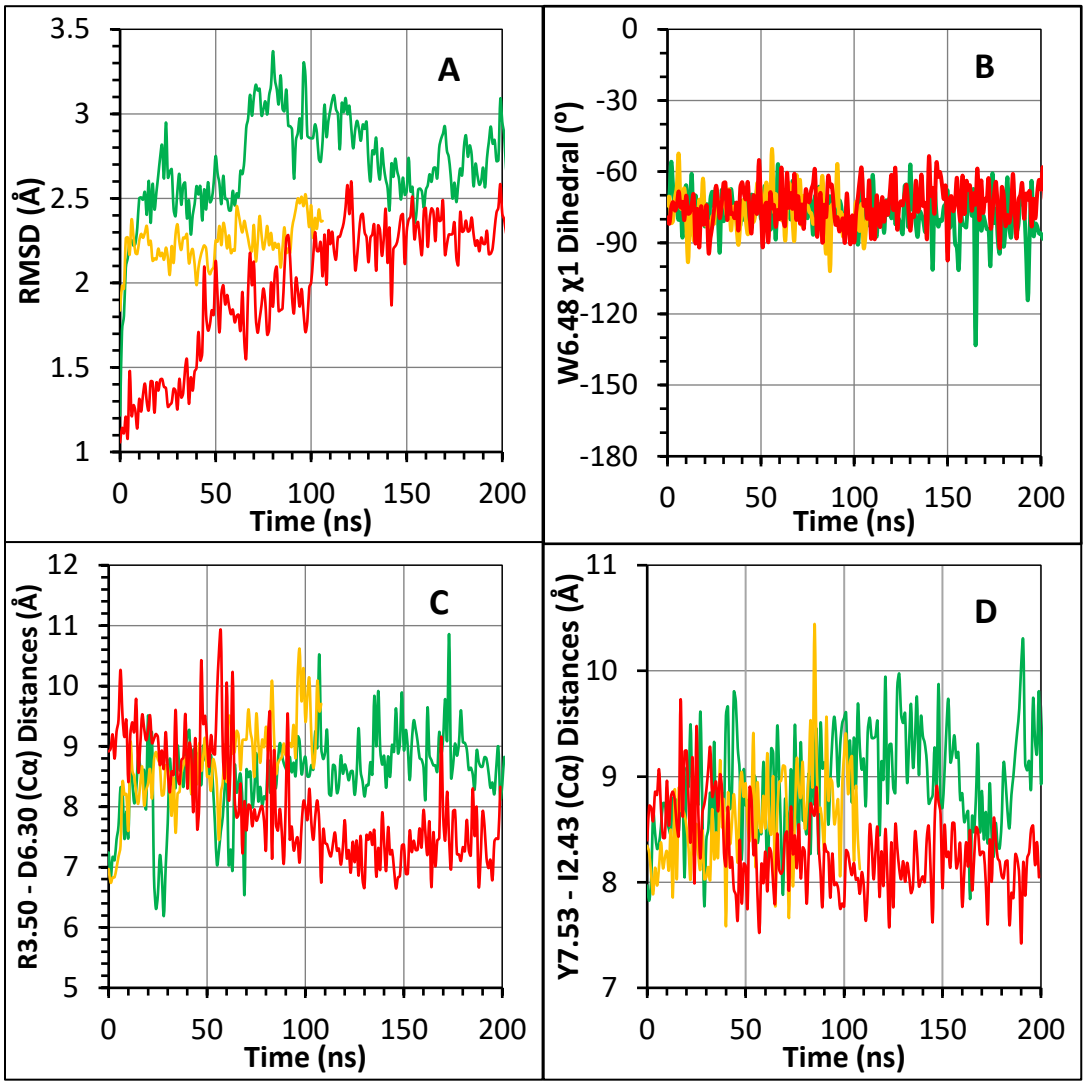

Figure 28. Stability of the Inactive State of the CB1 Receptor in Complex with 14h During MD Simulations. CB1–**14h** complex at the portal (green), CB1–**14h** docked in the CB1 receptor with the crystal structure original N-terminus (yellow), and CB1–**14h** docked in the CB1 receptor with modeled N-terminus (red). A) RMSD of the transmembrane region. B) χ1 dihedral of W6.48, the y-axis represents the radian of measured dihedrals. C) interhelical distances between the Cα of R3.50 and D6.30. D) interhelical distances between the Cα of Y7.53 and I2.43.

Discussion

Preparation of the CB1 receptor for docking and MD simulation: Two crystal structures of the CB1 receptor in its inactive state have been reported in complex with AM6538 and Taranabant, and with resolution of 2.8 Å[15] and 2.6 Å[16] respectively. The later (PDB ID: 5U09) was used for the docking and the MD simulations. The CB1 receptor construct in this crystal structure had single thermostabilizing mutation (T3.46A). In addition, the construct (lacking residues N-terminal to K90, and residues C-terminal from P421) had a fusion protein at the intracellular ends of TMH5 (A301) and TMH6(D333). While the electronic density of residues N-terminal to E100 or C-terminal from F412 was not resolved, the distal region of the N-terminus (specifically F102 and M103) occludes the receptor binding pocket. Thus, we aimed to model the proximal region (S88 to P113) of the N-terminus, adding the N-terminal disulfide bridge with F102 and M103 above the binding pocket while complying with the I105M mutation data (see Fig. 29).

Placement of a sodium ion inside the CB1 receptor bundle: Different studies reported that sodium allosterically stabilizes the inactive state of class A GPCRs. High resolution crystal structures of the δ-opioid,[149] β1-adrenergic,[103] and the adenosine[150] receptors revealed a high electronic density near D2.50 which has been attributed to the presence of sodium ion that coordinates with D2.50, S3.39. Sodium was not resolved in the CB1 receptor crystal structures. However, it has been shown to lower the binding affinity of CP-55940 to the WT receptor and to an D2.50E, but not D2.50N mutant.[151] In addition, the efficacy of Org-27569 (an allosteric modulator at the CB1

receptor) in inhibiting CP-55940 induced GTPγS binding to the CB1 receptor was significantly enhanced suggesting an increased stability of the inactive state of the receptor.[92] During the current work, we ran multiple MD simulations of the CB1 receptor without the addition of the sodium, and water inside the bundle was monitored during all simulations. It was noticed that sodium maintained the number of water molecules inside the sodium binding pocket to the original waters added, and prevented an overflow of water in that area.

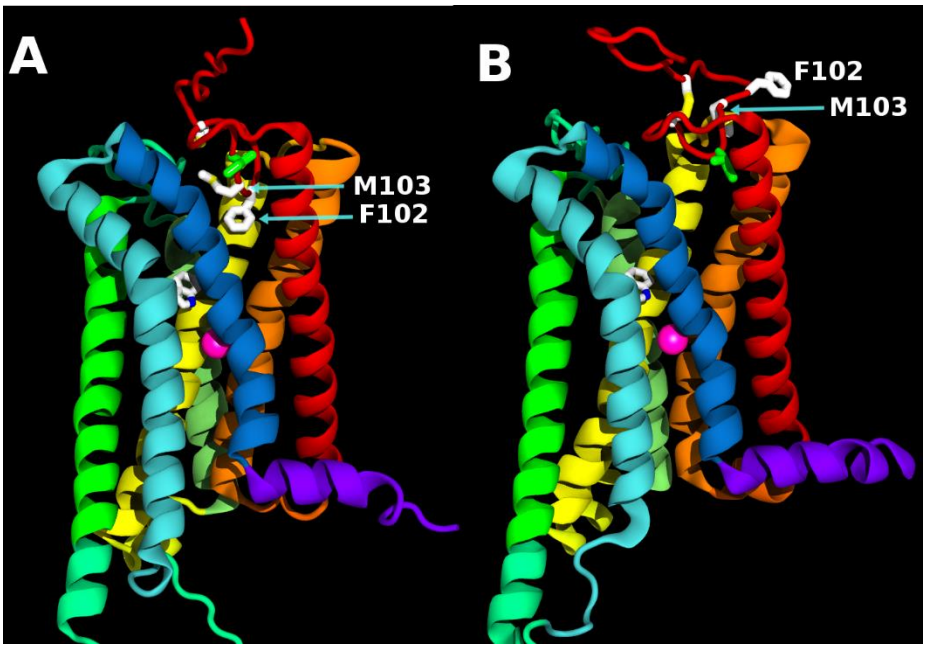

Figure 29. Structure of the CB1 Receptor's N-Terminus. A) CB1 receptor with the original N-terminus showing the F102 and M103 inside the binding pocket. B) CB1 receptor with the modeled N-terminus at 120ns of the simulation, F102 and M103 were stable outside the binding pocket. M105 in green licorice and the disulfide bridge at the N-terminus in white licorice.

MD simulations: In the effort to model the N-terminus of the CB1 receptor, our strategy was to dock **14h** inside the receptor and model the N-terminus guided by the I105M mutation data which affected **14h** binding to the receptor, and with the possibility that **14h** might have a different binding site compared to the crystallized ligands inside the CB1 receptor. Initial docking of **14h** inside the CB1 receptor yielded different orientations of the ligand inside the binding pocket. To better evaluate docking results, we ran a MD simulation of **14h** in a POPC bilayer to investigate its dynamics in the lipid bilayer. Results from the MD simulation show that **14h** would always orient its cyclohexanol ring towards the phospholipid headgroup forming stable hydrogen bond interaction with the polar head groups or interfacial water molecules, which eliminates some docking results that places the cyclohexanol near the D2.50. Next step was to decide on whether the chlorophenyl ring, or the methoxy-ethoxy tail would insert first into the transmembrane portal of the CB1 receptor. This is important because it would better determine the orientation of **14h** inside the receptor.

The CB1 receptor inactive state crystal structures show a transmembrane portal between TMH1 and TMH7 for CB1 receptor's antagonists.[15, 16] Thus, three MD simulation runs were done where **14h** was placed near the TMH1/7 portal in three different orientations: with either the chlorophenyl ring or the methoxyethoxy tail pointing towards the portal, or with both substituents at equidistance from the portal. In all simulations, the molecule rotated and placed its chlorophenyl ring in a groove between the two helices, while the cyclohexanol ring of **14h** was forming alternate H-bond interactions with the lipid headgroups or the top of the receptor, stabilizing the vertical

orientation of **14h** in the lipid bilayer. Such interactions require that the chlorophenyl ring be at an angle with the pyridine and the cyclohexanol ring (See Fig 30). This conformational requirement has been studied previously using different analogues of **14h**; analogues which have wide angle between the chlorophenyl and the cyclohexanol rings in their lowest energy conformations resulted in drastic loss of affinity.[127] It should be mentioned however, that the stable interaction of **14h** analogues with the lipid headgroups via their cyclohexanol ring dictates this requirement. SR-141716A on the other hand has a piperidine substituent attached to the amide with wide angle between the piperidine ring and the chlorophenyl ring. This compound can still bind to the receptor due to the free movement of SR-141716A in the lipid bilayer.

Results from previous simulations provided insight about the orientation of the ligand inside the receptor. Thus, one dock from our initial docking study was picked, this dock fits our MD simulation data obtained so far and it places **14h** high and near the portal so that **14h** could make headway freely into its binding pocket in a MD simulation. In its final dock inside the receptor, **14h** places its chlorophenyl ring on top of W6.48 and in a similar way to the Taranabant and AM6538 in the CB1 crystal structures, this positioning helps stabilizing the inactive rotameric state of W6.48, a conserved residue in class A GPCRs and has been shown to act as a toggle switch during the activation of these receptors where it changes its χ1 dihedral from g+ to trans during activation.[83-86] It could be noticed also, that **14h** forms stable VDW interactions with the I105, which fits I105M mutation data discussed previously. According to that, and in the effort to model the N-terminus, the spatial location of the I105 with respect to the rest of the receptor was

not changed from crystal structure`s location, while residues N-terminal to I105 were remodeled to solve crystallization artifact that places the F102 and M103 inside the receptor binding pocket. Finally, stability of the interaction of **14h** with the CB1 receptor with modified N-terminus was monitored in the last 100ns MD simulation, during which **14h** maintained its interaction with the I105, plus additional VDW and H-bond interactions with E106. Such interactions were not observed in the MD simulation of **14h** with the CB1 original crystal structure, and would require experimental validation.

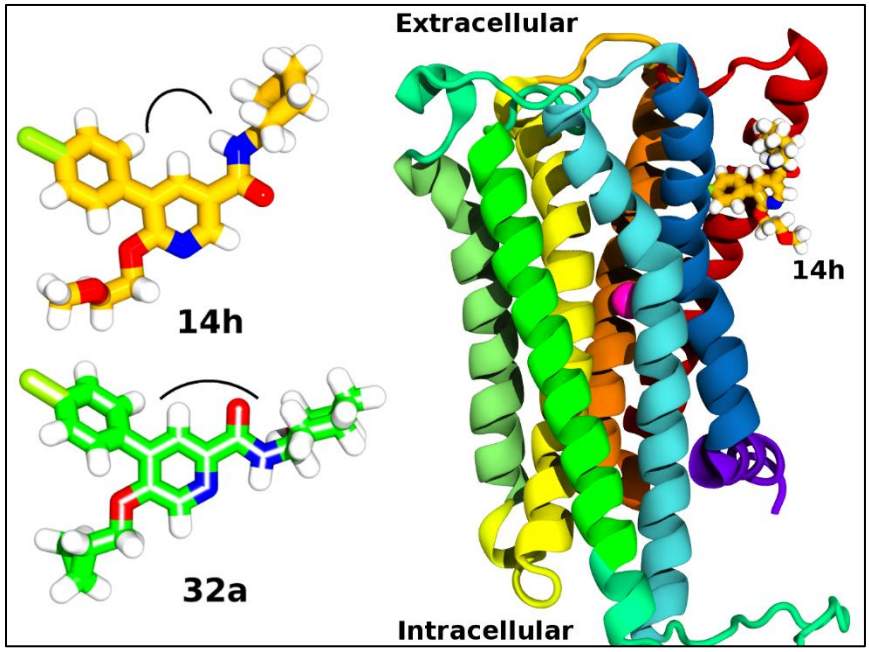

Figure 30. SAR of 6-Alkoxy-5-Aryl-3-Pyridinecarboxamides. Reported *Ki* values in hCB1 receptor against [^{3}H]CP55940 was >7000nM for the 32a analogue compared to 5.1 ± 1.6 nM for **14h**.[127] The narrow angle between the cyclohexanol and the chlorophenyl rings allows initial interaction with the CB1 receptor.

Conclusions

The current study illuminated the initial interaction of **14h** with the receptor, and shed a light on the differences in the structural requirements of different CB1 receptor antagonists based on their initial interaction with the receptor and their dynamics in the lipid bilayer. In addition, it provided a stable model of the N-terminus that still needs to be validated experimentally.

CHAPTER IV

PARAMETERIZATION AND ALL ATOM MOLECULAR DYNAMICS SIMULATION OF SR141716A IN A LIPID BILAYER

Introduction

The biarylpyrazole, 5-(4-Chlorophenyl)-1-(2,4-dichloro-phenyl)-4-methyl-N-(piperidin-1-yl)-1H-pyrazole-3-carboxamide (SR141716A, Rimonabant (**SR**)), is a potent and selective CB1 receptor antagonist and inverse agonist. **SR** (see Fig. 31) is widely used in pharmacological and in binding assay experiments due to the availability of tritiated version. It was the first approved CB1 receptor antagonist, developed by Sanofi-Aventis, and approved in Europe in 2006 as an anti-obesity drug, but was withdrawn two years later due to increased reports of suicidal ideation.[152, 153]

The SAR of biarylpyrazoles has been extensively studied through structural variation, and through mutation studies at the CB1 receptor binding site.[115] The two inactive state crystal structures for CB1 were resolved in complex with two different antagonists; AM6538 and Taranabant.[15, 16] However, mutation data at the CB1 receptor suggest that the binding site of SR is deeper inside the binding pocket compared to the crystallized antagonists, and involves a hydrogen bond interaction with a lysine residue at the third transmembrane helix of the receptor.[19, 118-120] Running MD study of **SR** with the CB1 receptor in an explicit membrane can reveal different ligands' interactions with the receptor at a molecular level. In addition, understanding such an

interaction will aid in the design of new ligands with modified pharmacological activity based on the **SR's** basic scaffold.

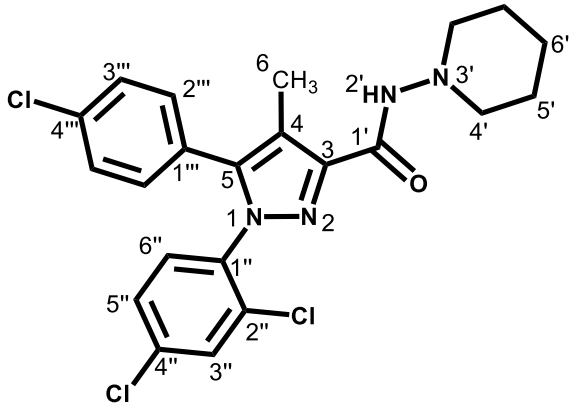

Figure 31. Chemical Structure and Numbering of SR-141716A.

Applying the CHARMM force field potential energy function to run all atom MD simulation necessitates the development of force field parameters for **SR**, such parameters have been well established and experimentally validated for biological molecules such as lipids and proteins [141]. This work describes the parameterization for **SR**, including evaluation of the internal (Bonded) and external (non-bonded) parameters, and two independent 300ns all atom MD simulation of **SR** in a fully hydrated POPC bilayer.

Methods

The Class I additive CHARMM potential energy function is given in eq. (1) [154].

$$E = \sum_{bonds} K_b\,(b - b_0)^2 + \sum_{angles} K_\theta\,(\theta - \theta_0)^2 + \sum_{Urey-Bradley} K_{b^{1-3}}\left(b^{1-3} - b_0^{1-3}\right)^2 + \sum_{dihedrals} K_\emptyset\,[1 + \cos(n\emptyset - \delta)] + \sum_{improper} K_\varphi\,(\varphi - \varphi_0)^2 + \sum_{nonbonded}\left\{\varepsilon_{ij}\left[\left(\frac{R_{min,ij}}{r_{ij}}\right)^{12} - 2\left(\frac{R_{min,ij}}{r_{ij}}\right)^{6}\right] + \frac{q_i q_j}{\epsilon r_{ij}}\right\} \quad \text{eq. (1)}$$

The internal (bonded) part of the equation includes potential energy functions for bonds (b), angles (θ), Urey-Bradley (b^{1-3}), dihedrals (ϕ), and improper dihedrals (φ). Subscript zero corresponds to the equilibrium value for each, and the K's are the corresponding force constants. The sinusoidal dihedral energy term also incorporates periodicity (n) and phase shift (δ). External (nonbonded) energy terms include Lennard-Jones 6-12 potential, and Coulombic potential for electrostatic interactions. In the nonbonded energy terms; ε_{ij} is the well depth calculated as the geometric mean ($\varepsilon_{ij} = \sqrt{\varepsilon_i \varepsilon_j}$), $R_{min,ij}$ is the arithmetic mean ($R_{min,ij} = (r_{min.i} + r_{min,j})/2$), q_i, q_j are the partial atomic charges, and (ϵ) is the dielectric constant which is set to 1 corresponding to vacuum and in calculations that incorporate explicit solvent.

Parameterization:

Target data: Crystal structures for **SR** were previously published [155], coordinates were obtained from Cambridge Crystallographic Data Centre (www.ccdc.cam.ac.uk/data request/cif). MP2/6-31G* level of theory was used to obtain target bond lengths, angles, and dihedrals by optimizing crystal structures' geometries in vacuum, as well as to generate quantum mechanical potential energy scans (QM PES) for missing bond lengths, angles and dihedrals using Spartan 08 molecular modeling program (Wavefunction, Inc., Irvine, CA [156]).

Initial charges, atom typing, and initial guess parameters for SR: A stream file used as a wild card for **SR** was obtained from CGenFF.ParamChem.org server; this stream file contains **SR**`s topology with estimated charges, Lennard-Jones (LJ) parameters, as well as the initial guess parameters for missing bond lengths, angles and dihedrals. LJ parameters for new atom types were copied from ParamChem-generated atom types.

Charge optimization: Charges for all molecular fragments were directly obtained from CGenFF except for molecular fragment (1). A stream file that describes the topology of molecular fragment 1 was downloaded from ParamChem website. Charges for all atoms in fragment 1 except the aliphatic hydrogens (which were set to +0.09 as recommended) were optimized to reproduce scaled QM interaction energies and distances between the model compound in its MP2/6-31G(d) optimized trans geometry (a geometry like the N-(piperidin-1-yl)-carboxamide moiety in **SR** global minima) and individual water molecules. To do that, a CHARMM script available in the CHARMM

parameterization tutorial was modified and used to place a TIP3P water molecule to form a linear hydrogen bond with each hydrogen bonding donor or acceptor atom in the model compound. Interaction distances between the model compound and individual water molecules were then optimized at the HF/6-31G* level in Jaguar [157] by performing rigid coordinate scan in which all other degrees of freedom are fixed. Resulting water interaction energies (calculated as $E_{Interaction} = E_{Complex} - E_{\mathbf{SR}} - E_{TIP3}$) were scaled by a factor 1.16 as recommended and used as target data for charges optimization. Charges for the whole **SR** were then calculated by removing atoms at which molecular fragments will be linked and adding their charges to their parent heavy atoms.

Bond-angle-dihedral optimization: Coordinates generated from QM PES were used as input geometries to generate CHARMM PES. Coordinates of interest were fixed, and other degrees of freedom could minimize in CHARMM while setting the correspondent force constant for bonds, angles, or dihedrals to zero in the stream file. Resulting energy profiles were then plotted against QM profiles, and parameters were adjusted until generated CHARMM PES fit the MP2-generated PES.

MD simulation: Two independent all atom MD simulations were performed for **SR** in a POPC bilayer. The simulation cell (73x73x79 $Å^3$, Z axis normal to the plane of the bilayer) was built using the freely available CHARMM-GUI input generator.[142] Each leaflet contained 81 POPC molecules hydrated with a layer of TIP3 water (22.5 Å thickness) above and below the lipid bilayer and including sodium chloride ions (0.15 M). In simulation I, three **SR** molecules were added randomly to each leaflet of the lipid bilayer by replacement method, and generated input file was checked for lipid penetration

into **SR** rings. While in simulation II, three **SR** molecules were added to the water layer at each side of the leaflet, and clashing waters or ions were removed while maintaining the neutrality of the system. Standard CHARMM-GUI minimization and equilibration steps were performed followed by 300ns, and 400ns production runs for simulation I and II respectively.[146] Isobaric-isothermic (NPT) simulations were performed with the GPU-enabled AMBER16 molecular dynamics package [Case et al., Amber 2016] using the CHARMM36m force field for proteins and lipids,[140, 141, 158] and a stream file that contains optimized **SR** parameters, and run at a temperature of 310K (using Langevin thermostat) and 1atm pressure (using MC barostat). Periodic boundary conditions (PBC) were employed, non-bonded cutoff distance was set to 12 Å, long-range electrostatic interactions beyond this cutoff were calculated using the particle mesh Ewald (PME) method, and all covalent bonds involving hydrogen atoms were constrained using the SHAKE algorithm.

Lipid order parameters and density distributions were calculated using LOOS [143]. Tcl tools in VMD were used to calculate area per lipid and dihedral angles probability distributions.[144]

Results

Parameterization:

Target data: Previously published crystal structures for **SR** show two different crystalline forms that have different dihedral angles between the chlorinated phenyl groups and the pyrazole ring, and between the amide group and the piperidine ring (see

Fig. 32). In addition, the crystal structure of form I has the dichlorophenyl ring rotated 180° in 10% of the molecules,[155] with energy barrier of 10 Kcal/mol between the two conformations calculated at HF 6-31G* level. To overcome crystal packing and solvation effects, and to obtain a reference geometry for CHARMM parameterization, crystal structures' geometries were optimized in vacuum using *ab initio* HF/6-31G* and MP2/6-31G* levels of theory.

Crystal structures' bond lengths were reproduced in the MP2 level of theory compared to the HF calculations. QM optimized dihedrals were slightly shifted from crystal structures' dihedrals in both QM methods. MP2 geometry optimization shows that form II has a higher (2 Kcal/mol) gas phase potential energy compared to form I, and form Ia is lower in energy (0.11 Kcal/mol) than form Ib. In addition, **SR** global minima identified by full conformational search at MP2 level of theory has a similar geometry to form Ia, and the rotation of the dichlorophenyl ring in form Ia is similar to the crystal structure of AM6538 in complex with the CB1 receptor [15]. Thus, form Ia was used as the target geometry for **SR** bonded parameter optimization, and will be referred to as **SR** global minima.

Evaluation of initial charges and guess parameters: Paramchem-generated charges and guess parameters show high penalties on some charges, bonds, angles and dihedrals. **SR** global minima was minimized in CHARMM to evaluate those parameters before starting a full parameterization. CHARMM minimized structure deviates from the global minima, specifically at the piperidinyl amide moiety which necessitates partial atomic charges and parameter optimization (see Fig. 33).

Charge optimization: Hinge on the hierarchical essence of CGenFF parameter optimization, charges for **SR** aromatic rings were obtained directly from the CGenFF, and charge optimization was only carried for the piperidinyl amide moiety. The amide functional group was capped with a methyl group, and a total of nine separate electrostatic interaction complexes were optimized (see Fig. 34). Table 5 shows interaction energies and distances for fragment 1-water complexes. Absolute average deviation for MM interaction energies and interaction distances compared to HF values were 0.11 Kcal/mol and 0.16 Å respectively. Charges of the whole **SR** were then calculated as described in Methods and are listed with atom typing in Table 6.

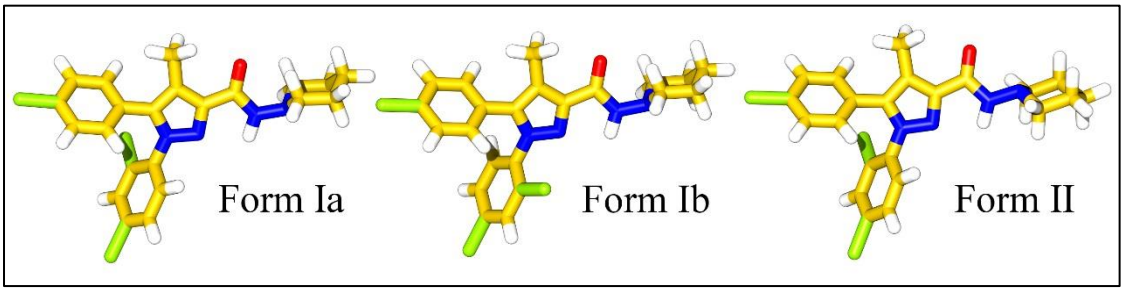

Figure 32. Crystal Structure Geometries for SR. In both conformations, the phenyl rings are tilted ~60 degrees from the plane of the pyrazole ring, the amide oxygen is ~20 degrees from the plane of the pyrazole with trans amide conformation, and the piperidine ring lone pair of electrons are either in trans (Form Ia,b), or in cis (Form II) conformation with the amide hydrogen.

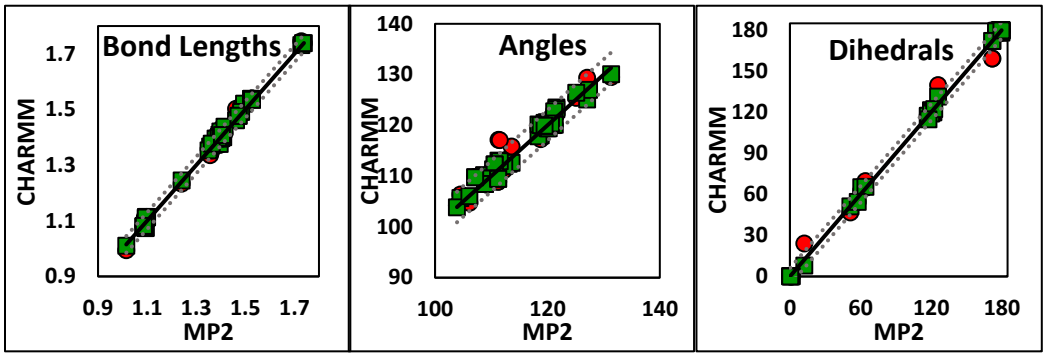

Figure 33. Bond Lengths, Angles, and Dihedrals for SR. Plots of bond lengths, angles, and dihedrals measured for **SR** global minima at MP2 geometry against CHARMM minimized structure using initial CGenFF guess parameters (Red circles), and optimized parameters (Green boxes). Black line corresponds to MP2 reference values, dotted lines correspond to ±0.03 Å, 3°, and 6° margins for bond lengths, angles and dihedrals respectively.

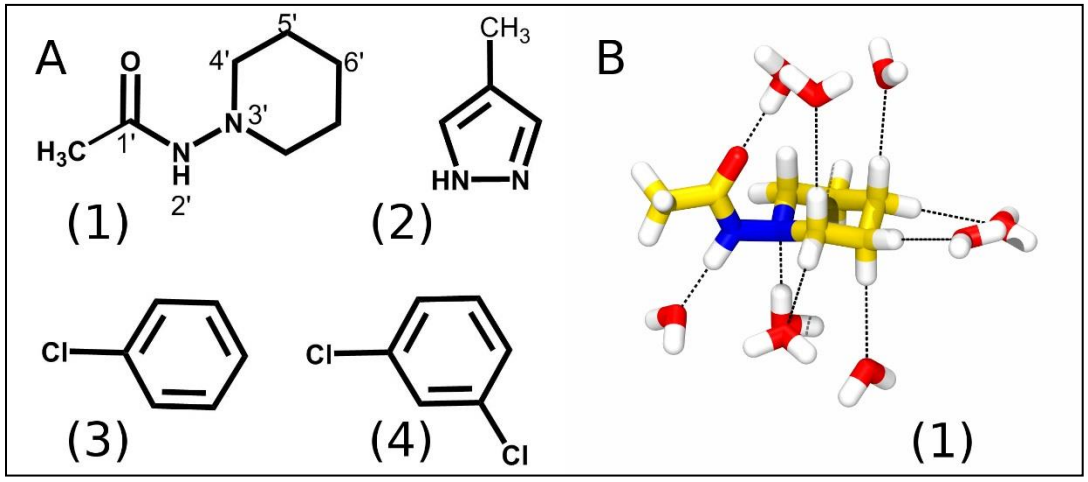

Figure 34. Setting SR-Water Interaction Complexes. A) Molecular fragments used to set charges for the whole **SR.** Atom numbers for molecular fragment 1 are indicated. B) Interaction complexes between fragment 1 and TIP3 water molecules. Each complex was set individually to calculate electrostatic interaction energies and distances for each indicated atom.

Bonded parameters: **SR** global minima geometry was minimized again in CHARMM using optimized partial charges. Charge optimization significantly enhanced the geometry of CHARMM minimized **SR**. Bonded parameters optimization was based on the reproduction of **SR** global minima geometry (see Fig. 33), as well as the reproduction of QM PES for bonds, angles, and dihedrals that deviated by more than 0.03 Å, 3°, and 6°, respectively from their measures in **SR** global minima (see Fig. 35, 36, 37). Bonded terms parameterization started with parameterizing bond lengths, then angles and dihedrals, and required multiple iterations specifically that the parameterization of one bonded term may affect the other. Following each iteration, bond lengths, angles, and dihedrals were measured for the whole compound and compared with **SR** global minima geometries. Dihedral angles were also measured for **SR** during the MD simulation and dihedral parameters were adjusted to ensure that the dihedral probability distributions are in agreement with the QM PES. For the dihedral between the pyrazole and the aromatic rings, two energy minima are present with low energy barrier between them, a planar geometry with the pyrazole ring is unfavorable due to steric clash with the ortho-substituents on the pyrazole ring (see Fig. 37A and 37B). The dihedral between the piperidine ring and the carboxamide shows a broad local minimum between -80° to -160° (see Fig. 37C), this is when the carboxamide oxygen is in cis with the piperidine lone pair of electrons and the equatorial aliphatic hydrogens on the piperidine ring (like form II crystal structure). Finally, the amid oxygen would have a cis geometry with the methyl substituent at the pyrazole ring, this is because the trans geometry would result in steric clash between the amide proton and that methyl.

Table 5. Interaction Energies and Distances Between Molecular Fragment 1 and Water. Differences in CHARMM (MM) and *ab-initio* (QM) interaction energies ΔE (Kcal/mol), and Distances Δr (Å), of Fragment 1-Water complexes.

Interacting complex	$\Delta\Delta$ ***E*** (MM-QM)	Δr (MM-QM)
O …HOH	0.1	-0.22
H2' … OHH	-0.06	-0.2
C4'H_a …OHH	0.25	0.43
C4'H_e …OHH	-0.07	-0.15
C5'H_a …OHH	0.13	-0.1
C5'H_e …OHH	-0.04	-0.09
C6'H_a …OHH	0	-0.02
C6'H_e…OHH	0.11	-0.09
N3' … HOH	0.2	-0.11
Abs Ave. Deviation	0.11	0.16
Abs. Std. Deviation	0.08	0.12

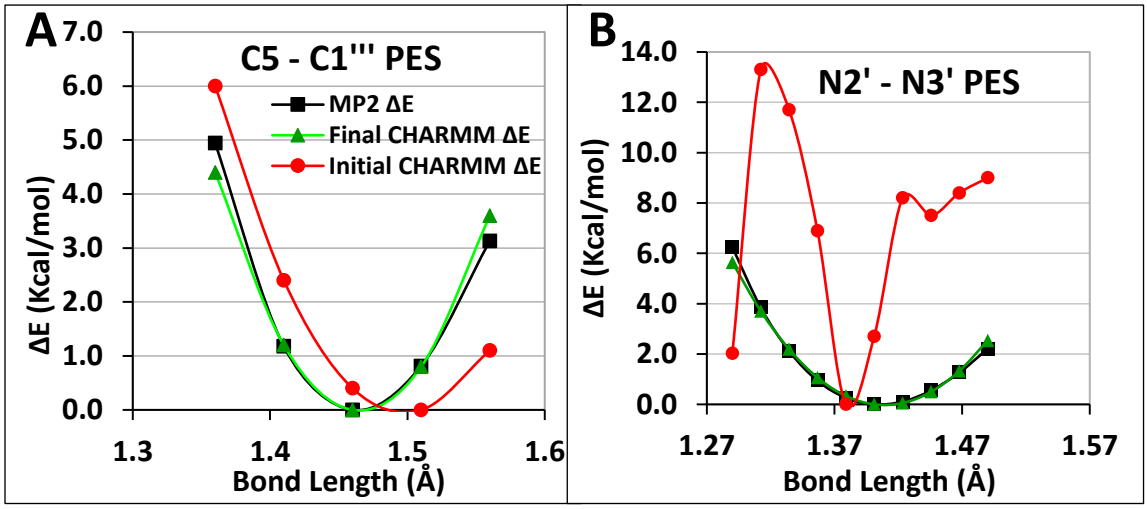

Figure 35. Potential Energy Scans for Two Bond Lengths in SR. A) Bond length between the pyrazole ring and the chlorophenyl ring. B) Bond length between the amide nitrogen and the piperidine nitrogen, with similar legend to graph A.

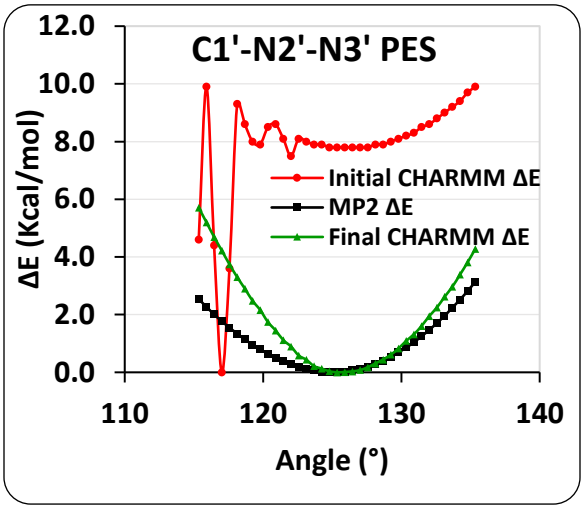

Figure 36. Potential Energy Scan for SR Angle. The angle described by the carboxamide carbon, the carboxamide nitrogen and piperidine nitrogen

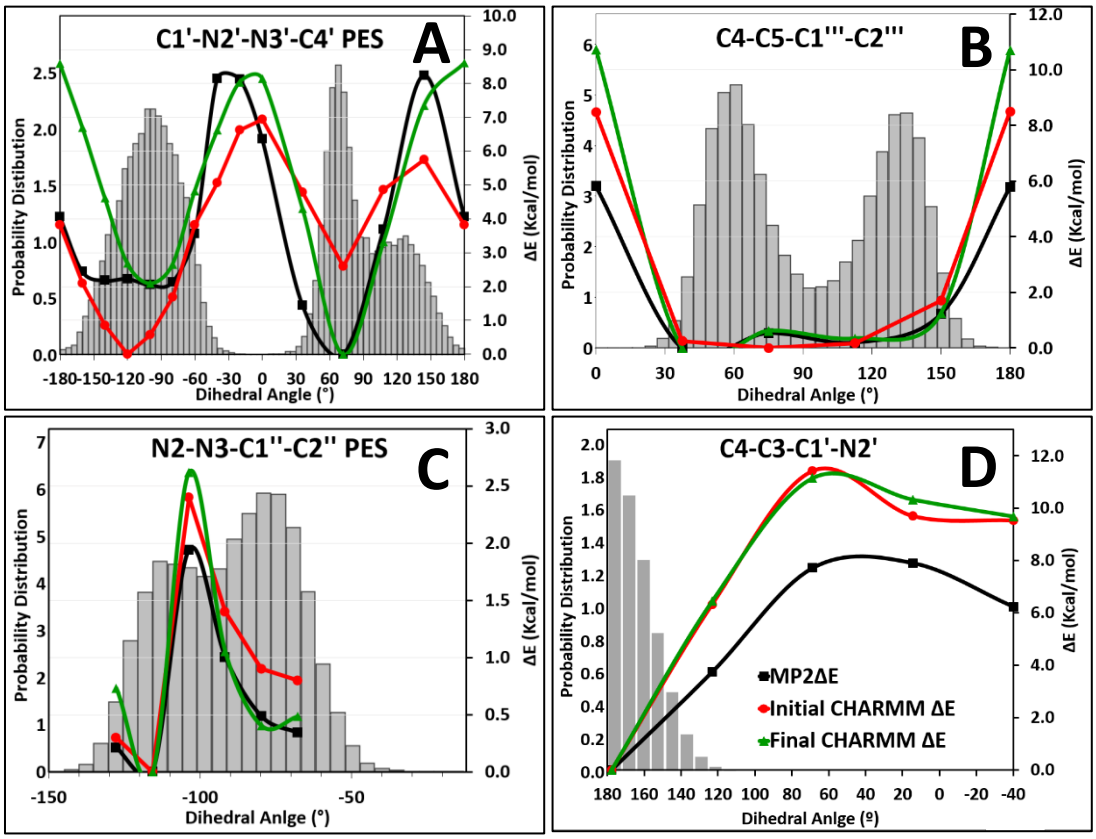

Figure 37. Potential Energy Scans and Probability Distributions for SR Dihedrals. Graphs show dihedrals between: the amide and the piperidine ring (A), pyrazole and the chlorophenyl rings (B), the pyrazole and the dichlorophenyl ring (C), and the pyrazole and the amide group (D). Right Axes show relative energies from PES and are displayed in black (MP2 PES), Red (initial CGenFF PES), and in green (CHARMM PES using optimized parameters). Left axes show the probability distribution from the MD simulations of **SR** in POPC bilayer and are displayed on each graph and colored Grey.

MD simulation: Two independent all atom MD simulations were done to study the dynamics of **SR** in a lipid bilayer. In the first simulation, **SR** was added directly to the lipid phase, and dynamics of all six **SR** molecules in the bilayer was monitored throughout the simulation. However, in the second simulation, three **SR** molecules were added to the water phase on each side of the bilayer, and the dynamics of **SR** partitioning

into, and inside the bilayer was monitored. In this simulation, only three **SR** molecules from one side of the bilayer partitioned into the lipid bilayer during the first 25ns of the simulation, while the remaining **SR** molecules on the other side of the bilayer clumped together inside the water phase and did not diffuse into the lipid phase during the period of the simulation.

Lipid parameters: For both simulations, area per lipid as well as the lipid acyl chain order parameters were calculated to verify the accuracy of the lipid simulation. Area per lipid was determined by dividing the lateral area, measured in VMD for each frame, by the number of phospholipids in each leaflet. Average area per lipid for the last 200ns for simulation I and II were 67 and 66 A^2 respectively, in agreement with experimental values (see Fig. 38). [147]

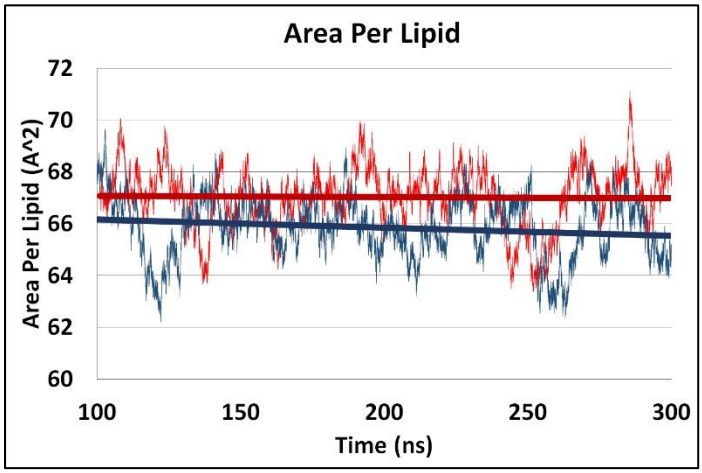

Figure 38. Area Per Lipid for the Last 200ns of MD Simulations of SR in POPC Bilayer. Simulation I (Red), and simulation II (Blue).

Palmitoyl (sn1), and oleoyl (sn2) acyl chains order parameters (S_{CH}) were also calculated for both simulations and compared to available experimental data. S_{CH} denotes an ensemble average of the relative orientation of the CH bonds with respect to the bilayer normal, and defined as (eq. 2):

$$S_{CH} = \frac{1}{2} \langle 3\cos^2\theta - 1 \rangle \qquad \text{eq. (2)}$$

Where θ is the angle between a C-H bond in acyl chain methylene groups and the normal to the bilayer (Z-axis). The angular brackets indicate an ensemble average.

A ^{2}H solid state NMR study at 35°C reported an increase in the order parameters of a dimyristoylphosphatidylcholine (DMPC) bilayer by the addition of 2 mol% AM281 which is an analogue of **SR** with a morpholino group substituent at the amide group and a p-iodophenyl group instead of the p-chlorophenyl ring in **SR**.[159] Experimentally determined order parameters for the sn1 and the sn2 POPC acyl chains are not available at 310K temperature. However, error bars of calculated S_{CH} values for both sn1 and sn2 chains in both simulations overlap with recently published (NMR-determined at 300K) order parameters,[148] and the sn2 oleoyl chain shows the characteristic dip in S_{CH} values at carbon 2 and 10 (see Fig. 39).

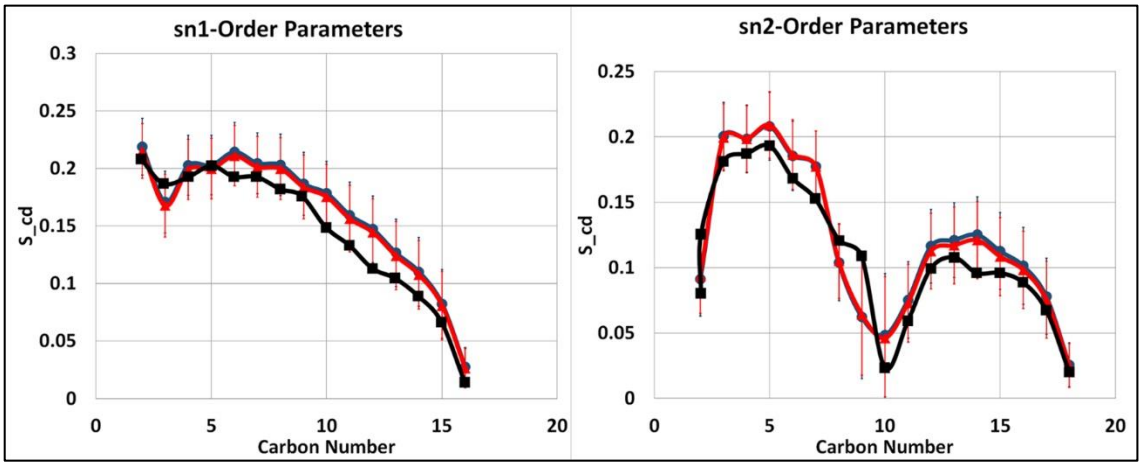

Figure 39. Lipid Order Parameters from MD Simulations of SR in POPC Bilayer. Calculated lipid order parameters for the sn1 (Palmitoyl) and the sn2 (Oleoyl) chains of POPC. Results from MD simulation run 1 (Blue), run 2 (Red), and NMR experimental values (Black).[148] Error bars represent standard error in each MD simulation run. NMR reference values were extracted by digitizing plotted graph in the reference paper.[148]

Density distribution: Density distributions for the bilayer components as well as for **SR** and **SR** subset groups were calculated and determined for the last 200 ns of each simulation. Visual monitoring of the **SR** behavior in the lipid bilayer shows that **SR** generally sets below the phospholipids glyceryl chain. SR can freely move, rotate and flip in all directions in the bilayer, and may also move between leaflets. This is obvious in the density distributions where it shows some molecules being distributed in both leaflets indicative of movement of **SR** from one leaflet to the other (see Fig. 40). In addition, the random distribution of **SR** subsets indicates the free behavior of the ligand in the bilayer. However, comparing the density distributions of the different subsets of **SR** shows a general trend where the piperidine ring and the amide groups are located closest to the phospholipid head groups, the chlorophenyl ring is shifted slightly towards the center of

the bilayer, and the dichlorophenyl ring is shifted further. In simulation II, the partitioning of **SR** into the lipid bilayer starts with an interaction of the piperidine and amide groups with the phospholipid head groups (see Fig. 41).

Dihedrals probability distributions: **SR** dihedrals were measured throughout both simulations and compared to QM PES. All dihedral probability distributions acquired from simulations were consistent with QM PES (see Fig. 37). Looking at the probability distribution of the dihedral between the piperidine and the amide that a piperidine could rotate in the bilayer, and despite that the starting structure had the piperidine ring rotated like form I crystal structure, the other form has been populated throughout the simulation (see Fig. 37C).

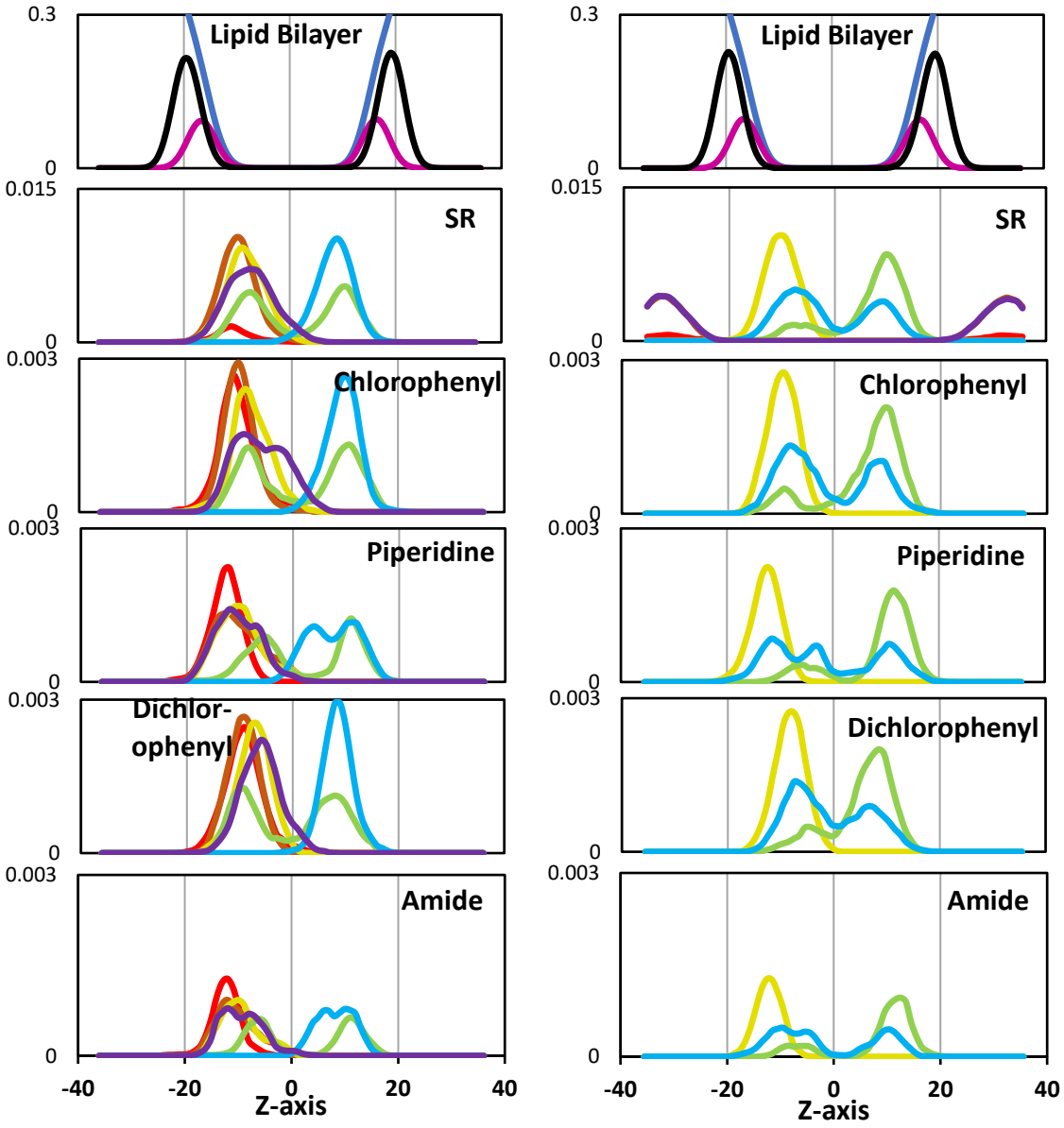

Figure 40. Mass-Density Distributions of SR in POPC Bilayer. At the y-axis: mass-density distributions. Right and Left panels show mass density distributions calculated for simulation I and II respectively, Upper most graphs are showing the density distributions for the phosphate atoms (Black), glycerol region (Pink) and water (Blue). The rest of the panels, each **SR** molecule is given a distinct color in those distributions, and the distribution of **SR** or **SR** subsets were calculated for each **SR** molecule. Measures were done for the last 200 ns of simulations. **SR** subset density distributions for simulation II were only done for the SR molecules that partitioned into the lipid.

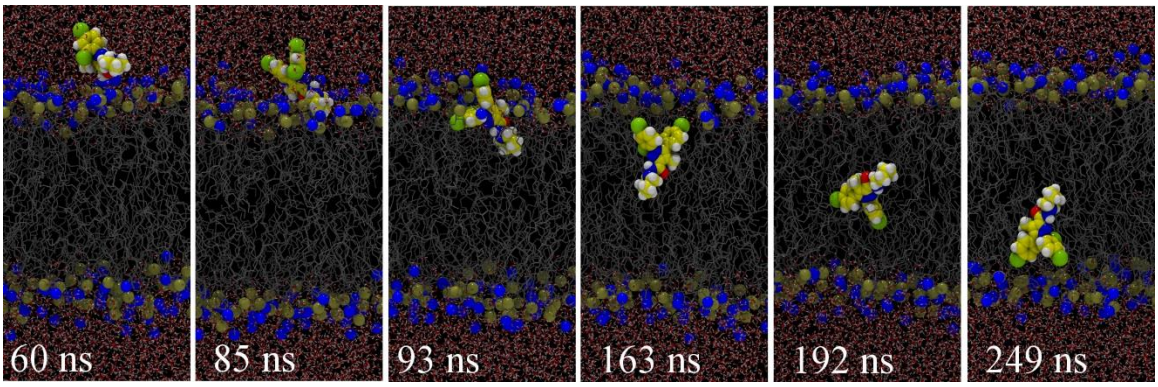

Figure 41. Snapshots from MD Simulation Showing the Diffusion of SR from Bulk Water into the POPC Bilayer. SR rotates in all directions and moves freely between bilayers. First entry of **SR** involves an interaction of the piperidine ring with the head groups. The phosphorous and nitrogen atoms of the POPC headgroups are shown as gold and blue spheres respectively, Water molecules are shown in tube display. POPC carbon tail in silver tubes. Color code for **SR** is: carbons (yellow), nitrogens (Blue), oxygen (Red), hydrogens (White) and chlorine (Yellow green).

Discussion

Advances in computer power and algorithms facilitated the use of molecular dynamics simulation to predict and understand drug receptor interactions. MD simulation studies were done to pursue ligand binding to GPCRs to correlate ligand structure to their binding affinity. Using multi-microsecond unbiased MD simulations, Dror and coworkers examined the pathway and the interaction dynamics of different ligands with the β_1- and β_2- adrenergic receptors. Their results suggest that ligands that access the receptor binding pocket from bulk water would face a large energy barrier during their initial association with the receptor due to dehydration process that is necessary to allow the hydrophobic interaction with the receptor.[160] Differently, it has been reported that lipid derived ligands for GPCRs diffuse from the lipid bilayer to the binding site through

transmembrane portal. As an example, 2-AG has been shown to diffuse from the phospholipid bilayer to the CB2 receptor's binding pocket through transmembrane portal that was formed between transmembrane helices six and seven upon interacting with the ligand.[161] Compared to ligands that access the binding site directly from bulk water, the orientation and the depth of lipophilic ligands in a bilayer will affect the binding affinity or the binding mode to the receptor.[162]

Biophysical studies using NMR, X-ray diffraction and differential scanning calorimetry were used to investigate the orientation and the dynamics of different cannabinoid ligands in the membrane.[159, 162-165] In addition, MD simulation studies were used to study the dynamics of anandamide in membrane.[166] Intuitively, cannabinoid ligands would orient in the membrane in a way that their polar region orients towards the lipid head groups, while their hydrophobic part orients towards the center of the bilayer. Results from current work show that **SR** can move freely in the lipid bilayer. Crystal structures of the CB1 receptor with the two different antagonists, Taranabant and AM6538, show a common orientation of those ligand in the receptor binding pocket having their aromatic rings setting the deepest in the receptor. The presence of aromatic residues at the second transmembrane helix near the ligand portal suggests an initial aromatic interaction between the ligand and the receptor, and the free movement of **SR** in the bilayer makes it possible for the ligand to form similar aromatic interactions with the receptor transmembrane portal.

The SAR of biarylpyrazole derivatives has been studied extensively, and the affinity of **SR** to different CB1 receptor mutants has been evaluated. It is worth

mentioning that mutating K3.28 in the third transmembrane helix had no effect on the binding affinity of Taranabant, while it lowered **SR's** binding affinity.[118] In a thermodynamic cycle study, this amino acid residue was determined to form a key hydrogen bond interaction between the carboxamide oxygen of **SR** and K3.28 that is essential for the inverse agonism of biarylpyrazoles.[120] The different effect of mutating K3.28 to alanine on the binding affinity of those ligands indicate a different way of the binding of those two ligands to the receptor. Availability of force field parameters for **SR** helps elucidating its interaction with the CB1 receptor.

Conclusions

The CHARMM General Force Field (CGenFF) was created for drug-like molecules to use in conjunction with the CHARMM additive biomolecular force field. It covers a broad space of chemical groups present in biomolecules and in drug-like molecules, including simple functional groups, aromatics, and heterocycles, and it allows the extension of the force field to cover additional functional groups with emphasis on quantum mechanical (QM) results as target data for parameter optimization.[154] In this study, we have reported the force field parameters for **SR**, which reproduced **SR** quantum mechanical and crystal structure's geometries during a MD simulation of **SR** in a lipid bilayer. Those parameters can be used to better understand the interaction dynamics of **SR** with the CB1 receptor, and to develop force field parameters for **SR** analogues, helping us better understand the binding affinity data of those analogues not only in the

context of drug-receptor interaction, but also in the context of ligand's behavior in the lipid bilayer.

Table 6. Listing of Atom Names, Types, and Partial Charges (Q) of SR.

Atom	Type	q	Atom	Type	Q
N1	NG2R51	0.251	H6’	HGA2	0.090
N2	NG2R54	-0.547	C1’’	CG2R65	0.048
C3	CG2R52	0.246	C2’’	CG2R65	0.047
C4	CG2R51	-0.072	C3’’	CG2R61	-0.047
C5	CG2R51	0.113	H3’’	HGR62	0.151
C6	CG331	-0.261	C4’’	CG2R61	0.047
H6	HGA8	0.090	C5’’	CG2R61	-0.117
C1’	CG2O8	0.431	H5’’	HGR62	0.165
O	OG2D1	-0.455	C6’’	CG2R61	-0.117
N2’	NG2S1	-0.323	H6’’	HGR61	0.115
H2’	HGP1	0.318	C1’’’	CG2R61	-0.006
N3’	NG3N1	-0.409	C2’’’	CG2R61	-0.116
C4’	CG321	0.045	H2’’’	HGR61	0.115
C5’	CG321	-0.183	C3’’’	CG2R61	-0.114
C6’	CG321	-0.186	H3’’’	HGR62	0.165
H4’	HGA2	0.090	C4’’’	CG2R61	0.052
H5’	HGA2	0.090	Cl	CLGR1	-0.146

Table 7. Lennard-Johns Parameters for Atom Types Used in SR Topology File. New atom types were added to the stream file to ensure that fixed angle or dihedral terms do not affect the force field parameters for other molecules already parameterized in CGenFF.

Atom type	ε	r_{min}	Atom type	ε	r_{min}
CG2O8	-0.110	2.0000	HGA8	-0.024	1.3400
CG2R51	-0.050	2.1000	HGP1	-0.046	0.2245
CG2R52	-0.020	2.2000	HGR61	-0.030	1.3582
CG2R61	-0.070	1.9924	HGR62	-0.046	1.1000
CG2R65	-0.070	1.9924	NG2R51	-0.200	1.8500
CG321	-0.050	2.0100	NG2R54	-0.200	1.8500
CG331	-0.780	2.0500	NG2S1	-0.200	1.8500
CLGR1	-0.320	1.9300	NG3N1	-0.060	2.0500
HGA2	-0.035	1.3400	OG2D1	-0.120	1.7000

Table 8. SR Bond Parameters.

Type	**Type**	K_b	b_0	**Type**	**Type**	K_b	b_0
CG2O8	CG2R52	300.0	1.4750	CG2R65	CLGR1	350.0	1.7260
CG2R51	CG2R61	400.0	1.4400	CG2R52	NG2R54	400.0	1.3560
CG2R65	NG2R51	400.0	1.4150	NG2R54	NG2R51	360.0	1.3500
CG321	NG3N1	263.0	1.4730	CG2O8	OG2D1	620.0	1.2400
NG2S1	NG3N1	360.0	1.4011	CG2O8	NG2S1	370.0	1.3450
CG2R65	CG2R65	394.0	1.3750	CG331	HGA8	170.0	1.0700
CG2R65	CG2R61	394.0	1.3750				

Table 9. SR Angle Parameters.

Type	Type	Type	K_θ	θ_0	$K_{b^{1-3}}$	b_0^{1-3}
CG2R52	CG2O8	NG2S1	80.00	113.57		
CG2R52	CG2O8	OG2D1	30.00	121.65		
CG2R51	CG2R51	CG2R61	45.80	131.33		
CG2R52	CG2R51	CG331	45.80	128.06		
CG2R61	CG2R51	NG2R51	45.80	122.45		
CG2R51	CG2R61	CG2R61	36.00	119.91		
CG321	CG321	NG3N1	0.04	108.70		
NG3N1	CG321	HGA2	32.40	109.50	50.00	2.13
CG2O8	NG2S1	NG3N1	50.00	120.00		
NG3N1	NG2S1	HGP1	35.00	115.93		
CG321	NG3N1	CG321	40.50	112.02	5.00	2.443
CG321	NG3N1	NG2S1	0.03	111.65	99.00	2.38
CG2R65	CG2R65	NG2R51	60.00	121.61		
CG2R61	CG2R65	NG2R51	60.00	118.45		
CG2R51	NG2R51	CG2R65	70.00	128.04		
CG2R65	NG2R51	NG2R54	70.00	118.83		
CG2R61	CG2R65	CLGR1	60.00	120.00		
CG2R65	CG2R65	CLGR1	60.00	120.00		
CG2R65	CG2R65	CG2R61	40.00	119.85	35.00	2.42
CG2R65	CG2R61	CG2R61	40.00	119.39	35.00	2.41
CG2R65	CG2R61	HGR61	30.00	119.98	22.00	2.15
CG2R65	CG2R61	HGR62	30.00	120.00	22.00	2.15
CG2R52	NG2R54	NG2R51	160.00	103.94		
CG2R51	NG2R51	NG2R54	160.00	113.13		
CG2R51	CG2R52	CG2O8	0.02	124.60	125.00	2.51
NG2R54	CG2R52	CG2O8	50.00	120.59		
CG2R51	CG2R52	NG2R54	110.00	112.33		
NG2S1	CG2O8	OG2D1	80.00	124.78		
CG2O8	NG2S1	HGP1	34.00	123.00	143.00	2.12
CG2R51	CG331	HGA8	55.00	110.33		
HGA8	CG331	HGA8	35.50	109.55	5.40	1.80

Table 10. SR Dihedral Parameters.

Type	Type	Type	Type	K_ϕ	n	δ
NG2S1	CG2O8	CG2R52	CG2R51	4.6	2	180
NG2S1	CG2O8	CG2R52	NG2R54	0.0	2	180
OG2D1	CG2O8	CG2R52	CG2R51	1.0	3	180
OG2D1	CG2O8	CG2R52	NG2R54	1.0	3	180
CG2R52	CG2O8	NG2S1	NG3N1	1.6	2	180
CG2R52	CG2O8	NG2S1	HGP1	4.0	2	180
OG2D1	CG2O8	NG2S1	NG3N1	1.0	2	180
CG2R52	CG2R51	CG2R51	CG2R61	0.0	2	180
CG2R61	CG2R51	CG2R51	CG331	0.0	2	180
CG2R51	CG2R51	CG2R52	CG2O8	2.0	2	180
CG331	CG2R51	CG2R52	CG2O8	6.9	2	180
CG331	CG2R51	CG2R52	NG2R54	15.0	2	180
CG2R51	CG2R51	CG2R61	CG2R61	3.0	2	180
NG2R51	CG2R51	CG2R61	CG2R61	3.0	2	180
CG2R61	CG2R51	NG2R51	NG2R54	1.0	2	180
CG2O8	CG2R52	NG2R54	NG2R51	1.0	2	180
CG2R51	CG2R61	CG2R61	CG2R61	10.0	2	180
CG2R51	CG2R61	CG2R61	HGR61	12.0	2	180
CG2R61	CG2R61	CG2R61	NG2R51	3.1	2	180
CG321	CG321	CG321	NG3N1	2.4	2	0
NG3N1	CG321	CG321	HGA2	5.0	3	0
CG321	CG321	NG3N1	CG321	0.4	3	0
CG321	CG321	NG3N1	NG2S1	0.2	3	0
HGA2	CG321	NG3N1	CG321	3.0	3	180
HGA2	CG321	NG3N1	NG2S1	2.0	3	180
CG2O8	NG2S1	NG3N1	CG321	0.0	2	0
HGP1	NG2S1	NG3N1	CG321	0.0	1	0
CG2R65	CG2R65	CG2R61	CG2R61	2.0	2	180
CG2R61	CG2R65	CG2R65	CG2R61	0.0	2	180
CG2R61	CG2R61	CG2R61	CG2R65	3.1	2	180
CG2R61	CG2R61	CG2R65	CLGR1	3.1	2	180
CG2R61	CG2R65	CG2R65	CLGR1	3.1	2	180
CG2R65	CG2R61	CG2R61	CLGR1	3.0	2	180
CG2R51	CG2R51	NG2R51	CG2R65	3.0	2	180
CG2R61	CG2R51	NG2R51	CG2R65	3.0	2	180
CG2R61	CG2R65	CG2R65	NG2R51	3.0	2	180
CG2R61	CG2R61	CG2R65	NG2R51	3.0	2	180
NG2R51	CG2R65	CG2R65	CLGR1	5.0	2	180

Table 10 (Continued), SR Dihedral Parameters.

Type	**Type**	**Type**	**Type**	K_ϕ	n	δ
NG2R51	CG2R65	CG2R61	HGR61	5.0	2	180
CG2R65	CG2R65	CG2R61	HGR61	2.4	2	180
CG2R65	CG2R61	CG2R61	HGR61	3.0	2	180
CG2R61	CG2R65	NG2R51	CG2R51	4.2	2	180
CG2R65	CG2R65	NG2R51	CG2R51	4.2	2	180
CG2R65	CG2R65	NG2R51	NG2R54	1.2	2	180
CG2R61	CG2R65	NG2R51	NG2R54	1.2	2	180
CG2R52	NG2R54	NG2R51	CG2R65	8.5	2	180
CG2R65	CG2R61	CG2R61	HGR62	4.2	2	180
CG2R65	CG2R65	CG2R61	HGR62	4.2	2	180
HGR62	CG2R61	CG2R65	CLGR1	3.0	2	180
CG2R51	CG2R51	CG2R52	NG2R54	8.5	2	180
CG2R51	CG2R51	NG2R51	NG2R54	10.0	2	180
CG2R52	NG2R54	NG2R51	CG2R51	12.0	2	180
CG2R51	CG2R52	NG2R54	NG2R51	12.0	2	180
OG2D1	CG2O8	NG2S1	HGP1	2.5	2	180
CG2R51	CG2R51	CG331	HGA8	0.1	3	180
CG2R52	CG2R51	CG331	HGA8	0.0	3	0
IMPROPERS						
CG2O8	CG2R52	NG2S1	OG2D1	120.0	0	0

CHAPTER V

CONCLUSIONS

Three different studies were presented in this work. In the first study, we could demonstrate the function of conserved amino acid residues in dictating the signaling pathways via the CB1 receptor. In specific, proposed mutants were focused on stabilizing a rotameric state of Y7.53 that biases the signaling of the CB1 receptor towards the β-arrestin pathway. Resulting mutants were well expressed, and were successful in generating a G-protein independent, yet β-arrestin dependent pERK signal. Orthosteric ligands that bias the signaling of the CB1 receptor towards the β-arrestin pathway are not known yet, and resulting mutants can be used in structure-based drug design of such selective ligands. In addition, biased mutants assist drug discovery for novel therapeutics that target the CB1 receptor, and provide the ability to study the correlation of CB1 receptor to different diseases including neurodegenerative diseases. Most importantly, the elucidation of the role of conserved amino acid residues in dictating conformational changes at the IC domain of the CB1 receptor is an integral part in understanding the selective coupling of this receptor to the different IC effector proteins, and can be applied to other members of class A GPCRs.

Availability of structural information of proteins and chemical compounds is integral in drug design. Computational methods provide a broader view of drug receptor interactions and better understanding of protein structure and its dynamics in its

biological environment away from the static crystalline state. In the second study, we addressed the N-terminus of the CB1 receptor in its inactive state crystal structure being invading the receptor's binding site, which will affect future modelling studies and structure-based drug design for new CB1 receptor antagonists based on the crystal structure. We could determine via MD simulations the binding site of 14h, as well as detailed description of the TMH1/7 portal at the CB1 receptor which allows the entry of CB1 receptor antagonists. In addition, the presented model of the N-terminus was stable, and improved the stability of the receptor in its inactive state determined via MD simulations.

Finally, results from the MD simulations of 14h and SR in POPC bilayer emphasize on the role of the ligand's dynamics in the lipid bilayer in dictating the initial interaction with the receptor at the transmembrane portal, thus controlling ligand's affinity. Presented studies provide new perspective in designing new antagonists that target the CB1 receptor.

REFERENCES

1. Ballesteros, J.A. and H. Weinstein, *[19] Integrated methods for the construction of three-dimensional models and computational probing of structure-function relations in G protein-coupled receptors*, in *Methods in Neurosciences*, C.S. Stuart, Editor. 1995, Academic Press. p. 366-428.

2. Devane, W.A., et al., *Determination and Characterization of a Cannabinoid Receptor in Rat Brain.* Molecular Pharmacology, 1988. 34(5): p. 605-613.

3. Matsuda, L.A., et al., *Structure of a cannabinoid receptor and functional expression of the cloned cDNA.* Nature, 1990. 346(6284): p. 561-564.

4. Gérard, C.M., et al., *Molecular cloning of a human cannabinoid receptor which is also expressed in testis.* The Biochemical journal, 1991. 279 (Pt 1: p. 129-134.

5. Munro, S., K.L. Thomas, and M. Abu-Shaar, *Molecular characterization of a peripheral receptor for cannabinoids.* Nature, 1993. 365(6441): p. 61-65.

6. Reggio, P.H., *Endocannabinoid Binding to the Cannabinoid Receptors: What Is Known and What Remains Unknown.* Curr Med Chem., 2010. 17(14): p. 1468-1486.

7. Glass, M., R.L.M. Faull, and M. Dragunow, *Cannabinoid receptors in the human brain: a detailed anatomical and quantitative autoradiographic study in the fetal, neonatal and adult human brain.* Neuroscience, 1997. 77(2): p. 299-318.

8. Pertwee, R.G., *The pharmacology of cannabinoid receptors and their ligands: an overview.* Int J Obes (Lond), 2006. 30 Suppl 1: p. S13-8.

9. Onaivi, E.S., *Cannabinoid Receptors in Brain.* 2009. 88: p. 335-369.

10. Fredriksson, R., et al., *The G-Protein-Coupled Receptors in the Human Genome Form Five Main Families. Phylogenetic Analysis, Paralogon Groups, and Fingerprints.* Molecular Pharmacology, 2003. 63(6): p. 1256-1272.

11. Devillé, J., J. Rey, and M. Chabbert, *An indel in transmembrane helix 2 helps to trace the molecular evolution of class A G-protein-coupled receptors.* Journal of Molecular Evolution, 2009. 68(5): p. 475-489.

12. Pel, J., et al., *Multidimensional scaling reveals the main evolutionary pathways of class A G-protein-coupled receptors.* PLoS ONE, 2011. 6(4): p. 1-10.

13. Surgand, J.S., et al., *A chemogenomic analysis of the transmembrane binding cavity of human G-protein-coupled receptors.* Proteins: Structure, Function and Genetics, 2006. 62(2): p. 509-538.

14. Chrencik, J.E., et al., *Crystal Structure of Antagonist Bound Human Lysophosphatidic Acid Receptor 1.* Cell, 2015. 161(7): p. 1633-1643.

15. Hua, T., et al., *Crystal Structure of the Human Cannabinoid Receptor CB1.* Cell, 2016. 167(3): p. 750-762 e14.

16. Shao, Z., et al., *High-resolution crystal structure of the human CB1 cannabinoid receptor.* Nature, 2016.

17. Hanson, M.A., et al., *Crystal Structure of a Lipid G Protein–Coupled Receptor.* Science, 2012. 335(6070): p. 851.

18. Vallée, M., et al., *Pregnenolone Can Protect the Brain from Cannabis Intoxication.* Science, 2014. 343(6166): p. 94-98.

19. McAllister, S.D., et al., *An Aromatic Microdomain at the Cannabinoid CB 1 Receptor Constitutes an Agonist / Inverse Agonist Binding Region.* Receptor, 2003: p. 5139-5152.

20. Mechoulam, R., et al., *Identification of an endogenous 2-monoglyceride, present in canine gut, that binds to cannabinoid receptors.* Biochemical Pharmacology, 1995. 50(1): p. 83-90.

21. Sugiura, T., et al., *2-Arachidonoylgylcerol: A Possible Endogenous Cannabinoid Receptor Ligand in Brain.* Biochemical and Biophysical Research Communications, 1995. 215(1): p. 89-97.

22. Devane, W.A., et al., *Isolation and structure of a brain constituent that binds to the cannabinoid receptor.* Science, 1992. 258(5090): p. 1946.

23. Wilson, R.I. and R.A. Nicoll, *Endogenous cannabinoids mediate retrograde signalling at hippocampal synapses.* Nature, 2001. 410(6828): p. 588-592.

24. Lu, H.-C. and K. Mackie, *An introduction to the endogenous cannabinoid system.* Biological psychiatry, 2016. 79(7): p. 516-525.

25. Rinaldi-Carmona, M., et al., *SR141716A, a potent and selective antagonist of the brain cannabinoid receptor.* FEBS Letters, 1994. 350(2): p. 240-244.

26. Kendall, D.A. and G.A. Yudowski, *Cannabinoid Receptors in the Central Nervous System: Their Signaling and Roles in Disease.* Frontiers in Cellular Neuroscience, 2016. 10: p. 294.

27. Flores-Otero, J., et al., *Ligand-specific endocytic dwell times control functional selectivity of the cannabinoid receptor 1.* Nature Communications, 2014. 5: p. 1-11.

28. Howlett, A.C., et al., *International Union of Pharmacology. XXVII. Classification of Cannabinoid Receptors.* Pharmacological Reviews, 2002. 54(2): p. 161.

29. Pertwee, R.G., *The pharmacology of cannabinoid receptors and their ligands: an overview.* Int J Obes, 2006. 30(S1): p. S13-S18.

30. Turu, G. and L. Hunyady, *Signal transduction of the CB1 cannabinoid receptor.* Journal of Molecular Endocrinology, 2010. 44(2): p. 75-85.

31. Abadji, V., et al., *Involvement of the Carboxyl Terminus of the Third Intracellular Loop of the Cannabinoid CB1 Receptor in Constitutive Activation of Gs.* Journal of Neurochemistry, 1999. 72(5): p. 2032-2038.

32. Glass, M. and C.C. Felder, *Concurrent stimulation of cannabinoid CB1 and dopamine D2 receptors augments cAMP accumulation in striatal neurons: evidence for a Gs linkage to the CB1 receptor.* (0270-6474).

33. Eldeeb, K., S. Leone-Kabler, and A.C. Howlett, *CB(1) cannabinoid receptor-mediated increases in cyclic AMP accumulation are correlated with reduced Gi/o function.* Journal of basic and clinical physiology and pharmacology, 2016. 27(3): p. 311-322.

34. Lauckner, J.E., B. Hille, and K. Mackie, *The cannabinoid agonist WIN55,212-2 increases intracellular calcium via CB(1) receptor coupling to G(q/11) G proteins.* Proceedings of the National Academy of Sciences of the United States of America, 2005. 102(52): p. 19144-19149.

35. Premont, R.T. and R.R. Gainetdinov, *Physiological roles of G protein-coupled receptor kinases and arrestins.* Annual review of physiology, 2007. 69: p. 511-534.

36. Reiter, E. and R.J. Lefkowitz, *GRKs and β-arrestins: roles in receptor silencing, trafficking and signaling.* Trends in Endocrinology and Metabolism, 2006. 17(4): p. 159-165.

37. Nobles, K.N., et al., *Distinct Phosphorylation Sites on the β₂-Adrenergic Receptor Establish a Barcode That Encodes Differential Functions of β-Arrestin.* Science Signaling, 2011. 4(185): p. ra51.

38. DeWire, S.M., et al., *β-Arrestins and Cell Signaling.* Annual Review of Physiology, 2007. 69(1): p. 483-510.

39. Smith, J.S. and S. Rajagopal, *The β-arrestins: Multifunctional regulators of G protein-coupled receptors.* Journal of Biological Chemistry, 2016: p. jbc.R115.713313-jbc.R115.713313.

40. Luttrell, L.M. and W.E. Miller, *Arrestins as regulators of kinases and phosphatases.* Prog Mol Biol Transl Sci, 2013. 118: p. 115-47.

41. Li, L., et al., *G Protein-coupled Receptor Kinases of the GRK4 Protein Subfamily Phosphorylate Inactive G Protein-coupled Receptors (GPCRs).* Journal of Biological Chemistry, 2015. 290(17): p. 10775-10790.

42. Cahill, T.J., et al., *Distinct conformations of GPCR–β-arrestin complexes mediate desensitization, signaling, and endocytosis.* Proceedings of the National Academy of Sciences, 2017. 114(10): p. 2562-2567.

43. Thomsen, A.R.B., et al., *GPCR-G Protein-β-Arrestin Super-Complex Mediates Sustained G Protein Signaling.* Cell, 2016. 166(4): p. 907-919.

44. Ferguson, S.S.G., *Evolving Concepts in G Protein-Coupled Receptor Endocytosis: The Role in Receptor Desensitization and Signaling.* Pharmacological Reviews, 2001. 53(1): p. 1-24.

45. Lefkowitz, R.J., K. Rajagopal, and E.J. Whalen, *New Roles for β-Arrestins in Cell Signaling: Not Just for Seven-Transmembrane Receptors.* Molecular Cell, 2006. 24(5): p. 643-652.

46. Namkung, Y. and D.R. Sibley, *Protein Kinase C Mediates Phosphorylation, Desensitization, and Trafficking of the D2 Dopamine Receptor.* Journal of Biological Chemistry, 2004. 279(47): p. 49533-49541.

47. Garcia, D.E., et al., *Protein Kinase C Disrupts Cannabinoid Actions by Phosphorylation of the CB1 Cannabinoid Receptor.* The Journal of Neuroscience, 1998. 18(8): p. 2834-2841.

48. Zhou, X.E., et al., *Identification of Phosphorylation Codes for Arrestin Recruitment by G Protein-Coupled Receptors.* Cell, 2017. 170(3): p. 457-469.e13.

49. Shukla, A.K., et al., *Structure of active β-arrestin-1 bound to a G-protein-coupled receptor phosphopeptide.* Nature, 2013. **497**: p. 137.

50. Jin, W., et al., *Distinct domains of the CB1 cannabinoid receptor mediate desensitization and internalization.* Journal of Neuroscience, 1999. 19(10): p. 3773-3780.

51. Daigle, T.L., C.S. Kearn, and K. Mackie, *Rapid CB1 cannabinoid receptor desensitization defines the time course of ERK1/2 MAP kinase signaling.* Neuropharmacology, 2008. 54(1): p. 36-44.

52. Straiker, A., J. Wager-Miller, and K. Mackie, *The CB(1) cannabinoid receptor C-terminus regulates receptor desensitization in autaptic hippocampal neurones.* British Journal of Pharmacology, 2012. 165(8): p. 2652-2659.

53. Delgado-Peraza, F., et al., *Mechanisms of Biased beta-Arrestin-Mediated Signaling Downstream from the Cannabinoid 1 Receptor.* Mol Pharmacol, 2016. 89(6): p. 618-29.

54. Blume, L.C., et al., *Cannabinoid Receptor Interacting Protein (CRIP) 1a competition with β-arrestin for CB1 receptor binding sites.* Molecular Pharmacology, 2016.

55. Morgan, D.J., et al., *Mutation of Putative GRK Phosphorylation Sites in the Cannabinoid Receptor 1 (CB1R) Confers Resistance to Cannabinoid Tolerance and Hypersensitivity to Cannabinoids in Mice.* Journal of Neuroscience, 2014. 34(15): p. 5152-5163.

56. Hsieh, C., et al., *Internalization and recycling of the CB1 cannabinoid receptor.* Journal of Neurochemistry, 1999. 73(2): p. 493-501.

57. Daigle, T.L., M.L. Kwok, and K. Mackie, *Regulation of CB(1) cannabinoid receptor internalization by a promiscuous phosphorylation-dependent mechanism.* Journal of neurochemistry, 2008. 106(1): p. 70-82.

58. Hajkova, A., et al., *SGIP1 alters internalization and modulates signaling of activated cannabinoid receptor 1 in a biased manner.* Neuropharmacology, 2016. 107: p. 201-14.

59. Breivogel, C.S., et al., *Sensitivity to delta9-tetrahydrocannabinol is selectively enhanced in beta-arrestin2 -/- mice.* Behavioural pharmacology, 2008. 19(4): p. 298-307.

60. Breivogel, C.S. and M.S. Vaghela, *The effects of beta-arrestin1 deletion on acute cannabinoid activity, brain cannabinoid receptors and tolerance to cannabinoids in mice.* J Recept Signal Transduct Res, 2015. 35(1): p. 98-106.

61. Leterrier, C., et al., *Constitutive Activation Drives Compartment-Selective Endocytosis and Axonal Targeting of Type 1 Cannabinoid Receptors.* The Journal of Neuroscience, 2006. 26(12): p. 3141-3153.

62. Niehaus, J.L., et al., *CB₁ Cannabinoid Receptor Activity Is Modulated by the Cannabinoid Receptor Interacting Protein CRIP 1a.* Molecular Pharmacology, 2007. 72(6): p. 1557-1566.

63. Smith, T.H., et al., *Cannabinoid Receptor-Interacting Protein 1a Modulates CB1 Receptor Signaling and Regulation.* Molecular Pharmacology, 2015. 87(4): p. 747-765.

64. Blume, L.C., et al., *Cannabinoid receptor interacting protein suppresses agonist-driven CB1 receptor internalization and regulates receptor replenishment in an agonist-biased manner.* J Neurochem, 2016. 139(3): p. 396-407.

65. Kenakin, T., *The Effective Application of Biased Signaling to New Drug Discovery.* Molecular Pharmacology, 2015(12): p. 1055-1061.

66. Katritch, V., et al., *Allosteric sodium in class A GPCR signaling.* Trends in Biochemical Sciences, 2014. 39(5): p. 233-244.

67. Gyombolai, P., et al., *Mutations in the 'DRY' motif of the CB1 cannabinoid receptor result in biased receptor variants.* Journal of Molecular Endocrinology, 2014. 54(1): p. 75-89.

68. Wei, H., et al., *Independent beta-arrestin 2 and G protein-mediated pathways for angiotensin II activation of extracellular signal-regulated kinases 1 and 2.* Proceedings of the National Academy of Sciences of the United States of America, 2003. 100(19): p. 10782-7.

69. Shenoy, S.K., et al., *β-arrestin-dependent, G protein-independent ERK1/2 activation by the β2 adrenergic receptor.* Journal of Biological Chemistry, 2006. 281(2): p. 1261-1273.

70. Fenalti, G., et al., *Molecular control of δ-opioid receptor signalling.* Nature, 2014. 506(7487): p. 191-6.

71. Ahn, K.H., et al., *Distinct roles of b-arrestin 1 and b-arrestin 2 in ORG27569-induced biased signaling and internalization of the cannabinoid receptor 1 (CB1).* Journal of Biological Chemistry, 2013. 288(14): p. 9790-9800.

72. Laprairie, R.B., et al., *Biased Type 1 Cannabinoid Receptor Signalling Influences Neuronal Viability in a Cell Culture Model of Huntington Disease.* Molecular Pharmacology, 2015. 89: p. 364-375.

73. Laprairie, R.B., et al., *Type 1 cannabinoid receptor ligands display functional selectivity in a cell culture model of striatal medium spiny projection neurons.* Journal of Biological Chemistry, 2014. 289(36): p. 24845-24862.

74. Ahn, K.H., M.M. Mahmoud, and D.A. Kendall, *Allosteric modulator ORG27569 induces CB1 cannabinoid receptor high affinity agonist binding state, receptor internalization, and Gi protein-independent ERK1/2 kinase activation.* Journal of Biological Chemistry, 2012. 287(15): p. 12070-12082.

75. Wisler, J.W., et al., *A unique mechanism of beta-blocker action: carvedilol stimulates beta-arrestin signaling.* Proceedings of the National Academy of Sciences of the United States of America, 2007. 104(42): p. 16657-16662.

76. Laprairie, R.B., et al., *Mapping Cannabinoid Receptor 1 Allosteric Site(S): Critical Molecular Determinant and Signaling Profile of Gat100 - a Novel, Potent and Irreversibly Binding Probe.* ACS Chemical Neuroscience, 2016: p. acschemneuro.6b00041-acschemneuro.6b00041.

77. Ahn, K.H., et al., *Distinct roles of Beta-arrestin 1 and Beta-arrestin 2 in ORG27569-induced biased signaling and internalization of the cannabinoid receptor 1 (CB1).* Journal of Biological Chemistry, 2013. 288(14): p. 9790-9800.

78. Breivogel, C.S. and M.S. Vaghela, *The effects of beta-arrestin1 deletion on acute cannabinoid activity, brain cannabinoid receptors and tolerance to cannabinoids in mice.* Journal of Receptors and Signal Transduction, 2015. 35(1): p. 98-106.

79. Glass, M. and J.K. Northup, *Agonist selective regulation of G proteins by cannabinoid CB(1) and CB(2) receptors.* Molecular pharmacology, 1999. 56(6): p. 1362-9.

80. Georgieva, T., et al., *Unique agonist-bound cannabinoid CB1 receptor conformations indicate agonist specificity in signaling.* European Journal of Pharmacology, 2008. 581(1-2): p. 19-29.

81. Kahsai, A.W., et al., *Multiple ligand-specific conformations of the β(2)-adrenergic receptor.* Nature Chemical Biology, 2011. 7(10): p. 692-700.

82. Carpenter, B. and C.G. Tate, *Active state structures of G protein-coupled receptors highlight the similarities and differences in the G protein and arrestin coupling interfaces.* Current Opinion in Structural Biology, 2017. 45(Supplement C): p. 124-132.

83. Shi, L., et al., *Beta-2 adrenergic receptor activation: Modulation of the proline kink in transmembrane 6 by a rotamer toggle switch.* Journal of Biological Chemistry, 2002. 277(43): p. 40989-40996.

84. Altenbach, C., et al., *High-resolution distance mapping in rhodopsin reveals the pattern of helix movement due to activation.* Proceedings of the National Academy of Sciences of the United States of America, 2008. 105(21): p. 7439-7444.

85. Rasmussen, S.G.F., et al., *Crystal structure of the b 2 adrenergic receptor – Gs protein complex.* Nature, 2011. 477(7366): p. 549-555.

86. Hua, T., et al., *Crystal structures of agonist-bound human cannabinoid receptor CB1.* Nature, 2017. 547(7664): p. 468-471.

87. Singh, R., et al., *Activation of the cannabinoid CB1 receptor may involve a W6.48/F3.36 rotamer toggle switch.* The Journal of Peptide Research, 2002. 60(6): p. 357-370.

88. Venkatakrishnan, A.J., et al., *Diverse activation pathways in class A GPCRs converge near the G-protein-coupling region.* Nature, 2016. 536: p. 484.

89. Valentin-Hansen, L., et al., *Biased Gs versus Gq proteins and β-arrestin signaling in the NK1 receptor determined by interactions in the water hydrogen bond network.* Journal of Biological Chemistry, 2015. 290.

90. Yuan, S., et al., *Activation of G-protein-coupled receptors correlates with the formation of a continuous internal water pathway.* Nature communications, 2014. 5(May): p. 4733-4733.

91. D'Antona, A.M., et al., *A cannabinoid receptor 1 mutation proximal to the DRY motif results in constitutive activity and reveals intramolecular interactions involved in receptor activation.* Brain Research, 2006. 1108(1): p. 1-11.

92. Fay, J.F. and D.L. Farrens, *Structural dynamics and energetics underlying allosteric inactivation of the cannabinoid receptor CB1.* Proceedings of the National Academy of Sciences of the United States of America, 2015. 112(27): p. 8469-74.

93. Liu, W., et al., *Structural basis for allosteric regulation of GPCRs by sodium ions.* Science (New York, N.Y.), 2012. 337(6091): p. 232-6.

94. Carpenter, B., et al., *Structure of the adenosine A2A receptor bound to an engineered G protein.* Nature, 2016. 536: p. 104.

95. Cherezov, V., et al., *High-resolution crystal structure of an engineered human beta2-adrenergic G protein-coupled receptor.* Science, 2007. **318**(5854): p. 1258-1265.

96. Manglik, A., et al., *Crystal structure of the μ-opioid receptor bound to a morphian antagonist.* Nature, 2012. 485(7398): p. 321-326.

97. Huang, W., et al., *Structural insights into μ-opioid receptor activation.* Nature, 2015. 524(7565): p. 315-321.

98. Haga, K., et al., *Structure of the human M2 muscarinic acetylcholine receptor bound to an antagonist.* Nature, 2012. 482: p. 547.

99. Kruse, A.C., et al., *Activation and allosteric modulation of a muscarinic acetylcholine receptor.* Nature, 2013. 504: p. 101.

100. Rahmeh, R., et al., *Structural insights into biased G protein-coupled receptor signaling revealed by fluorescence spectroscopy.* Proceedings of the National Academy of Sciences of the United States of America, 2012. 109(17): p. 6733-8.

101. Liu, J.J., et al., *Biased signaling pathways in β(2)-adrenergic receptor characterized by (19)F-NMR.* Science (New York, N.y.), 2012. 335(6072): p. 1106-1110.

102. Wacker, D., et al., *Crystal Structure of an LSD-Bound Human Serotonin Receptor.* Cell, 2017. 168(3): p. 377-389.e12.

103. Miller-Gallacher, J.L., et al., *The 2.1 Å Resolution Structure of Cyanopindolol-Bound β(1)-Adrenoceptor Identifies an Intramembrane Na(+) Ion that Stabilises the Ligand-Free Receptor.* PLoS ONE, 2014. 9(3): p. e92727.

104. Zhang, C., et al., *High-resolution crystal structure of human protease-activated receptor 1.* Nature, 2012. 492(7429): p. 387-392.

105. Segala, E., et al., *Controlling the Dissociation of Ligands from the Adenosine A2A Receptor through Modulation of Salt Bridge Strength.* Journal of Medicinal Chemistry, 2016. 59(13): p. 6470-6479.

106. Tao, Q. and M.E. Abood, *Mutation of a Highly Conserved Aspartate Residue in the Second Transmembrane Domain of the Cannabinoid Receptors, CB1 and CB2, Disrupts G-Protein Coupling.* Journal of Pharmacology and Experimental Therapeutics, 1998. 285(2): p. 651.

107. Angel, T.E., M.R. Chance, and K. Palczewski, *Conserved waters mediate structural and functional activation of family A (rhodopsin-like) G protein-coupled receptors.* Proceedings of the National Academy of Sciences of the United States of America, 2009. 106(21): p. 8555-8560.

108. Yuan, S., et al., *Activation of G-protein-coupled receptors correlates with the formation of a continuous internal water pathway.* Nature Communications, 2014. 5: p. 4733.

109. Nygaard, R., et al., *Conserved Water-mediated Hydrogen Bond Network between TM-I , -II , -VI , and -VII in 7TM Receptor Activation* * □. 2010. 285(25): p. 19625-19636.

110. Yuan, S., H. Vogel, and S. Filipek, *The role of water and sodium ions in the activation of the μ-opioid receptor.* Angewandte Chemie - International Edition, 2013. 52(38): p. 10112-10115.

111. Sun, X., H. Ågren, and Y. Tu, *Functional Water Molecules in Rhodopsin Activation.* The Journal of Physical Chemistry B, 2014. 118(37): p. 10863-10873.

112. Angel, T.E., et al., *Structural waters define a functional channel mediating activation of the GPCR, rhodopsin.* Proceedings of the National Academy of Sciences of the United States of America, 2009. 106(34): p. 14367-14372.

113. Munk, C., et al., *GPCRdb: the G protein-coupled receptor database – an introduction.* British Journal of Pharmacology, 2016. **173**(14): p. 2195-2207.

114. Isberg, V., et al., *GPCRdb: an information system for G protein-coupled receptors.* Nucleic Acids Research, 2016. 44(D1): p. D356-D364.

115. Reggio, P.H., *Toward the design of cannabinoid CB1 receptor inverse agonists and neutral antagonists.* Drug Development Research, 2009. 70(8): p. 585-600.

116. Bonner, T.I. and Z.H. Song, *A lysine residue of the cannabinoid receptor is critical for receptor recognition by several agonists but not WIN55212-2.* Molecular pharmacology, 1996. 49(5): p. 891-896.

117. Chin, C.N., et al., *Ligand binding and modulation of cyclic AMP levels depend on the chemical nature of residue 192 of the human cannabinoid receptor 1.* Journal of neurochemistry, 1998. 70(1): p. 366-373.

118. Lin, L.S., et al., *Conformational Analysis and Receptor Docking of N - [(1 S , 2 S) -3- (4-Chlorophenyl) -2- (3-cy- anophenyl) -1-methylpropyl] -2-methyl-2- \\{[5- (trifluoromethyl) pyridin-2-yl] oxy } propanamide (Taranabant , MK-0364), a Novel , Acyclic Canna.* Journal of medicinal chemistry, 2008. 51: p. 2108-2114.

119. Hurst, D., et al., *Biarylpyrazole Inverse Agonists at the Cannabinoid CB1 Receptor: Importance of the C-3 Carboxamide Oxygen/Lysine3.28(192) Interaction.* Journal of Medicinal Chemistry, 2006. 49(20): p. 5969-5987.

120. Hurst, D.P., et al., *N-(Piperidin-1-yl)-5-(4-chlorophenyl)-1-(2,4-dichlorophenyl)-4-methyl-1H-pyrazole-3-carboxamide (SR141716A) Interaction with LYS 3.28(192) Is Crucial for Its Inverse Agonism at the Cannabinoid CB1 Receptor.* Molecular Pharmacology, 2002. 62(6): p. 1274-1287.

121. Pan, X., S.R. Ikeda, and D.L. Lewis, *SR 141716A Acts as an Inverse Agonist to Increase Neuronal Voltage-Dependent Ca 2 ∂ Currents by Reversal of Tonic CB1 Cannabinoid Receptor Activity.* 1998. 1072: p. 1064-1072.

122. Ahn, K.H., et al., *Computationally-predicted CB1 cannabinoid receptor mutants show distinct patterns of salt-bridges that correlate with their level of constitutive activity reflected in G protein coupling levels, thermal stability, and ligand binding.* Proteins, 2013. 81(8): p. 1304-17.

123. Fay, J.F. and D.L. Farrens, *The Membrane Proximal Region of the Cannabinoid Receptor CB1 N-Terminus Can Allosterically Modulate Ligand Affinity.* Biochemistry, 2013. 52(46): p. 8286-8294.

124. Murphy, J.W. and D.A. Kendall, *Integrity of extracellular loop 1 of the human cannabinoid receptor 1 is critical for high-affinity binding of the ligand CP 55,940 but not SR 141716A.* Biochemical Pharmacology, 2003. 65(10): p. 1623-1631.

125. Andersson, H., et al., *Membrane Assembly of the Cannabinoid Receptor 1: Impact of a Long N-Terminal Tail.* Molecular Pharmacology, 2003. 64(3): p. 570-577.

126. *UniProt: the universal protein knowledgebase.* Nucleic Acids Research, 2017. 45(D1): p. D158-D169.

127. Rover, S., et al., *6-alkoxy-5-aryl-3-pyridinecarboxamides, a new series of bioavailable cannabinoid receptor type 1 (CB1) antagonists including peripherally selective compounds.* Journal of Medicinal Chemistry, 2013. 56(24): p. 9874-9896.

128. Iyer, M.R., et al., *Structural Basis of Species-dependent Differential Affinity of 6-Alkoxy-5-aryl-3-pyridinecarboxamide Cannabinoid Receptor 1 Antagonists Running Title: Species-specific affinity of CB1 receptor antagonists.* at ASPET Journals on, 2015: p. 238-244.

129. Šali, A. and T.L. Blundell, *Comparative Protein Modelling by Satisfaction of Spatial Restraints.* Journal of Molecular Biology, 1993. 234(3): p. 779-815.

130. Fiser, A., R.K. Do, and A. Sali, *Modeling of loops in protein structures.* Protein Science : A Publication of the Protein Society, 2000. 9(9): p. 1753-1773.

131. Ulfers, A.L., et al., *Structure of the third intracellular loop of the human cannabinoid 1 receptor.* Biochemistry, 2002. 41(38): p. 11344-11350.

132. Jacobson, M.P., et al., *On the Role of the Crystal Environment in Determining Protein Side-chain Conformations.* Journal of Molecular Biology, 2002. 320(3): p. 597-608.

133. Jacobson, M.P., et al., *A hierarchical approach to all-atom protein loop prediction.* Proteins: Structure, Function, and Bioinformatics, 2004. 55(2): p. 351-367.

134. Nie, J. and D.L. Lewis, *Structural domains of the CB1 cannabinoid receptor that contribute to constitutive activity and G-protein sequestration.* The Journal of neuroscience : the official journal of the Society for Neuroscience, 2001. 21(22): p. 8758-8764.

135. Chillakuri, C.R., C. Reinhart, and H. Michel, *C-terminal truncated cannabinoid receptor 1 coexpressed with G protein trimer in Sf9 cells exists in a precoupled state and shows constitutive activity.* FEBS J, 2007. 274(23): p. 6106-15.
136. Stadel, R., K.H. Ahn, and D.A. Kendall, *The cannabinoid type-1 receptor carboxyl-terminus, more than just a tail.* J Neurochem, 2011. 117(1): p. 1-18.

137. Oddi, S., et al., *Effects of palmitoylation of Cys(415) in helix 8 of the CB(1) cannabinoid receptor on membrane localization and signalling.* British Journal of Pharmacology, 2012. 165(8): p. 2635-2651.

138. Lomize, A.L., et al., *Positioning of proteins in membranes: A computational approach.* Protein Science : A Publication of the Protein Society, 2006. 15(6): p. 1318-1333.

139. Sherman, W., et al., *Novel Procedure for Modeling Ligand/Receptor Induced Fit Effects.* Journal of Medicinal Chemistry, 2006. 49(2): p. 534-553.

140. Huang, J., et al., *CHARMM36m: an improved force field for folded and intrinsically disordered proteins.* Nature Methods, 2016. 14: p. 71.

141. Huang, J. and A.D. MacKerell, *CHARMM36 all-atom additive protein force field: Validation based on comparison to NMR data.* Journal of Computational Chemistry, 2013. 34(25): p. 2135-2145.

142. Jo, S., et al., *CHARMM-GUI: A web-based graphical user interface for CHARMM.* Journal of Computational Chemistry, 2008. 29(11): p. 1859-1865.

143. Romo, T.D., N. Leioatts, and A. Grossfield, *Lightweight Object Oriented Structure analysis: Tools for building Tools to Analyze Molecular Dynamics Simulations.* Journal of computational chemistry, 2014. 35(32): p. 2305-2318.

144. Humphrey, W., A. Dalke, and K. Schulten, *VMD: Visual molecular dynamics.* Journal of Molecular Graphics, 1996. 14(1): p. 33-38.

145. Wu, E.L., et al., *CHARMM-GUI Membrane Builder Toward Realistic Biological Membrane Simulations.* Journal of computational chemistry, 2014. 35(27): p. 1997-2004.

146. Lee, J., et al., *CHARMM-GUI Input Generator for NAMD, GROMACS, AMBER, OpenMM, and CHARMM/OpenMM Simulations Using the CHARMM36 Additive Force Field.* Journal of Chemical Theory and Computation, 2016. 12(1): p. 405-413.

147. Hyslop, P.A., B. Morel, and R.D. Sauerheber, *Organization and interaction of cholesterol and phosphatidylcholine in model bilayer membranes.* Biochemistry, 1990. 29(4): p. 1025-1038.
148. Ferreira, T.M., et al., *Cholesterol and POPC segmental order parameters in lipid membranes: solid state 1H-13C NMR and MD simulation studies.* Physical Chemistry Chemical Physics, 2013. 15(6): p. 1976-1989.

149. Fenalti, G., et al., *Molecular Control of δ -Opioid Receptor Signaling.* 2015. 506(7487): p. 191-196.

150. Liu, W., et al., *Structural basis for allosteric regulation of GPCRs by sodium ions.* Science (New York, N.Y.), 2012. **337**(6091): p. 232-6.

151. Tao, Q. and M.E. Abood, *Mutation of a highly conserved aspartate residue in the second transmembrane domain of the cannabinoid receptors, CB1 and CB2, disrupts G-protein coupling.* The Journal of pharmacology and experimental therapeutics, 1998. 285(2): p. 651-8.

152. Rinaldi-Carmona, M., et al., *SR141716A, a potent and selective antagonist of the brain cannabinoid receptor.* FEBS Letters, 1994. **350**(2): p. 240-244.

153. Kang, J.G. and C.-Y. Park, *Anti-Obesity Drugs: A Review about Their Effects and Safety.* Diabetes & Metabolism Journal, 2012. 36(1): p. 13-25.

154. Vanommeslaeghe, K., et al., *CHARMM general force field: A force field for drug-like molecules compatible with the CHARMM all-atom additive biological force fields.* J Comput Chem, 2010. 31(4): p. 671-90.

155. Perrin, M.-A., et al., *Rimonabant dimorphism and its pressure–temperature phase diagram: A delicate case of overall monotropic behavior.* Journal of Pharmaceutical Sciences, 2013. 102(7): p. 2311-2321.

156. Shao, Y., et al., *Advances in methods and algorithms in a modern quantum chemistry program package.* Physical Chemistry Chemical Physics, 2006. 8(27): p. 3172-3191.

157. Bochevarov, A.D., et al., *Jaguar: A high-performance quantum chemistry software program with strengths in life and materials sciences.* International Journal of Quantum Chemistry, 2013. 113(18): p. 2110-2142.

158. Huang, J. and A.D. MacKerell, *CHARMM36 all-atom additive protein force field: Validation based on comparison to NMR data.* Journal of Computational Chemistry, 2013. **34**(25): p. 2135-2145.

159. Tiburu, E.K., et al., *Structural divergence among cannabinoids influences membrane dynamics: A 2H Solid-State NMR analysis.* Biochimica et Biophysica Acta (BBA) - Biomembranes, 2007. 1768(9): p. 2049-2059.

160. Dror, R.O., et al., *Pathway and mechanism of drug binding to G-protein-coupled receptors.* Proceedings of the National Academy of Sciences, 2011. 108(32): p. 13118-13123.

161. Hurst, D.P., et al., *A lipid pathway for ligand binding is necessary for a cannabinoid G protein-coupled receptor*. Journal of Biological Chemistry, 2010. 285(23): p. 17954-17964.

162. Makriyannis, A., X. Tian, and J. Guo, *How lipophilic cannabinergic ligands reach their receptor sites.* Prostaglandins & Other Lipid Mediators, 2005. 77(1): p. 210-218.

163. Mavromoustakos, T., et al., *Small angle X-ray diffraction studies on the topography of cannabinoids in synaptic plasma membranes.* Pharmacology Biochemistry and Behavior, 1991. **40**(3): p. 547-552.

164. Kimura, T., et al., *Location, Structure, and Dynamics of the Synthetic Cannabinoid Ligand CP-55,940 in Lipid Bilayers.* Biophysical Journal, 2009. 96(12): p. 4916-4924.

165. Tian, X., et al., *The interaction of cannabinoid receptor agonists, CP55940 and WIN55212-2 with membranes using solid state (2)H NMR.* Biochimica et biophysica acta, 2011. 1808(9): p. 2095-2101.

166. Lynch, D.L. and P.H. Reggio, *Molecular Dynamics Simulations of the Endocannabinoid N-Arachidonoylethanolamine (Anandamide) in a Phospholipid Bilayer: Probing Structure and Dynamics.* Journal of Medicinal Chemistry, 2005. 48(15): p. 4824-4833.